

TRAINING EFFICIENCY AND ROBUSTNESS IN DEEP LEARNING

by

Fartash Faghri

A thesis submitted in conformity with the requirements
for the degree of Doctor of Philosophy

Department of Computer Science
University of Toronto

Training Efficiency and Robustness in Deep Learning

Fartash Faghri

Doctor of Philosophy

Department of Computer Science

University of Toronto

2022

Abstract

Deep Learning has revolutionized machine learning and artificial intelligence, achieving superhuman performance in several standard benchmarks. It is well-known that deep learning models are inefficient to train; they learn by processing millions of training data multiple times and require powerful computational resources to process large batches of data in parallel at the same time rather than sequentially. Deep learning models also have unexpected failure modes; they can be fooled into misbehaviour, producing unexpectedly incorrect predictions.

In this thesis, we study approaches to improve the training efficiency and robustness of deep learning models. In the context of learning visual-semantic embeddings, we find that prioritizing learning on more informative training data increases convergence speed and improves generalization performance on test data. We formalize a simple trick called hard negative mining as a modification to the learning objective function with no computational overhead. Next, we seek improvements to optimization speed in general-purpose optimization methods in deep learning. We show that a redundancy-aware modification to the sampling of training data improves the training speed and develops an efficient method for detecting the diversity of training signal, namely, gradient clustering. Finally, we study adversarial robustness in deep learning and approaches to achieve maximal adversarial robustness without training with additional data. For linear models, we prove guaranteed maximal robustness achieved only by appropriate choice of the optimizer, regularization, or architecture.

Acknowledgements

Throughout the years, David Fleet was the best supervisor I could ever hope to have. He provided a calm environment without typical pressures, encouraged research wanderings, and valued my approaches. His responses to strange ideas were either constructive and kind feedback or a surprisingly deep and thought-provoking question. As an absolute ethical role model, David always promptly responded with intelligent resolutions. His generous support went beyond financial to caring for my physical and mental wellness. It has been an honour to have David as my sage mentor.

I have been blessed to have the support and company of my cheerful, considerate, kindhearted, encouraging, and simply amazing wife, Sara Sabour.

I have been fortunate enough to receive lasting influences from numerous mentors. I highly appreciate the guidance, encouragement, and constructive feedback of my supervisory committee, David Duvenaud, Roger Grosse, Graham Taylor, and Chris Maddison. I am also grateful for the wisdom, unique perspective, and pivotal advice of Ian Goodfellow, Nicolas Le Roux, Fabian Pedregosa, Jimmy Ba, Daniel Roy, Sanja Fidler, Foteini Agrafioti, Alexey Kurakin, Nicholas Carlini, Mohammad Norouzi, Mehrdad Farajtabar, Mohammad Amin Sadeghi, Ehsan Fazl Ersi, Aideen NasiriShargh, Afshin Nikzad, Kian Mirjalali, and Vahid Liaghat.

I appreciate the enjoyable, fun and fruitful collaborations with my coauthors Yanshuai Cao, Ali Ramezani-Kebrya, Iman Tabrizian, Avery Ma, Justin Gilmer, Nicolas Papernot, Jamie Kiros, and Sven Gowal.

Thanks to my friends, lab-mates and coworkers for making my graduate studies a pleasurable journey. Among many others at the University of Toronto and the Vector Institute, I would like to thank Alireza Shekaramiz, Saeed Seddighin, Jake Snell, Nona Naderi, Kevin Swersky, Eleni Triantafillou, Micha Livne, Ladislav Rampasek, Alimohammad Rabbani, Bahareh Mostafazadeh, Sepideh Mahabadi, Kaveh Ghasemloo, Sajad Norouzi, Aryan Arbabi, Rahmtin Rotabi, Farzaneh Derakhshan, Alireza Makhzani, Farzaneh Mahdisoltani, Taylor Killian, Ehsan Amiri, and Sobhan Foroughi.

I would like to thank the staff at the University of Toronto, the Department of Computer Science, and the Vector Institute for their support. A special thanks to Relu Patrascu for providing technical support throughout the years.

I am grateful to my family Laleh Kordavani, Hassan Faghri, Faraz Faghri, and Ali Faghri, for their foundational role in my growth and development.

I am grateful to various organizations for financial support. These include the Department of Computer Science and the University of Toronto, and the Ontario Graduate Scholarship (OGS). Resources used in my research were also provided, in part, by the Province of Ontario, the Government of Canada through CIFAR, and companies sponsoring the Vector Institute.¹ In addition, part of the research in this thesis was initiated during an internship with the Brain Team in Google Research.

¹ www.vectorinstitute.ai/#partners

Contents

1	Introduction	1
1.1	Publications	6
2	Background	8
2.1	Optimization for Deep Learning	8
2.1.1	Stochastic Gradient Descent	10
2.1.2	Momentum	12
2.1.3	Second Order Methods	12
2.1.4	Adaptive Gradient Methods	13
2.1.5	Initialization	14
2.1.6	Generalization	15
2.1.7	Implicit Bias of Optimization Methods	16
2.2	Contrastive Learning	17
3	VSE++: Improving Visual-Semantic Embeddings with Hard Negative Mining	20
3.1	Introduction	21
3.2	Learning Visual-Semantic Embeddings	23
3.2.1	Visual-Semantic Embedding	23
3.2.2	Emphasis on Hard Negatives	25
3.2.3	Probability of Sampling the Hardest Negative	27
3.3	Experiments	27

3.3.1	Datasets	29
3.3.2	Details of Training	29
3.3.3	Results on MS-COCO	29
3.3.4	Results on Flickr30K	31
3.3.5	Improving Order Embeddings	32
3.3.6	Behavior of Loss Functions	33
3.3.7	Examples of Hard Negatives	33
3.3.8	Distribution of distances	34
3.3.9	Effect of Negative Set Size on <i>MH</i> Loss	34
3.4	Conclusion	35
4	Gradient Clustering and A Study of Gradient Variance in Deep Learning	39
4.1	Introduction	40
4.2	Related Work	43
4.3	Mini-batch Gradient with Stratified Sampling	45
4.3.1	Weighted Gradient Clustering	46
4.3.2	Efficient Gradient Clustering (GC)	47
4.4	Experiments	49
4.4.1	MNIST: Low Variance, CIFAR-10: Noisy Estimates, ImageNet: No Structure	51
4.4.2	Random Features Models: How Does Overparametrization Affect the Variance?	54
4.4.3	Duplicates: Back to the Motivation for Gradient Clustering	56
4.5	Conclusion	57
5	Bridging the Gap Between Adversarial Robustness and Optimization Bias	59
5.1	Introduction	60
5.2	No Trade-offs with Maximally Robust Classifiers	62
5.2.1	Maximally Robust Classifier	64

5.2.2	Linear Models: Maximally Robust is the Minimum Norm Classifier	65
5.3	Implicit Robustness of Optimizers	66
5.3.1	Steepest Descent on Fully-Connected Networks	67
5.3.2	Gradient Descent on Linear Convolutional Networks	68
5.3.3	Fourier Attacks	70
5.4	Explicit Regularization	71
5.5	Experiments	73
5.5.1	Maximally Robust to ℓ_∞ , ℓ_2 , ℓ_1 , and Fourier- ℓ_∞ Bounded Attacks	74
5.5.2	Plotting the Trade-offs	75
5.5.3	CIFAR-10 Fourier- ℓ_∞ Robustness	76
5.6	Related work	77
5.6.1	Investigating the Gap in the Convergence of Linear Convolutional Networks	81
5.7	Conclusion	82
6	Conclusion and Future Work	84
A	Appendices to the Chapter on Gradient Clustering	87
A.1	Additional Details of Gradient Clustering	87
A.1.1	Proof of Proposition 4.3.1	87
A.2	Additional Details of Efficient GC	88
A.2.1	Convolutional Layers	88
A.2.2	Complexity Analysis	89
A.3	Additional Details for Experiments	90
A.3.1	Experimental Details for Image Classification Models	90
A.3.2	Experimental Details for Random Features Models	92
A.4	Normalized Variance and Convergence Analysis	92

B	Appendices to the Chapter on Bridging the Gap Chapter	94
B.1	Generalization of the Maximally Robust Classifier	94
B.2	Proofs	95
B.2.1	Proof of Lemma 5.2.1	95
B.2.2	Proof of Maximally Robust to Perturbations Bounded in Fourier Domain (Corollary 2)	96
B.3	Linear Operations in Discrete Fourier Domain	97
B.3.1	ℓ_∞ Complex Projection	97
B.3.2	Steepest Ascent Direction w.r.t. Fourier- ℓ_∞	98
B.4	Non-linear Maximally Robust Classifiers	99
B.5	Extended Experiments	101
B.5.1	Details of Linear Classification Experiments	101
B.5.2	Details of CIFAR-10 experiments	102
B.5.3	Margin Figures	103
B.5.4	Visualization of Fourier Adversarial Attacks	104
B.6	Visualization of Norm-balls	105
	Bibliography	113

Chapter 1

Introduction

Deep Learning has revolutionized machine learning and artificial intelligence, achieving superhuman performance in several standard benchmarks, including image classification [78], the game of Go [185], and natural language translation [157]. Deep neural networks have become major components of emerging technologies such as autonomous driving [71], robotics [193], and drug discovery [28].

It is also well-known that deep learning models are inefficient to train [192]; they learn by processing millions of training data multiple times [78, 185, 157]. They require powerful computational resources to process large batches of data in parallel at the same time rather than sequentially [159, 163, 21]. Vast amounts of image and text data gathered in the past few decades, and technological advancements in processing hardware, allowed breakthroughs in deep learning applications [40, 16, 118]. However, this recipe is challenging to scale. For example, significant advances in language modelling require vast amounts of data and have yet to achieve superhuman performance on some datasets [21].

Deep learning models also have unexpected failure modes; they can be fooled into misbehaviour, producing incorrect predictions [196, 67]. Adversarial perturbations are small modifications to the input that change the output of a model. Adversarial perturbations against deep learning image models can be designed to be sufficiently subtle that they become imperceptible to humans. Adversarial samples are particularly troubling in applications with

significant security and privacy requirements [107, 101]. Moreover, adversarial samples are not only security flaws but an intriguing example of our limitation in understanding deep learning models [59]. The lack of explanation for adversarial samples limits our trust and confidence in the decisions and predictions of machine learning models. Understanding and mitigating the impact of adversarial samples provides ways to improve robustness and efficiency of models [174].

This thesis comprises three parts, each of which explores aspects of efficiency and robustness in deep learning from different perspectives.

The first problem concerns training efficiency in computer vision. We hypothesize that training data are not equally important; the available training signal from some inputs is stronger than others. Moreover, we hypothesize that prioritizing learning on more informative training data increases convergence speed and improves generalization performance on test data. In **Chapter 3** (originally published in [50]) we illustrate how a simple trick referred to as hard negative mining speeds up training and improves test performance. Although previously used in ad-hoc ways, we formalize hard negative mining as a modification to the learning objective function. We demonstrate these improvements in learning joint embeddings that is a standard benchmark for representation learning.

Joint embeddings enable a wide range of tasks in image, video and language understanding. Examples include shape-image embeddings [115] for shape inference, bilingual word embeddings [238], human pose-image embeddings for 3D pose inference [113], fine-grained recognition [166], zero-shot learning [56], and modality conversion via synthesis [165, 166]. Such embeddings entail mappings from two (or more) domains into a common vector space in which semantically associated inputs (e.g., text and images) are mapped to similar locations. The embedding space thus represents the underlying domain structure, where location and often direction are semantically meaningful.

Visual-semantic embeddings have been central to image-caption retrieval and generation [103, 98], visual question-answering [128], and more recently in large-scale multi-modal representation learning such as CLIP [159]. One approach to visual question-answering,

for example, is to first describe an image by a set of captions, and then to find the nearest caption in response to a question [1, 237]. For image synthesis from text, one could map from text to the joint embedding space, and then back to image space [165, 166].

It is common to use a contrastive loss function to learn representations with a meaningful distance metric that resembles a conceptual contrast in the input space [76]. For example, we would use a contrastive loss to learn representations of images such that the representation of a dog is closer to other dogs relative to any cat. In particular, triplet ranking losses consist of terms that contrast a positive similar pair with a dissimilar negative sample. A non-zero loss is incurred if the representations of the similar pair are farther from each other than they are individually from the negative sample. A triplet loss requires a ground-truth collection of matching pairs but the negative sample often requires no annotation as it can be any non-matching input from the database. Triplet losses are defined given a distance metric (or more generally a similarity score) and differ in how the loss scales with the magnitude of the distance violation.

Our main contribution is to incorporate hard negatives in the loss function with no computational overhead. A hard negative for any positive pair is defined as the training sample incurring the maximum triplet loss. Finding the hardest negative is computationally expensive. Instead, we use semi-hard negatives that are the hardest contrastive triplets in each mini-batch. This simple change has no additional computational cost while significantly improving the training performance.

Various works have extended our work and applied semi-hard negative mining in visual-semantic embeddings and related applications. Examples are visual-semantic embedding with generalized pooling operator [29], Consensus-aware visual-semantic embedding [213], and top ranking methods in video retrieval competition tasks [8] for ad-hoc video search and video-to-text description generation. These examples illustrate the effectiveness of our simple modification to the loss function in computer vision applications.

The second problem addressed in this thesis is training efficiency as a general challenge in training deep neural networks. Instead of focusing on a task-specific loss function, we

seek improvements to optimization speed in gradient-based optimization methods for deep learning. We revisit our hypothesis from the first problem that training data are not all equally important. We hypothesize that training deep learning models on diverse and heterogeneous data distributions should be slower than homogeneous data distributions with less diversity. In [Chapter 4](#) and the publication [48], we develop a method for detecting the diversity of training signal and propose it as a method for improving training speed. Our method can generally be used with any gradient-based optimization method. In contrast to [Chapter 3](#), very few general-purpose ideas exist that consistently increase training efficiency.

We motivate our hypothesis with a simple example for which there exist duplicate data points. To decrease the processing time per iteration, it is common to uniformly sample mini-batches of data during training. As illustrated in the following example, uniform sampling is not always ideal. Suppose there are duplicate data points in a training set. We can save computation time by removing all but one of the duplicates. To get the same gradient update, in expectation, it is sufficient to rescale the gradient of the remaining samples in proportion to the number of duplicates. In this example, standard optimization methods for deep learning will be inefficient because with uniform sampling there is a chance of sampling mini-batches containing duplicates of one data type.

In general, redundancy can be extended from exact duplicates to points that are very similar to each other according to a similarity metric. In [Chapter 4](#), we focus on the similarity in the gradient space and establish the connection between gradient redundancy and training speed through a connection to gradient variance reduction. Prior works have theoretically established that smaller gradient variance results in faster training. Through an illustrative example, we show that a redundancy-aware modification to the sampling of training data reduces the gradient variance. We prove that the gradient variance is minimized if the elements are sampled from a weighted clustering in gradient space. Accordingly, we propose a gradient clustering method as a computationally efficient method for clustering in the gradient space.

Although outside the scope of this thesis, we also note that we have used our observations

about the gradient distribution during training in designing gradient quantization methods to speed up data-parallel optimization for deep learning [49, 164].

The third and last problem studied in this thesis concerns adversarial robustness in deep learning. We hypothesize that deep learning models are not inherently weak; their robustness depends on the implicit and explicit training mechanisms. In [Chapter 5](#), we show that these mechanisms imply maximal robustness to the types of perturbations not commonly considered in adversarial attacks. This observation allows us to find alternative approaches to adversarial robustness that introduce no additional training overhead compared to standard robustness methods. Hence, increasing training efficiency in the task of adversarial robustness. Next, we introduce adversarial robustness and standard robustness methods in more detail.

Deep neural networks achieve high accuracy on standard test sets. Nevertheless, [196] showed that any natural input correctly classified by a neural network can be modified with adversarial perturbations that fool the network into misclassification. They observed that adversarial perturbations exist even when they are constrained to be small enough that they do not significantly affect human perception. Adversarially perturbed inputs are also commonly referred to as Adversarial samples or adversarial examples.

Adversarial training [67] was proposed to improve the robustness of models through training on adversarial samples and further generalized as a saddle-point optimization problem [126]. In practice, adversarial training refers to methods that solve the saddle-point problem approximately by minimizing the loss on adversarial samples.

The state-of-the-art approach to increase adversarial robustness is adversarial training, i.e., empirical risk minimization on adversarial samples. Adversarial training is another example of inefficient training; i.e., in addition to training on large datasets, for robustness, we need to create and train on artificial adversarial samples to improve models. Adversarial training also exhibits a trade-off between standard generalization and adversarial robustness. That is, it achieves improved *robust accuracy*, on adversarially perturbed data, at the expense of *standard accuracy*, the probability of correct predictions on natural data [204].

In [Chapter 5](#), we discuss an alternative formulation to adversarial robustness, namely, maximally robust classification, with no robustness trade-off. By connecting this problem to the literature on the implicit bias of optimization methods[72], we also find maximally robust classifiers at no additional computational cost. This link allows for the bidirectional transfer of results between the two literatures on adversarial robustness and optimization bias.

Finally, we conclude in [Chapter 6](#) with a summary of the main results, and a discussion of future directions.

1.1 Publications

The contents of this thesis have largely been taken from the following publications and technical reports:

- **Faghri, Fartash** and Fleet, David J. and Kiros, Jamie R. and Fidler, Sanja, “*VSE++: Improving Visual-Semantic Embeddings with Hard Negatives*”, British Machine Vision Conference (BMVC), 2018. ([Chapter 3](#))
- **Faghri, Fartash** and Duvenaud, David and Fleet, David J. and Ba, Jimmy, “*A Study of Gradient Variance in Deep Learning*”, arXiv, 2020. ([Chapter 4](#))
- **Faghri, Fartash** and Duvenaud, David and Fleet, David J. and Ba, Jimmy, “*Gluster: Variance Reduced Mini-Batch SGD with Gradient Clustering*”, Conference on Neural Information Processing Systems (NeurIPS), Workshop on Beyond First Order Methods in ML, 2019. ([Chapter 4](#))
- **Faghri, Fartash** and Gowal, Sven, Vasconcelos, Cristina and Fleet, David J. and Pedregosa, Fabian and Le Roux, Nicolas, “*Bridging the Gap Between Adversarial Robustness and Optimization Bias*”, Workshop on Security and Safety in Machine Learning Systems, International Conference on Learning Representations (ICLR), 2021. ([Chapter 5](#))

During my PhD studies, beyond the research in this thesis, I have authored and contributed to the following papers. We do not discuss the details of the following papers in this thesis.

- **Faghri, Fartash**¹, Tabrizian, Iman* and Markov, Ilia and Alistarh, Dan and Roy, Dan M. and Ramezani-Kebrya, Ali, “*Adaptive Gradient Quantization for Data-Parallel SGD*”, Conference on Neural Information Processing Systems (NeurIPS), 2020.
- Ramezani-Kebrya, Ali and **Faghri, Fartash** and Markov, Ilya and Aksenov, Vitalii and Alistarh, Dan and Roy, Dan M. et al., “*NUQSGD: Provably Communication-efficient Data-parallel SGD via Nonuniform Quantization*”, Journal of Machine Learning Research 22.114 (2021): 1-43..
- Ma, Avery and **Faghri, Fartash** and Papernot, Nicolas and Farahmand, Amir-massoud, “*SOAR: Second-Order Adversarial Regularization*”, ArXiv, 2020.
- Zhang, Qingru and Wu, Yuhuai and **Faghri, Fartash** and Zhang, Tianzong and Ba, Jimmy, “*A Non-asymptotic comparison of SVRG and SGD: tradeoffs between compute and speed*”, ArXiv, 2020.
- Gilmer, Justin and Metz, Luke and **Faghri, Fartash** and Schoenholz, Samuel S. and Raghu, Maithra and Wattenberg, Martin and Goodfellow, Ian, “*Adversarial Spheres*”, ICLR Workshop, 2018.
- Sabour, Sara and Cao, Yanshuai and **Faghri, Fartash** and Fleet David J. “*Adversarial Manipulation of Deep Representations*”, International Conference on Learning Representations (ICLR), 2016.

¹ * joint first co-authors

Chapter 2

Background

In this section, we will cover the general background for the thesis and review common standard practices for optimization in deep learning. Further related work that is specific to individual chapters is developed in subsequent chapters. We refer the reader to [65] for a general introduction to deep learning.

2.1 Optimization for Deep Learning

Minimizing an objective is at the core of deep learning. In this section, we focus on methods and ideas for solving or simplifying optimization problems in deep learning.

Many machine learning tasks entail the minimization of the risk, $\mathbb{E}_{(\mathbf{x}, y) \sim D}[\ell(\mathbf{x}, y; \boldsymbol{\theta})]$, where the input \mathbf{x}, y are random variables distributed according to the data distribution D , and ℓ is the per-example loss function parametrized by $\boldsymbol{\theta}$, the parameters of the neural network. In supervised learning, y denotes the ground-truth label. Empirical risk approximates the population risk by the risk of i.i.d. samples $\{(\mathbf{x}_i, y_i)\}_{i=1}^N$, the training set, as $L(\boldsymbol{\theta}) = \sum_{i=1}^N \ell(\mathbf{x}_i, y_i; \boldsymbol{\theta})/N$. For differentiable loss functions, the gradient of ℓ is defined as $\frac{\partial}{\partial \boldsymbol{\theta}} \ell(\mathbf{x}_i, y_i; \boldsymbol{\theta})$, i.e., the gradient of the loss with respect to the parameters evaluated at a point \mathbf{x}_i [207].

Optimization algorithms used for deep learning are predominantly iterative [17]. An

iterative optimizer starts with an initial estimate of the parameters and improves the estimate iteratively [150]. Each iteration is often broken into two parts, i.e., choosing a direction and choosing the step size to move along this direction.

Optimization methods are mainly evaluated based on their rate of convergence to a local or global minimum of the loss function. Such evaluation is either by theoretically proving convergence rates on specific families of functions (e.g., convex functions) [17] or empirically, by training a model on benchmark datasets (e.g., a convolutional network on the MNIST dataset [111]). The rate of convergence is either measured by the number of iterations or the total wall-clock time in non-distributed settings. [33] suggests guidelines for empirical evaluation of optimization methods in deep learning.

Generalization, the ability to perform well on unseen data, is one of the key elements of machine learning [15]. Empirically, generalization is measured by evaluating a trained model on a held out test set. It is known that the choice of optimizer affects generalization performance [72, 209, 4]).

The scope of this section is restricted to optimization methods popular in deep learning. We focus on continuous parameters and assume that the gradient of the loss is defined and exists almost everywhere. Optimizing neural networks is often an unconstrained problem but regularization methods are commonly used. The functions minimized in deep learning are often non-convex with multiple local minima. Nevertheless, we focus on local optimization methods as they are more popular. Bayesian learning [147] and evolution strategies [172] are examples of non-local methods not covered in this chapter.

Within the optimization framework, **Chapter 3** can be described as a modification to an optimization problem to better match the task's objective, **Chapter 4** is an improvement to solving common optimization problems in deep learning, and **Chapter 5** characterizes the implicit bias of optimization on adversarial metrics.

2.1.1 Stochastic Gradient Descent

Gradient Descent (GD) or Steepest Descent [150], is an iterative optimization method that assumes access to the first-order derivative of the objective or loss function, e.g., $\ell(\mathbf{x}, y; \boldsymbol{\theta})$ defined above. We use GD to optimize a neural network by evaluating the gradient over the full training set. The update rule for GD is

$$\boldsymbol{\theta}^t = \boldsymbol{\theta}^{t-1} - \alpha_t \sum_{i \in S} \frac{\partial}{\partial \boldsymbol{\theta}} \ell(\mathbf{x}_i, y_i; \boldsymbol{\theta}) \Big|_{\boldsymbol{\theta}=\boldsymbol{\theta}^{t-1}}, \quad (2.1)$$

where ℓ is the loss function parameterized at the t -th iteration of optimization by $\boldsymbol{\theta}^t$ on the training data \mathbf{x}_i . α_t is the optimization step size, or learning rate, at iteration t .

GD requires the computation of gradients on the entire training set in each step while the alternative, Stochastic Gradient Descent (SGD), uses the gradient of a uniformly sampled data point from the training set. The gradient from a single sample is an unbiased estimate of the average gradient on the training set such that they are equivalent in expectation. Nevertheless, there exists a trade-off between the performance of GD versus SGD (discussed in Chapter 4). In mini-batch Stochastic Gradient Descent (mini-batch SGD) we can control the trade-off between GD and SGD by instead sampling B training samples, which comprise a mini-batch in each step. The mini-batch size is a hyper-parameter that provides flexibility in trading per-step computation time for potentially fewer total steps. The update rule for mini-batch SGD is

$$\boldsymbol{\theta}^t = \boldsymbol{\theta}^{t-1} - \alpha_t \sum_{i \in B_t} \frac{\partial}{\partial \boldsymbol{\theta}} \ell(\mathbf{x}_i, y_i; \boldsymbol{\theta}) \Big|_{\boldsymbol{\theta}=\boldsymbol{\theta}^{t-1}}, \quad (2.2)$$

where B_t is the mini-batch of training samples at iteration t . In GD the mini-batch is the entire training set while in SGD it is a single sample.

GD and SGD are guaranteed to converge under specific assumptions [17, 167]. Theoretically the convergence rates for GD/SGD are known under certain conditions [141]. The effect of the mini-batch size in deep learning has been studied extensively [181, 229].

To use GD/SGD to train deep neural networks, we usually need to compute the gradient of the loss function with respect to the network parameters. Back-Propagation [170] is one way of numerically computing these gradients. In feed-forward networks, layers are composed such that the inputs of a layer are the outputs of lower layers or the inputs of the model. Back-propagation (back-prop) is the application of the chain rule to this decomposition.

Although GD/SGD are popular optimizers in deep learning, they have known limitations. In [195], two problems are identified, namely, the elongated ravine problem and the unlearning problem. An elongated ravine refers to a special shape of the loss function in the space of the model parameters. There are two directions in an elongated ravine, the principal direction of the ravine and the perpendicular steep direction of the ravine's wall. The optimization step size has to be small enough to prevent divergence in the steepest direction while the loss decreases along the principal direction. The convergence rate is determined by the ratio of the two slopes.

The unlearning problem, more recently known as catastrophic forgetting, is when the optimizer ruins well-optimized parameters to learn new concepts, even though the model has underemployed parameters. Catastrophic forgetting is a challenge for training models in the setting of continual learning [120]. In continual learning, there exist multiple tasks and we only get the training data of a task after we are done with learning with previous tasks. A model should perform well on all tasks seen so far. In this setting, current optimizers quickly lose the performance on previous tasks, when they are trained only with the data of a new task.

2.1.2 Momentum

The most commonly used variant of SGD in deep learning incorporates Polyak’s momentum [156] (also known as the heavy ball momentum)

$$\mathbf{v}^t = \beta \mathbf{v}^{t-1} + \sum_{i \in B_t} \frac{\partial}{\partial \boldsymbol{\theta}} \ell(\mathbf{x}_i, y_i; \boldsymbol{\theta}) \Big|_{\boldsymbol{\theta} = \boldsymbol{\theta}^{t-1}} \quad (2.3)$$

$$\boldsymbol{\theta}^t = \boldsymbol{\theta}^{t-1} - \alpha_t \mathbf{v}^t, \quad (2.4)$$

where $\beta \in [0, 1)$ is the momentum coefficient and \mathbf{v} is a velocity vector. Empirically, SGD with momentum is often significantly faster than SGD [181]. Polyak’s momentum has the same convergence rate as GD with an improved constant. [149] proposed an acceleration method with an improved convergence rate on convex and continuously differentiable functions with a Lipschitz continuous gradient [17]. This method was later revitalized as Nesterov’s momentum by [194] in a similar form to Polyak’s momentum, where the gradient estimate for the current step is computed not at the current parameter value, but at the anticipated next value. In practice as well as certain convex settings, momentum increases flexibility in the choice of the step size and mini-batch size [62, 229].

Polyak’s momentum can also be interpreted as a gradient noise reduction method that connects it to the ideas discussed in [Chapter 4](#).

2.1.3 Second Order Methods

Second-order methods address the elongated ravine problem by incorporating the curvature information into the optimization. The Hessian, $H(\boldsymbol{\theta}) = \frac{\partial^2}{\partial \boldsymbol{\theta}^2} \ell(\mathbf{x}_i, y_i; \boldsymbol{\theta})$, represents the information about the curvature. The generalization of Newton’s method is to replace \mathbf{g} in the GD update step ([Eq. \(2.1\)](#)) with $H^{-1} \mathbf{g}$ where $\mathbf{g} = \frac{\partial}{\partial \boldsymbol{\theta}} \ell(\mathbf{x}_i, y_i; \boldsymbol{\theta})$. Given the Hessian, Newton’s method normalizes the gradients along the direction of the walls to prevent overshooting and allows consistent improvements in all directions.

Computing the inverse of the Hessian is computationally demanding when the parameter

space is high dimensional. As such, approximations have been suggested. A diagonal approximation is suggested in [11]. Hessian-Free optimization [130] is a second-order method that neither computes the Hessian, nor any approximation to it. Instead, Conjugate Gradient iterations are used to choose the next optimization direction.

Natural gradient descent, e.g., K-FAC [132], methods can also be viewed as second-order methods [3]. Natural gradient [3] is defined as $F^{-1}\mathbf{g}$, where

$$F(\boldsymbol{\theta}) = \mathbb{E}_{\mathbf{x} \sim p(\mathbf{x})} \mathbb{E}_{\mathbf{y} \sim p(\mathbf{y}|\mathbf{x}, \boldsymbol{\theta})} \left[\frac{\partial \log p(\mathbf{y}|\mathbf{x}, \boldsymbol{\theta})}{\partial \boldsymbol{\theta}} \frac{\partial \log p(\mathbf{y}|\mathbf{x}, \boldsymbol{\theta})}{\partial \boldsymbol{\theta}}^T \right], \quad (2.5)$$

is the Fisher information matrix where \mathbf{x} is sampled from the underlying data distribution and \mathbf{y} is sampled from the distribution of model predictions (See [106] for common errors in the definition). The Fisher information matrix captures the uncertainty due to sampling of the training set and the sampling of mini-batches. Under certain conditions, the Fisher information matrix is equivalent to a positive semi-definite approximation to the Hessian [134].

Second order methods are still not widely used in deep learning, often because of implementation challenges. Recent work have demonstrated wall-clock time improvements with scalable implementations [5]. Besides, second order methods and more generally preconditioned optimization exhibit alternative generalization properties [4]. Our results in Chapter 5 can be extended to preconditioned optimization methods to imply alternative robustness guarantees.

2.1.4 Adaptive Gradient Methods

In settings where gradients have known characteristics such as sparsity, specialized methods are preferred over SGD with momentum. ADAGRAD [45] proposes an update direction that works well when gradients are sparse. In this method, each gradient dimension is divided by $\sqrt{\sum_{i=1}^T g_{i,d}^2}$, where $g_{i,d}$ is the d th gradient dimension at the i th training iteration. RMSprop [201] has a similar update rule that uses an exponentially-weighted average of

the gradients over time instead of equally-weighted averaging gradients of all iterations. Adam [102] is a popular adaptive gradient method that combines Polyak’s momentum with RMSprop’s adaptive gradient. The update rule for Adam divides the velocity vector from Polyak’s momentum by the second moment of the gradients.

ADAGRAD, RMSprop, and Adam propose dividing the gradient vector by a function of its second moment per dimension. Under certain conditions, these methods can be interpreted as approximate second-order methods that use diagonal approximations to the Hessian or the Fisher information matrix [17].

Numerous optimization methods have been proposed for deep learning, yet Adam and SGD with Nesterov momentum still match or exceed the performance of the most recent ones with proper hyper-parameter tuning [144, 178]. We use Adam in Chapter 3 as the optimization method. Our method in Chapter 4 can be interpreted as an adaptive gradient method with per-example reweighing. Adaptive gradient methods have unique generalization properties with robustness implications covered in Chapter 5.

2.1.5 Initialization

For non-convex functions, poor initialization can cause slow convergence or convergence to a local minimum significantly worse than the global minimum. Practical initializations in deep learning are often based on analysis of the distribution of activations and gradients. For example, the initialization should be such that neither gradients nor activations vanish or explode during back-propagation [82, 78].

Common initializations in deep learning are often based on sampling from zero-mean uniform or Gaussian distributions [61, 79]. The variance of the distribution is determined by the type of activation function and usually depends on the number of inputs and outputs of a unit. Orthogonal initialization has also been explored for deep linear and non-linear networks [175, 155].

Initialization for deep non-linear models affects the entire training trajectory and results in varying properties of a converged model [140]. We expect similar results to Chapter 5

would show the choice of initialization implicitly affects the robustness.

2.1.6 Generalization

In Machine Learning, we seek accurate models that generalize to unseen data that is estimated empirically on held out test data. For performance on test data to be an accurate estimate of generalization, test data should not be reused. Model selection and hyper-parameter tuning require an estimate of the test performance that is often estimated on a validation set that is held out from the training set. A generalization gap between training and test performance can be due to model misspecification, data limitations, or loss function shortcomings [15]. The optimizer can also affect the generalization gap if the choice of the model and loss function form an underspecified optimization problem [72].

Modifications to a model, data, or loss function that improve the generalization gap can be problem/domain specific. For example, we often seek to learn computer vision models invariant or equivariant to affine image transformations. Using convolutional layers instead of fully-connected layers, we achieve translation invariance/equivariance at no additional computational cost but with reduced model flexibility. A more flexible but computationally expensive approach is data augmentation that trains on transformations of the training data. Alternatively, the loss function can be changed to penalize disagreements between the model outputs on transformations of a single input, providing both flexibility and potentially lower computational cost. In Chapter 3, we propose a similar loss function alternative that results in both faster training and better generalization.

The optimization problems in deep learning are often underspecified, i.e., the model is complex enough to fit the training data accurately in more than one way. As such, there are generic modifications to the model, loss function, and optimization that restrict the model complexity. Dropout [191] applied to a layer deactivates units randomly and forces the model to learn a compact representation but with some redundancy. Regularization penalizes the model by adding additional penalty terms to the loss function. Norm penalties such as ℓ_0 , ℓ_1 , and ℓ_2 encourage sparsity or parameter shrinkage and can be interpreted as assuming a

prior distribution over parameters [142]. Early stopping addresses overfitting by selecting the best performing model during training according to the validation performance. A model is overfitting to the training data if the test performance worsens while the training performance improves.

A trade-off exists between model complexity and generalization that can be characterized by a bias-variance decomposition of the risk in some problems [15]. The relation between complexity and generalization can be a double-descent curve where the generalization performance of a family of models is worst at a critical model size while improves monotonically for more or less complex models [77].

In [Chapter 5](#), we discuss how common modifications for improving generalization such as model architecture, regularization, and optimization method indirectly affect model robustness.

2.1.7 Implicit Bias of Optimization Methods

Minimizing the empirical risk for an overparametrized model with more parameters than the training data has multiple solutions. [228] observed that overparametrized deep models can even fit to randomly labeled training data, yet given the correct labels they consistently generalize to test data. This behavior has been explained using the implicit bias of optimization methods towards particular solutions. [72] proved that minimizing the empirical risk using steepest descent and mirror descent have an implicit bias towards minimum norm solutions in overparametrized linear classification. Characterizing the implicit bias in linear regression proved to be more challenging and dependent on the initialization. [92] proved that training a deep linear classifier using gradient descent not only implicitly converges to the minimum norm classifier in the space of the product of parameters, each layer is also biased towards rank-1 matrices aligned with adjacent layers. [73] proved the implicit bias of gradient descent in training linear convolutional classifiers is towards minimum norm solutions in the Fourier domain that depends on the number of layers. [91] has established the directional alignment in the training of deep linear networks using gradient flow (gradient descent with

infinitesimal step size) as well as the implicit bias of training deep 2-homogeneous networks. In the case of gradient flow the implicit bias of training multi-layer linear models is towards rank-1 layers that satisfy directional alignment with adjacent layers [91, Proposition 4.4]. Recently, [226] has proposed a unified framework for implicit bias of neural networks using tensor formulation that includes fully-connected, diagonal, and convolutional networks and weakened the convergence assumptions.

The recent theory of generalization in deep learning, in particular the double descent phenomenon, studies the generalization properties of minimum norm solutions for finite and noisy training sets [77]. Characterization of the double descent phenomenon relies on the implicit bias of optimization methods while using additional assumptions about the data distribution. In contrast, our results in Chapter 5 only rely on the implicit bias of optimization and hence are independent of the data distribution.

2.2 Contrastive Learning

Contrastive losses [76] have been used widely in computer vision and machine learning. Triplet losses are widely used in retrieval problems where the task is to learn a mapping such that similar inputs are mapped close to each other and farther from dissimilar inputs [216]. Examples are image retrieval [57, 26], learning to rank problems [112], and max-margin structured prediction [25, 108]. Let $f(\mathbf{x}; \boldsymbol{\theta})$ denote a mapping of input $\mathbf{x} \in X$ parametrized by $\boldsymbol{\theta}$. A triplet loss function $\ell(\mathbf{q}, \mathbf{k}_+, \mathbf{k}_-)$ takes a query input, $\mathbf{q} \in X$, together with a similar and dissimilar key inputs, $\mathbf{k}_+, \mathbf{k}_- \in X$. The loss function encourages the mappings of the query and the similar key to be close to each other while discouraging proximity to the dissimilar key. A hinge triplet loss is commonly used in image retrieval where the similarity is measured by cosine similarity and the model is penalized if the proximity between the negative pair is not more than the positive pair by a preset margin [103, 98, 235, 189]. The pairwise hinge loss is an alternative in which elements of positive pairs are encouraged to lie within a hypersphere of radius ρ_1 , while negative pairs should be no closer than $\rho_2 > \rho_1$. A

pairwise loss restricts the mapping more than a triplet loss and requires two hyper-parameters rather than one. In [Chapter 3](#), we propose a modification to the hinge triplet loss function. Focal loss is a similar recent work that modifies the cross-entropy loss to handle imbalance in classes and training data when there are many easy samples but few hard samples such as when there are few foreground samples but numerous background samples [\[117\]](#).

Recently, contrastive losses have been successfully employed for unsupervised representation learning in methods such as MoCo [\[80, 31\]](#) and SimCLR [\[30\]](#). In contrast to ranking and retrieval applications, new applications of contrastive losses are in unsupervised representation learning where the positive pair is usually the input itself with some perturbation. As an alternative to hinge losses and others [\[80\]](#), the InfoNCE [\[152\]](#) loss and its variants are based on the cross-entropy loss,

$$\ell(\mathbf{q}, \mathbf{k}_+, \mathbf{K}_-) = -\log \frac{\exp(\mathbf{q} \cdot \mathbf{k}_+ / \tau)}{\exp(\mathbf{q} \cdot \mathbf{k}_+ / \tau) + \sum_{\mathbf{k}_- \in \mathbf{K}_-} \exp(\mathbf{q} \cdot \mathbf{k}_- / \tau)} \quad (2.6)$$

where \mathbf{q} is a query input, \mathbf{k}_+ a similar key and \mathbf{K}_- a dissimilar set of keys to the query. τ is the temperature hyper-parameter that controls the expected separation between similar and dissimilar samples.

An interpretation of $\ell(\mathbf{q}, \mathbf{k}_+, \mathbf{K}_-)$ is as the cross-entropy loss where the set of positive and negative keys are the categories and $\exp(\mathbf{q} \cdot \mathbf{k} / \tau)$ is the unnormalized probability of the event $\mathbf{q} = \mathbf{k}$. The cross-entropy loss is commonly used with a fixed set of categories while with in [Eq. \(2.6\)](#) the set of keys is specific to each query.

The equivalence to the standard cross-entropy loss is exact if the normalizing term consists of all negative keys. Suppose we use cross-entropy but use a sampled subset of all categories in the denominator that decreases the computation cost. The drawback is some queries will influence the training more than others because of modified probabilities. A fix is to use importance sampling according to the unnormalized probabilities of the negative keys at the cost of losing the advantage of subsampling. In the literature on triplet losses such ideas are often referred to as hard negative mining where instead of using any negative,

we mine hard negatives. Our proposed method in [Chapter 3](#) is an example of hard negative mining in contrastive losses.

In recent works on contrastive losses, the query is uniformly selected from the training set and k_+ is generated by perturbing the query using common input augmentations. For images, common perturbations are random resize, random crop, random color jitter, and random flip. The novelty in works such as MoCo is to keep an adaptive queue of keys to be used as dissimilar examples. This ensures the cost of training is reduced by not back-propagating through the network for negative examples while keeping an up-to-date set of negatives with enough contrast. Another novelty in works such as SimCLR and MoCo v2 is to use more diverse and aggressive data augmentations to generate a larger set of possible similar and dissimilar pairs and hence better contrastive examples.

Chapter 3

VSE++: Improving Visual-Semantic Embeddings with Hard Negative Mining

The first problem studied in this thesis concerns training efficiency in computer vision. We hypothesize that training data are not equally important; training signal from some inputs is stronger than others. Moreover, we hypothesize that prioritizing learning on more informative training data increases convergence speed and improves generalization performance on test data.

To this end, we present a new technique for learning visual-semantic embeddings for cross-modal retrieval. Inspired by hard negative mining, the use of hard negatives in structured prediction, and ranking loss functions, we introduce a simple change to common loss functions used for multi-modal embeddings. That, combined with fine-tuning and use of augmented data, yields significant gains in retrieval performance. We showcase our approach, *VSE++*, on MS-COCO and Flickr30K datasets, using ablation studies and comparisons with existing methods. On MS-COCO our approach outperforms state-of-the-art methods by 8.8% in caption retrieval and 11.3% in image retrieval (at R@1).

The content of this chapter have appeared in the following publication:

- **Faghri, Fartash** and Fleet, David J. and Kiros, Jamie R. and Fidler, Sanja, “VSE++: Improving Visual-Semantic Embeddings with Hard Negatives”, British Machine Vision Conference (BMVC), 2018.

To ensure reproducibility, our code is publicly available ¹.

3.1 Introduction

Joint embeddings enable a wide range of tasks in image, video and language understanding. Examples include shape-image embeddings [115] for shape inference, bilingual word embeddings [238], human pose-image embeddings for 3D pose inference [113], fine-grained recognition [166], zero-shot learning [56], and modality conversion via synthesis [165, 166]. Such embeddings entail mappings from two (or more) domains into a common vector space in which semantically associated inputs (e.g., text and images) are mapped to similar locations. The embedding space thus represents the underlying domain structure, where location and often direction are semantically meaningful.

Visual-semantic embeddings have been central to image-caption retrieval and generation [103, 98], and visual question-answering [128]. One approach to visual question-answering, for example, is to first describe an image by a set of captions, and then to find the nearest caption in response to a question [1, 237]. For image synthesis from text, one could map from text to the joint embedding space, and then back to image space [165, 166].

Here we focus on visual-semantic embeddings for cross-modal retrieval; i.e., the retrieval of images given captions, or of captions for a query image. As is common in retrieval, we measure performance by $R@K$, i.e., recall at K – the fraction of queries for which the correct item is retrieved in the closest K points to the query in the embedding space (K is usually a small integer, often 1). More generally, retrieval is a natural way to assess the quality of joint embeddings for image and language data [84].

¹ <https://github.com/fartashf/vsepp>

The basic problem is one of ranking; the correct target(s) should be closer to the query than other items in the corpus, not unlike *learning to rank* problems [e.g., 112], and max-margin structured prediction [25, 108]. The formulation and model architecture in this paper are most closely related to those of [103], learned with a triplet ranking loss. In contrast to that work, we advocate a novel loss, the use of augmented data, and fine-tuning, which, together, produce a significant increase in caption retrieval performance over the baseline ranking loss on well-known benchmark data. We outperform the best reported result on MS-COCO by almost 9%. We also show that the benefit of a more powerful image encoder, with fine-tuning, is amplified with the use of our stronger loss function. We refer to our model as *VSE++*.

Our main contribution is to incorporate hard negatives in the loss function. This was inspired by the use of hard negative mining in classification tasks [38, 53, 129], and by the use of hard negatives for improving image embeddings for face recognition [179, 219]. Minimizing a loss function using hard negative mining is equivalent to minimizing a modified non-transparent loss function with uniform sampling. We extend the idea with the explicit introduction of hard negatives in the loss for multi-modal embeddings, without any additional cost of mining.

We also note that our formulation complements other recent articles that propose new architectures or similarity functions for this problem. To this end, we demonstrate improvements to [210]. Among other methods that could be improved with a modified loss, [214] propose an embedding network to fully replace the similarity function used for the ranking loss. An attention mechanism on both images and captions is used by [146], where the authors sequentially and selectively focus on a subset of words and image regions to compute the similarity. In [86], the authors use a multi-modal context-modulated attention mechanism to compute the similarity between images and captions. Our proposed loss function and triplet sampling could be extended and applied to other such problems.

3.2 Learning Visual-Semantic Embeddings

For image-caption retrieval the query is a caption and the task is to retrieve the most relevant image(s) from a database. Alternatively, the query may be an image, and the task is to retrieve relevant captions. The goal is to maximize recall at K ($R@K$), i.e., the fraction of queries for which the most relevant item is ranked among the top K items returned.

Let $S = \{(i_n, c_n)\}_{n=1}^N$ be a training set of image-caption pairs. We refer to (i_n, c_n) as *positive pairs* and $(i_n, c_{m \neq n})$ as *negative pairs*; i.e., the most relevant caption to the image i_n is c_n and for caption c_n , it is the image i_n . We define a similarity function $s(i, c) \in \mathbb{R}$ that should, ideally, give higher similarity scores to positive pairs than negatives. In caption retrieval, the query is an image and we rank a database of captions based on the similarity function; i.e., $R@K$ is the percentage of queries for which the positive caption is ranked among the top K captions using $s(i, c)$. Likewise for image retrieval. In what follows the similarity function is defined on the joint embedding space. This differs from other formulations, such as [214], which use a similarity network to directly classify an image-caption pair as matching or non-matching.

3.2.1 Visual-Semantic Embedding

Let $\phi(i; \theta_\phi) \in \mathbb{R}^{D_\phi}$ be a feature-based representation computed from image i (e.g., the representation before logits in VGG19 [187] or ResNet152 [78]). Similarly, let $\psi(c; \theta_\psi) \in \mathbb{R}^{D_\psi}$ be a representation of caption c in a caption embedding space (e.g., a GRU-based text encoder). Here, θ_ϕ and θ_ψ denote model parameters for the respective mappings to these initial image and caption representations.

Then, let the mappings into the *joint embedding space* be defined by linear projections:

$$f(i; W_f, \theta_\phi) = W_f^T \phi(i; \theta_\phi) \quad (3.1)$$

$$g(c; W_g, \theta_\psi) = W_g^T \psi(c; \theta_\psi) \quad (3.2)$$

where $W_f \in \mathbb{R}^{D_\phi \times D}$ and $W_g \in \mathbb{R}^{D_\psi \times D}$. We further normalize $f(i; W_f, \theta_\phi)$, and $g(c; W_g, \theta_\psi)$,

to lie on the unit hypersphere. Finally, we define the similarity function in the joint embedding space to be the usual inner product:

$$s(i, c) = f(i; W_f, \theta_\phi) \cdot g(c; W_g, \theta_\psi). \quad (3.3)$$

Let $\theta = \{W_f, W_g, \theta_\psi\}$ be the model parameters. If we also fine-tune the image encoder, then we would also include θ_ϕ in θ .

Training entails the minimization of empirical loss with respect to θ , i.e., the cumulative loss over training data $S = \{(i_n, c_n)\}_{n=1}^N$:

$$e(\theta, S) = \frac{1}{N} \sum_{n=1}^N \ell(i_n, c_n) \quad (3.4)$$

where $\ell(i_n, c_n)$ is a suitable loss function for a single training exemplar. Inspired by the use of a triplet loss for image retrieval [e.g., 57, 26], recent approaches to joint visual-semantic embeddings have used a hinge-based triplet ranking loss [103, 98, 235, 189]:

$$\ell_{SH}(i, c) = \sum_{\hat{c}} [\alpha - s(i, c) + s(i, \hat{c})]_+ + \sum_{\hat{i}} [\alpha - s(i, c) + s(\hat{i}, c)]_+, \quad (3.5)$$

where α serves as a margin parameter, and $[x]_+ \equiv \max(x, 0)$. This hinge loss comprises two symmetric terms. The first sum is taken over all negative captions \hat{c} , given query i . The second is taken over all negative images \hat{i} , given caption c . Each term is proportional to the expected loss (or *violation*) over sets of negative samples. If i and c are closer to one another in the joint embedding space than to any negative, by the margin α , the hinge loss is zero. In practice, for computational efficiency, rather than summing over all negatives in the training set, it is common to only sum over (or randomly sample) the negatives in a mini-batch of stochastic gradient descent [103, 189, 98]. The runtime complexity of computing this loss approximation is quadratic in the number of image-caption pairs in a mini-batch.

Of course there are other loss functions that one might consider. One is a pairwise hinge loss in which elements of positive pairs are encouraged to lie within a hypersphere

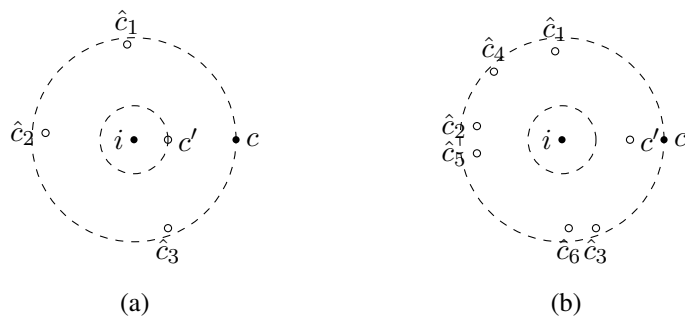


Figure 3.1: An illustration of typical positive pairs and the nearest negative samples. Here assume similarity score is the negative distance. Filled circles show a positive pair (i, c) , while empty circles are negative samples for the query i . The dashed circles on the two sides are drawn at the same radii. Notice that the hardest negative sample c' is closer to i in **a**. Assuming a zero margin, **b** has a higher loss with the *SH* loss compared to **a**. The *MH* loss assigns a higher loss to **a**.

of radius ρ_1 in the joint embedding space, while negative pairs should be no closer than $\rho_2 > \rho_1$. This is problematic as it constrains the structure of the latent space more than does the ranking loss, and it entails the use of two hyper-parameters which can be very difficult to set. Another possible approach is to use Canonical Correlation Analysis to learn W_f and W_g , thereby trying to preserve correlation between the text and images in the joint embedding [e.g., 104, 46]. By comparison, when measuring performance as $R@K$, for small K , a correlation-based loss will not give sufficient influence to the embedding of negative items in the local vicinity of positive pairs, which is critical for $R@K$.

3.2.2 Emphasis on Hard Negatives

Inspired by common loss functions used in structured prediction [205, 225, 53], we focus on hard negatives for training, i.e., the negatives closest to each training query. This is particularly relevant for retrieval since it is the hardest negative that determines success or failure as measured by $R@1$.

Given a positive pair (i, c) , the hardest negatives are given by $i' = \arg \max_{j \neq i} s(j, c)$

and $c' = \arg \max_{d \neq c} s(i, d)$. To emphasize hard negatives we define our loss as

$$\ell_{MH}(i, c) = \max_{c'} [\alpha - s(i, c) + s(i, c')]_+ + \max_{i'} [\alpha - s(i, c) + s(i', c)]_+ . \quad (3.6)$$

Like Eq. 3.5, this loss comprises two terms, one with i and one with c as queries. Unlike Eq. 3.5, this loss is specified in terms of the hardest negatives, c' and i' . We refer to the loss in Eq. 3.6 as *Max of Hinges* (MH) loss, and the loss in Eq. 3.5 as *Sum of Hinges* (SH) loss. There is a spectrum of loss functions from the SH loss to the MH loss. In the MH loss, the winner takes all the gradients, where instead we use re-weighted gradients of all the triplets. We only discuss the MH loss as it was empirically found to perform the best.

One case in which the MH loss is superior to SH is when multiple negatives with small violations combine to dominate the SH loss. For example, Fig. 3.1 depicts a positive pair together with two sets of negatives. In Fig. 3.1a, a single negative is too close to the query, which may require a significant change to the mapping. However, any training step that pushes the hard negative away, might cause a number of small violating negatives, as in Fig. 3.1b. Using the SH loss, these ‘new’ negatives may dominate the loss, so the model is pushed back to the first example in Fig. 3.1a. As a result, the optimization may oscillate between two states with no reduction in the SH loss while in a similar scenario the MH loss would decrease monotonically because it focuses on the hardest negative.

For computational efficiency, instead of finding the hardest negatives in the entire training set, we find them within each mini-batch. This has the same quadratic complexity as the complexity of the SH loss. With random sampling of the mini-batches, this approximation yields other advantages. One is that there is a high probability of getting hard negatives that are harder than at least 90% of the entire training set (see Section 3.2.3 for the explanation). Moreover, the loss is potentially robust to label errors in the training data because the probability of sampling the hardest negative over the entire training set is somewhat low.

3.2.3 Probability of Sampling the Hardest Negative

Let $S = \{(i_n, c_n)\}_{n=1}^N$ denote a training set of image-caption pairs, and let $C = \{c_n\}$ denote the set of captions. Suppose we draw M samples in a mini-batch, $Q = \{(i_m, c_m)\}_{m=1}^M$, from S . Let the permutation, π_m , on C refer to the rankings of captions according to the similarity function $s(i_m, c_n)$ for $c_n \in S \setminus \{c_m\}$. We can assume permutations, π_m , are uncorrelated.

Given a query image, i_m , we are interested in the probability of getting no captions from the 90th percentile of π_m in the mini-batch. Assuming i.i.d. samples, this probability is simply $.9^{(M-1)}$, the probability that no sample in the mini-batch is from the 90th percentile. This probability tends to zero exponentially fast, falling below 1% for $M \geq 44$. Hence, for large enough mini-batches, with high probability we sample negative captions that are harder than 90% of the entire training set. The probability for the 99.9th percentile of π_m tends to zero more slowly; it falls below 1% for $M \geq 6905$, which is a relatively large mini-batch.

While we get strong signals by randomly sampling negatives within mini-batches, such sampling also provides some robustness to outliers, such as negative captions that better describe an image compared to the ground-truth caption. Mini-batches as small as 128 can provide strong enough training signal and robustness to label errors. Of course by increasing the mini-batch size, we get harder negative examples and possibly a stronger training signal. However, by increasing the mini-batch size, we lose the benefit of SGD in finding good optima and exploiting the gradient noise. This can lead to getting stuck in local optima or as observed by [179], extremely long training time.

3.3 Experiments

Below we perform experiments with our approach, *VSE++*, comparing it to a baseline formulation with *SH* loss, denoted *VSE0*, and other state-of-the-art approaches. Essentially, the baseline formulation, *VSE0*, is similar to that in [103], denoted *UVS*.

We experiment with two image encoders: VGG19 by [187] and ResNet152 by [78]. In

#	Model	Trainset	Caption Retrieval				Image Retrieval			
			R@1	R@5	R@10	Med r	R@1	R@5	R@10	Med r
1K Test Images										
3.1.1	<i>UVS</i> ([103], GitHub)	<i>IC</i> (1 fold)	43.4	75.7	85.8	2	31.0	66.7	79.9	3
3.1.2	<i>Order</i> [210]	<i>IOC+rV</i>	46.7	-	88.9	2.0	37.9	-	85.9	2.0
3.1.3	Embedding Net [214]	<i>IOC+rV</i>	50.4	79.3	69.4	-	39.8	75.3	86.6	-
3.1.4	sm-LSTM [86]	?	53.2	83.1	91.5	1	40.7	75.8	87.4	2
3.1.5	2WayNet [46]	<i>IOC+rV</i>	55.8	75.2	-	-	39.7	63.3	-	-
3.1.6	<i>VSE++</i>	<i>IC</i> (1 fold)	43.6	74.8	84.6	2.0	33.7	68.8	81.0	3.0
3.1.7	<i>VSE++</i>	<i>RC</i>	49.0	79.8	88.4	1.8	37.1	72.2	83.8	2.0
3.1.8	<i>VSE++</i>	<i>RC+rV</i>	51.9	81.5	90.4	1.0	39.5	74.1	85.6	2.0
3.1.9	<i>VSE++ (FT)</i>	<i>RC+rV</i>	57.2	86.0	93.3	1.0	45.9	79.4	89.1	2.0
3.1.10	<i>VSE++ (ResNet)</i>	<i>RC+rV</i>	58.3	86.1	93.3	1.0	43.6	77.6	87.8	2.0
3.1.11	<i>VSE++ (ResNet, FT)</i>	<i>RC+rV</i>	64.6	90.0	95.7	1.0	52.0	84.3	92.0	1.0
5K Test Images										
3.1.12	<i>Order</i> [210]	<i>IOC+rV</i>	23.3	-	65.0	5.0	18.0	-	57.6	7.0
3.1.13	<i>VSE++ (FT)</i>	<i>RC+rV</i>	32.9	61.7	74.7	3.0	24.1	52.8	66.2	5.0
3.1.14	<i>VSE++ (ResNet, FT)</i>	<i>RC+rV</i>	41.3	71.1	81.2	2.0	30.3	59.4	72.4	4.0

Table 3.1: Results of experiments on MS-COCO.

what follows, we use VGG19 unless specified otherwise. As in previous work we extract image features directly from FC7, the penultimate fully connected layer. The dimensionality of the image embedding, D_ϕ , is 4096 for VGG19 and 2048 for ResNet152.

In more detail, we first resize the image to 256×256 , and then use either a single crop of size 224×224 or the mean of feature vectors for multiple crops of similar size. We refer to training with one center crop as *IC*, and training with 10 crops at fixed locations as *IOC*. These image features can be pre-computed once and reused. We also experiment with using a single random crop, denoted by *RC*. For *RC*, image features are computed on the fly. Recent works have mostly used *RC/IOC*. In our preliminary experiments, we did not observe significant differences between *RC/IOC*. As such, we perform most experiments with *RC*.

For the caption encoder, we use a GRU similar to the one used in [103]. We set the dimensionality of the GRU, D_ψ , and the joint embedding space, D , to 1024. The dimensionality of the word embeddings that are input to the GRU is set to 300.

We further note that in [103], the caption embedding is normalized, while the image embedding is not. Normalization of both vectors means that the similarity function is cosine similarity. In *VSE++* we normalize both vectors. Not normalizing the image embedding changes the importance of samples. In our experiments, not normalizing the image embedding helped the baseline, *VSE0*, to find a better solution. However, *VSE++* is not significantly

affected by this normalization.

3.3.1 Datasets

We evaluate our method on the Microsoft COCO dataset [118] and the Flickr30K dataset [224]. Flickr30K has a standard 30,000 images for training. Following [98], we use 1000 images for validation and 1000 images for testing. We also use the splits of [98] for MS-COCO. In this split, the training set contains 82,783 images, 5000 validation and 5000 test images. However, there are also 30,504 images that were originally in the validation set of MS-COCO but have been left out in this split. We refer to this set as rV . Some papers use rV for training (113,287 training images in total) to further improve accuracy. We report results using both training sets. Each image comes with 5 captions. The results are reported by either averaging over 5 folds of 1K test images or testing on the full 5K test images.

3.3.2 Details of Training

We use the Adam optimizer [102]. Models are trained for at most 30 epochs. Except for fine-tuned models, we start training with learning rate 0.0002 for 15 epochs, and then lower the learning rate to 0.00002 for another 15 epochs. The fine-tuned models are trained by taking a model trained for 30 epochs with a fixed image encoder, and then training it for 15 epochs with a learning rate of 0.00002. We set the margin to 0.2 for most experiments. We use a mini-batch size of 128 in all experiments. Notice that since the size of the training set for different models is different, the actual number of iterations in each epoch can vary. For evaluation on the test set, we tackle over-fitting by choosing the snapshot of the model that performs best on the validation set. The best snapshot is selected based on the sum of the recalls on the validation set.

3.3.3 Results on MS-COCO

The results on the MS-COCO dataset are presented in Table 3.1. To understand the effect of training and algorithmic variations we report ablation studies for the baseline *VSE0* (see

#	Model	Trainset	Caption Retrieval				Image Retrieval			
			R@1	R@5	R@10	Med r	R@1	R@5	R@10	Med r
3.2.1	VSE0	IC (1 fold)	43.2	73.9	85.0	2.0	33.0	67.4	80.7	3.0
3.1.6	VSE++	IC (1 fold)	43.6	74.8	84.6	2.0	33.7	68.8	81.0	3.0
3.2.2	VSE0	RC	43.1	77.0	87.1	2.0	32.5	68.3	82.1	3.0
3.1.7	VSE++	RC	49.0	79.8	88.4	1.8	37.1	72.2	83.8	2.0
3.2.3	VSE0	RC+rV	46.8	78.8	89.0	1.8	34.2	70.4	83.6	2.6
3.1.8	VSE++	RC+rV	51.9	81.5	90.4	1.0	39.5	74.1	85.6	2.0
3.2.4	VSE0 (FT)	RC+rV	50.1	81.5	90.5	1.6	39.7	75.4	87.2	2.0
3.1.9	VSE++ (FT)	RC+rV	57.2	86.0	93.3	1.0	45.9	79.4	89.1	2.0
3.2.5	VSE0 (ResNet)	RC+rV	52.7	83.0	91.8	1.0	36.0	72.6	85.5	2.2
3.1.10	VSE++ (ResNet)	RC+rV	58.3	86.1	93.3	1.0	43.6	77.6	87.8	2.0
3.2.6	VSE0 (ResNet, FT)	RC+rV	56.0	85.8	93.5	1.0	43.7	79.4	89.7	2.0
3.1.11	VSE++ (ResNet, FT)	RC+rV	64.6	90.0	95.7	1.0	52.0	84.3	92.0	1.0

Table 3.2: The effect of data augmentation and fine-tuning. We copy the relevant results for VSE++ from Table 3.1 to enable an easier comparison. Notice that after applying all the modifications, VSE0 model reaches 56.0% for R@1, while VSE++ achieves 64.6%.

Table 3.2). Our best result with VSE++ is achieved by using ResNet152 and fine-tuning the image encoder (row 3.1.11), where we see 21.2% improvement in R@1 for caption retrieval and 21% improvement in R@1 for image retrieval compared to UVS (rows 3.1.1 and 3.1.11).

Effect of MH loss. Using ResNet152 and fine-tuning can only lead to 12.6% improvement using the VSE0 formulation (rows 3.2.6 and 3.1.1), while our MH loss function brings a significant additional gain of 8.6% (rows 3.1.11 and 3.2.6).

Effect of the training set. We compare VSE0 and VSE++ by incrementally improving the training data. Comparing the models trained on IC (rows 3.1.1 and 3.1.6), we only see 2.7% improvement in R@1 for image retrieval but no improvement in caption retrieval performance. However, when we train using RC (rows 3.1.7 and 3.2.2) or RC+rV (rows 3.1.8 and 3.2.3), we see that VSE++ gains an improvement of 5.9% and 5.1%, respectively, in R@1 for caption retrieval compared to VSE0. This shows that VSE++ can better exploit the additional data.

Effect of a better image encoding. We also investigate the effect of a better image encoder on the models. Row 3.1.9 and row 3.2.4 show the effect of fine-tuning the VGG19 image encoder. We see that the gap between VSE0 and VSE++ increases to 6.1%. If we use ResNet152 instead of VGG19 (row 3.1.10 and row 3.2.5), the gap is 5.6%. As for our best result, if we use ResNet152 and also fine-tune the image encoder (row 3.1.11 and row 3.2.6)

#	Model	Trainset	Caption Retrieval				Image Retrieval			
			R@1	R@5	R@10	Med r	R@1	R@5	R@10	Med r
3.3.1	<i>UVS</i> [103]	<i>IC</i>	23.0	50.7	62.9	5	16.8	42.0	56.5	8
3.3.2	<i>UVS</i> (GitHub)	<i>IC</i>	29.8	58.4	70.5	4	22.0	47.9	59.3	6
3.3.3	Embedding Net [214]	<i>IOC</i>	40.7	69.7	79.2	-	29.2	59.6	71.7	-
3.3.4	DAN [146]	?	41.4	73.5	82.5	2	31.8	61.7	72.5	3
3.3.5	sm-LSTM [86]	?	42.5	71.9	81.5	2	30.2	60.4	72.3	3
3.3.6	2WayNet [46]	<i>IOC</i>	49.8	67.5	-	-	36.0	55.6	-	-
3.3.7	DAN (ResNet) [146]	?	55.0	81.8	89.0	1	39.4	69.2	79.1	2
3.3.8	<i>VSE0</i>	<i>IC</i>	29.8	59.8	71.9	3.0	23.0	48.8	61.0	6.0
3.3.9	<i>VSE0</i>	<i>RC</i>	31.6	59.3	71.7	4.0	21.6	50.7	63.8	5.0
3.3.10	<i>VSE++</i>	<i>IC</i>	31.9	58.4	68.0	4.0	23.1	49.2	60.7	6.0
3.3.11	<i>VSE++</i>	<i>RC</i>	38.6	64.6	74.6	2.0	26.8	54.9	66.8	4.0
3.3.12	<i>VSE0 (FT)</i>	<i>RC</i>	37.4	65.4	77.2	3.0	26.8	57.6	69.5	4.0
3.3.13	<i>VSE++ (FT)</i>	<i>RC</i>	41.3	69.1	77.9	2.0	31.4	60.0	71.2	3.0
3.3.14	<i>VSE0 (ResNet)</i>	<i>RC</i>	36.6	67.3	78.4	3.0	23.3	52.6	66.0	5.0
3.3.15	<i>VSE++ (ResNet)</i>	<i>RC</i>	43.7	71.9	82.1	2.0	32.3	60.9	72.1	3.0
3.3.16	<i>VSE0 (ResNet, FT)</i>	<i>RC</i>	42.1	73.2	84.0	2.0	31.8	62.6	74.1	3.0
3.3.17	<i>VSE++ (ResNet, FT)</i>	<i>RC</i>	52.9	80.5	87.2	1.0	39.6	70.1	79.5	2.0

Table 3.3: Results on the Flickr30K dataset.

the gap becomes 8.6%. The increase in the performance gap shows that the improved loss of *VSE++* can better guide the optimization when a more powerful image encoder is used.

Comparison with state-of-the-art. Comparing *VSE++ (ResNet, FT)* to the state-of-the-art on MS-COCO at the time of publication, *2WayNet* (row 3.1.11 and row 3.1.5), we see 8.8% improvement in R@1 for caption retrieval and compared to *sm-LSTM* (row 3.1.11 and row 3.1.4), 11.3% improvement in image retrieval. We also report results on the full 5K test set of MS-COCO in rows 3.1.13 and 3.1.14.

3.3.4 Results on Flickr30K

Tables 3.3 summarizes the performance on Flickr30K. We obtain 23.1% improvement in R@1 for caption retrieval and 17.6% improvement in R@1 for image retrieval (rows 3.3.1 and 3.3.17). We observed that *VSE++* over-fits when trained with the pre-computed features of *IC*. The reason is potentially the limited size of the Flickr30K training set. As explained in Sec. 3.3.2, we select a snapshot of the model before over-fitting occurs, based on performance with the validation set. Over-fitting does not occur when the model is trained using the *RC* training data. Our results show the improvements incurred by our *MH* loss persist across datasets, as well as across models.

3.3.5 Improving Order Embeddings

Given the simplicity of our approach, our proposed loss function can complement the recent approaches that use more sophisticated model architectures or similarity functions. Here we demonstrate the benefits of the *MH* loss by applying it to another approach to joint embeddings called order-embeddings [210]. The main difference with the formulation above is the use of an asymmetric similarity function, i.e., $s(i, c) = -\|\max(0, g(c; W_g, \theta_\psi) - f(i; W_f, \theta_\phi))\|^2$. Again, we simply replace their use of the *SH* loss by our *MH* loss.

Like their experimental setting, we use the training set *IOC+rV*. For our *Order++*, we use the same learning schedule and margin as our other experiments. However, we use their training settings to train *Order0*. We start training with a learning rate of 0.001 for 15 epochs and lower the learning rate to 0.0001 for another 15 epochs. Like [210] we use a margin of 0.05. Additionally, [210] takes the absolute value of embeddings before computing the similarity function which we replicate only for *Order0*.

Table 3.4 reports the results when the *SH* loss is replaced by the *MH* loss. We replicate their results using our *Order0* formulation and get slightly better results (row 3.4.1 and row 3.4.3). We observe 4.5% improvement from *Order0* to *Order++* in R@1 for caption retrieval (row 3.4.3 and row 3.4.5). Compared to the improvement from *VSE0* to *VSE++*, where the improvement on the *IOC+rV* training set is 1.8%, we gain an even higher improvement here. This shows that the *MH* loss can potentially improve numerous similar loss functions used in retrieval and ranking tasks.

#	Model	Caption Retrieval				Image Retrieval			
		R@1	R@5	R@10	Med r	R@1	R@5	R@10	Med r
1K Test Images									
3.4.1	<i>Order</i> [210]	46.7	-	88.9	2.0	37.9	-	85.9	2.0
3.4.2	<i>VSE0</i>	49.5	81.0	90.0	1.8	38.1	73.3	85.1	2.0
3.4.3	<i>Order0</i>	48.5	80.9	90.3	1.8	39.6	75.3	86.7	2.0
3.4.4	<i>VSE++</i>	51.3	82.2	91.0	1.2	40.1	75.3	86.1	2.0
3.4.5	<i>Order++</i>	53.0	83.4	91.9	1.0	42.3	77.4	88.1	2.0

Table 3.4: Comparison on MS-COCO. Training set for all the rows is *IOC+rV*.

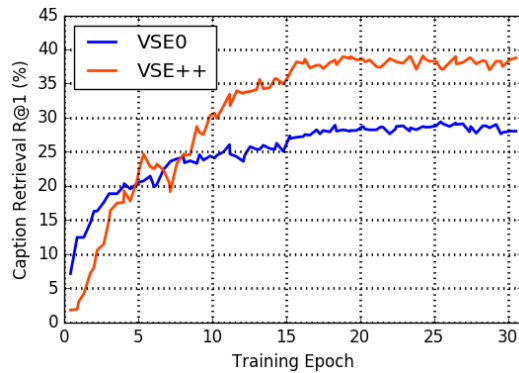


Figure 3.2: Analysis of the behavior of the MH loss on the Flickr30K dataset training with RC . This figure compares the SH loss to the MH loss (Table 3.3, row 3.3.9 and row 3.3.11). Notice that, in the first 5 epochs the SH loss achieves a better performance, however, from there-on the MH loss leads to much higher recall rates.

3.3.6 Behavior of Loss Functions

We observe that the MH loss can take a few epochs to ‘warm-up’ during training. Fig. 3.2 depicts such behavior on the Flickr30K dataset using RC . Notice that the SH loss starts off faster, but after approximately 5 epochs MH loss surpasses SH loss. To explain this, the MH loss depends on a smaller set of triplets compared to the SH loss. Early in training the gradient of the MH loss is influenced by a relatively small set of triples. As such, it can take more iterations to train a model with the MH loss. We explored a simple form of curriculum learning [14] to speed-up the training. We start training with the SH loss for a few epochs, then switch to the MH loss for the rest of the training. However, it did not perform much better than training solely with the MH loss.

In [179], it is reported that with a mini-batch size of 1800, training is extremely slow. We experienced similar behavior with large mini-batches up to 512. However, mini-batches of size 128 or 256 exceeded the performance of the SH loss within the same training time.

3.3.7 Examples of Hard Negatives

Fig. 3.3 shows the hard negatives in a random mini-batch. These examples illustrate that hard negatives from a mini-batch can provide useful gradient information.

Fig. 3.4 provides additional examples comparing the outputs of *VSE++* and *VSE0*.

3.3.8 Distribution of distances

Fig. 3.5 compares the distribution of distances for hard negatives using *MH* loss versus the *SH* loss after 10 and 30 epochs. For the *MH* loss, the distribution of distances is negatively skewed after 10 epochs, while the distribution using the *SH* loss is approximately symmetric. The reason is, the *MH* loss disproportionately focuses on the hardest negatives that results in a sharp drop in the number of hard negatives after cosine similarity 0.4 while a large stack of hard negatives is created before 0.4. As the training progresses to epoch 30, the stack of hard negatives is dispersed but the drop to zero probability is still sharper than the *SH* loss. At Epoch 30, this margin is reduced to 0.3.

3.3.9 Effect of Negative Set Size on *MH* Loss

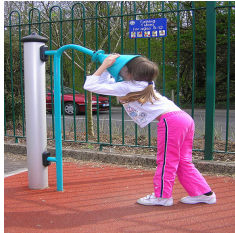
Our proposed hard negatives are found in the mini-batch of triplets in each training step that is a uniformly sampled subset of the training set. Instead, one could find the hardest negatives within the training set which is computationally expensive but potentially performs better. We study the effective sample size over which we searched for negatives (while keeping the mini-batch size fixed at 128). In the extreme case, when the negative set is the training set, we get the hardest negatives in the entire training set. As discussed in Sec. 3.2.2, sampling a negative set smaller than the training set can potentially be more robust to label errors.

In Fig. 3.6, we show the effect of the negative sample set size on the performance of *MH* loss. We compare the caption retrieval performance for different negative set sizes varied from 2 to 512. In practice, for negative set sizes smaller than the mini-batch size, 128, we randomly sample the negative set from the mini-batch, and when the mini-batch size is smaller than the negative set size, we randomly sample the mini-batch from the negative set. We observe that on this dataset, the optimal negative set size is around 128. Interestingly, for negative sets as small as 2, R@1 is slightly below *VSE0*. We observe a drop

in performance as the negative set size is increased to 512. We hypothesize that this number is dataset dependant and for a small dataset like Flickr30K, the probability of sampling a noisy example increases significantly. Even though the performance drops with larger mini-batch sizes, it still performs better than the *SH* loss.

3.4 Conclusion

This chapter focused on learning visual-semantic embeddings for cross-modal, image-caption retrieval. Inspired by structured prediction, we proposed a new loss based on violations incurred by relatively hard negatives compared to current methods that used expected errors [103, 210]. We performed experiments on the MS-COCO and Flickr30K datasets and showed that our proposed loss significantly improves performance on these datasets. We observed that the improved loss can better guide a more powerful image encoder, ResNet152, and also guide better when fine-tuning an image encoder. At the time of publication, with all modifications, our *VSE++* model achieved state-of-the-art performance on the MS-COCO dataset, and was slightly below the best model at the time on the Flickr30K dataset. Our proposed loss function can be used to train more sophisticated models that have been using a similar ranking loss for training.



GT: A little girl wearing pink pants, pink and white tennis shoes and a white shirt with a little girl on it puts her face in a blue Talking Tube.
HN: [0.26] Blond boy jumping onto deck.



GT: A teal-haired woman in a very short black dress, pantyhose, and boots standing with right arm raised and left hand obstructing her mouth in microphone-singing fashion is standing.
HN: [0.08] Two dancers in azure appear to be performing in an alleyway.



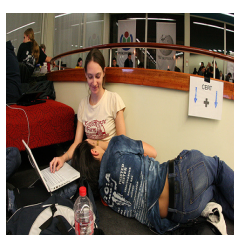
GT: Two men, one in a dark blue button-down and the other in a light blue tee, are chatting as they walk by a small restaurant.
HN: [0.41] Two men with guitars strapped to their back stand on the street corner with two other people behind them.



GT: A man wearing a black jacket and gray slacks, stands on the sidewalk holding a sheet with something printed on it in his hand.
HN: [0.26] Two men with guitars strapped to their back stand on the street corner with two other people behind them.



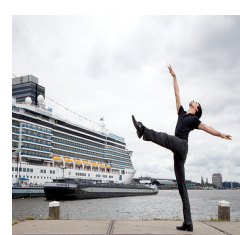
GT: There is a wall of a building with several different colors painted on it and in the distance one person sitting down and another walking.
HN: [0.06] A woman with luggage walks along a street in front of a large advertisement.



GT: A man is laying on a girl's lap, she is looking at him, she also has her hand on her notebook computer.
HN: [0.18] A woman sits on a carpeted floor with a baby.

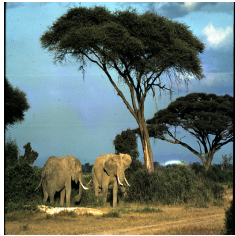


GT: A young blond girl in a pink sweater, blue skirt, and brown boots is jumping over a puddle on a cloudy day.
HN: [0.51] An Indian woman is sitting on the ground, amongst drawings, rocks and shrubbery.



GT: One man dressed in black is stretching his leg up in the air, behind him is a massive cruise ship in the water.
HN: [0.24] A topless man straps surfboards on top of his blue car.

Figure 3.3: Examples from the Flickr30K training set along with their hard negatives in a random mini-batch according to the loss of a trained VSE++ model. The value in brackets is the cost of the hard negative and is in the range $[0, 2]$ in our implementation. HN is the hardest negative in a random sample of size 128. GT is the positive caption used to compute the cost of NG.



GT: Two elephants are standing by the trees in the wild.

VSE0: [9] Three elephants kick up dust as they walk through the flat by the bushes.

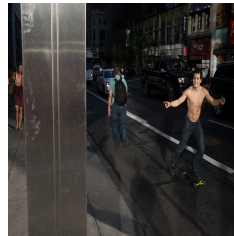
VSE++: [1] A couple elephants walking by a tree after sunset.



GT: A large multi layered cake with candles sticking out of it.

VSE0: [1] A party decoration containing flowers, flags, and candles.

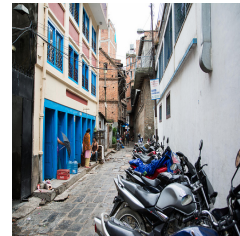
VSE++: [1] A party decoration containing flowers, flags, and candles.



GT: The man is walking down the street with no shirt on.

VSE0: [24] A person standing on a skate board in an alley.

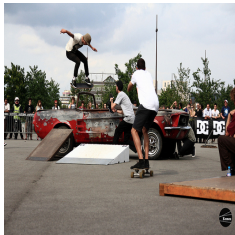
VSE++: [10] Two young men are skateboarding on the street.



GT: A row of motorcycles parked in front of a building.

VSE0: [2] a parking area for motorcycles and bicycles along a street

VSE++: [1] A number of motorbikes parked on an alley



GT: some skateboarders doing tricks and people watching them

VSE0: [39] Young skateboarder displaying skills on sidewalk near field.

VSE++: [3] Two young men are outside skateboarding together.



GT: a brown cake with white icing and some walnut toppings

VSE0: [6] A large slice of angel food cake sitting on top of a plate.

VSE++: [16] A baked loaf of bread is shown still in the pan.



GT: A woman holding a child and standing near a bull.

VSE0: [1] A woman holding a child and standing near a bull.

VSE++: [1] A woman holding a child looking at a cow.



GT: A woman in a short pink skirt holding a tennis racquet.

VSE0: [6] A man playing tennis and holding back his racket to hit the ball.

VSE++: [1] A woman is standing while holding a tennis racket.

Figure 3.4: Examples of MS-COCO test images and the top 1 retrieved captions for *VSE0* and *VSE++* (ResNet)-finetune. The value in brackets is the rank of the highest ranked ground-truth caption. GT is a sample from the ground-truth captions.

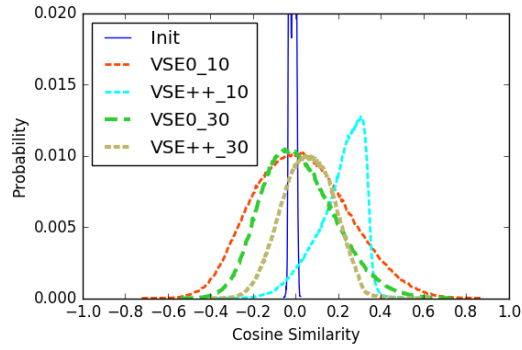


Figure 3.5: Distribution of distances for Flickr30K training set averaged over 10 fixed examples over the course of training. The distribution for the *MH* loss and the *SH* loss is shown for snapshots of the model at epoch 10 and 30. For comparison, the distribution for a randomly initialized model is also depicted.

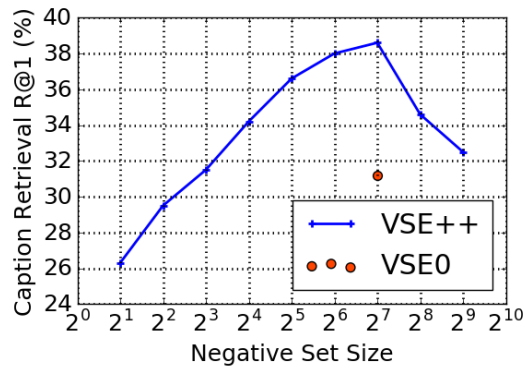


Figure 3.6: The effect of the negative set size on the R@1 performance. The optimal R@1 is achieved near mini-batch size 128.

Chapter 4

Gradient Clustering and A Study of Gradient Variance in Deep Learning

The second problem addressed in this thesis is training efficiency as a general challenge in training deep neural networks. Instead of focusing on a particular task-specific loss function, we seek improvements to optimization speed in gradient-based optimization methods for deep learning. We revisit our hypothesis from the first problem that training data are not equally important. We hypothesize that training deep learning models on diverse and heterogeneous data distributions is slower than homogeneous data distributions with less diversity.

In this context, we study the distribution of gradients during training. We introduce a method, Gradient Clustering, to minimize the variance of average mini-batch gradient with stratified sampling. We prove that the variance of average mini-batch gradient is minimized if the elements are sampled from a weighted clustering in the gradient space. We measure the gradient variance on common deep learning benchmarks and observe that, contrary to common assumptions, gradient variance increases at the beginning of the training, and smaller learning rates coincide with higher variance. In addition, we introduce normalized gradient variance as a statistic that better correlates with the speed of convergence compared to gradient variance.

The content of this chapter have appeared in the following publication:

- **Faghri, Fartash** and Duvenaud, David and Fleet, David J. and Ba, Jimmy, “*Gluster: Variance Reduced Mini-Batch SGD with Gradient Clustering*”, Conference on Neural Information Processing Systems (NeurIPS), Workshop on Beyond First Order Methods in ML, 2019.

Additionally, the results have been further developed in the following publications:

- **Faghri, Fartash**, Tabrizian, Iman and Markov, Ilia and Alistarh, Dan and Roy, Dan M. and Ramezani-Kebrya, Ali, “*Adaptive Gradient Quantization for Data-Parallel SGD*”, Conference on Neural Information Processing Systems (NeurIPS), 2020.
- Ramezani-Kebrya, Ali and **Faghri, Fartash** and Markov, Ilya and Aksenov, Vitalii and Alistarh, Dan and Roy, Dan M. et al., “*NUQSGD: Provably Communication-efficient Data-parallel SGD via Nonuniform Quantization*”, Journal of Machine Learning Research 22.114 (2021): 1-43.

To ensure reproducibility, our code is publicly available ^{1 2 3}.

4.1 Introduction

Many machine learning tasks entail the minimization of the risk, $\mathbb{E}_{\mathbf{x}}[\ell(\mathbf{x}; \boldsymbol{\theta})]$, where \mathbf{x} is an i.i.d. sample from a data distribution, and ℓ is the per-example loss parametrized by $\boldsymbol{\theta}$. In supervised learning, inputs and ground-truth labels comprise \mathbf{x} , and $\boldsymbol{\theta}$ is a vector of model parameters. Empirical risk approximates the population risk by the risk of a sample set $\{\mathbf{x}_i\}_{i=1}^N$, the training set, as $L(\boldsymbol{\theta}) = \sum_{i=1}^N \ell(\mathbf{x}_i; \boldsymbol{\theta})/N$. Empirical risk is often minimized using gradient-based optimization (first-order methods). For differentiable loss functions, the gradient of $\boldsymbol{\theta}$ is defined as $\frac{\partial}{\partial \boldsymbol{\theta}} \ell(\mathbf{x}; \boldsymbol{\theta})$, i.e., the gradient of the loss with respect

¹ https://github.com/fartashf/gvar_code

² <https://github.com/fartashf/foptim>

³ <https://github.com/fartashf/nuqsgd>

to the parameters evaluated at a point \mathbf{x} . Popular in deep learning, Mini-batch Stochastic Gradient Descent (mini-batch SGD) iteratively takes small steps in the opposite direction of the average gradient of B training samples. The mini-batch size is a hyper-parameter that provides flexibility in trading per-step computation time for potentially fewer total steps. In GD the mini-batch is the entire training set while in SGD it is a single sample.

In general, using any unbiased stochastic estimate of the gradient and sufficiently small step sizes, SGD is guaranteed to converge to a minimum for various function classes [167]. Common convergence bounds in stochastic optimization improve with smaller gradient variance [18]. Mini-batch SGD is said to converge faster because the variance of the gradient estimates is reduced by a rate linear in the mini-batch size. In practice however, we observe **diminishing returns** in speeding up the training of almost any deep model on deep learning benchmarks [181]. The transition point to diminishing returns is known to depend on the choice of data, model and optimization method. [229] observed that the limitation of acceleration in large batches is reduced when momentum or preconditioning is used. Other works suggest that very small mini-batch sizes can still converge fast enough using a collection of tricks [63, 135, 116]. One hypothesis is that the stochasticity due to small mini-batches improves generalization by finding “flat minima” and avoiding “sharp minima” [68, 100]. But this hypothesis does not explain why diminishing returns also happens in the training loss.

Motivated by the diminishing returns phenomena, we study and model the distribution of the gradients. Given a data distribution characterized by its probability density function, $\mathbb{P}(\mathbf{x})$, the gradient distribution is defined as a transformation of the data distribution by the gradient of the loss function, $\frac{\partial}{\partial \theta} \ell(\mathbf{x}; \theta)$. The transformation is a function of the model parameters that can be deterministic, e.g., with a linear model or stochastic, for example, when using random data augmentation or dropout. As such, the gradient distribution varies across model architectures and evolves during the training.

An unbiased gradient estimator is an estimate of the mean of the gradient distribution that is commonly evaluated by its variance. In the noisy gradient view, the average mini-

batch gradient (or the mini-batch gradient) is an unbiased estimator of the expected gradient where increasing the mini-batch size reduces the variance of this estimator. We propose a distributional view and argue that knowledge of the gradient distribution can be exploited to analyze and improve optimization speed as well as generalization to test data. A mean-aware optimization method is at best as strong as a distributional-aware optimization method. In our distributional view, the mini-batch gradient is only an estimate of the mean of the gradient distribution.

Questions: We identify the following questions about the gradient distribution.

Structure of gradient distribution. Is there structure in the distribution over gradients of standard learning problems?

Impact of gradient distribution on optimization. What characteristics of the gradient distribution correlate with the convergence speed and the minimum training/test loss reached?

Impact of optimization on gradient distribution. To what extent do the following factors affect the gradient distribution: data distribution, learning rate, model architecture, mini-batch size, optimization method, and the distance to local optima?

As we review in [Section 4.2](#), recent work have begun to investigate aforementioned questions but we are far from a comprehensive understanding.

Contributions:

Exploiting clustered distributions. We consider gradient distributions with distinct modes, i.e., the gradients can be clustered. We prove that the variance of average mini-batch gradient is minimized if the elements are sampled from a weighted clustering in gradient space ([Section 4.3](#)).

Efficient clustering to minimize variance. We propose Gradient Clustering (GC) as a computationally efficient method for clustering in the gradient space ([Section 4.3.2](#)).

[Fig. 4.1](#) shows an example of clusters found by GC.

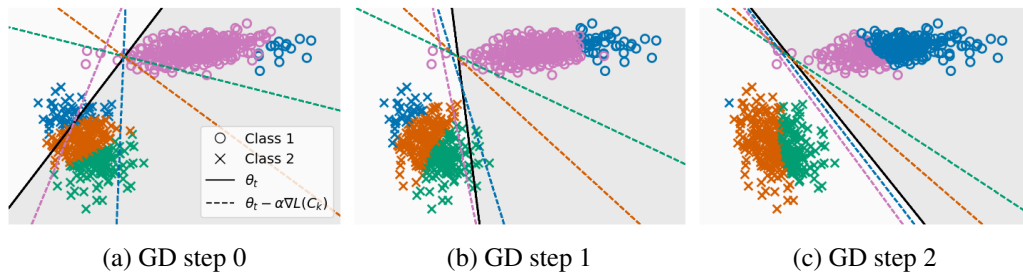


Figure 4.1: **Example of clusters found using Gradient Clustering.** A linear classifier visualized during training with gradient descent on 2 linearly separable classes (o, x). Gradients are assigned to 4 clusters (different colors) using Gradient Clustering (GC). Black line depicts current decision boundary. Colored dashed lines depict decision boundaries predicted from current boundary and each of the 4 individual clusters. Here, blue points belong to both classes; they have similar gradients, but are far apart in input space. By exploiting the knowledge of GC we can get low variance average mini-batch gradients.

Relation between gradient variance and optimization. We study the gradient variance on common deep learning benchmarks (MNIST, CIFAR-10, and ImageNet) as well as Random Features models recently studied in deep learning theory (Section 4.4). We observe that gradient variance increases for most of the training, and smaller learning rates coincide with higher variance.

An alternative statistic. We introduce normalized gradient variance as a statistic that better correlates with the speed of convergence compared to gradient variance (Section 4.4).

We emphasize that some of our contributions are primarily empirical yet unexpected. We believe our results provide an opportunity for future theoretical and empirical work.

4.2 Related Work

Modeling gradient distribution. Despite various assumptions on the mini-batch gradient variance, only recently these assumptions have been scrutinized for deep learning models. It is common to assume bounded variance in convergence analyses [18]. Works on variance reduction propose alternative estimates of the gradient mean with low variance [110, 95]

but they do not plot the variance which is the actual quantity they seek to reduce. Their ineffectiveness in deep learning has been observed but still requires explanation [39]. There are works that present gradient variance plots [137, 217] but they are usually for a single gradient coordinate and synthetic problems. The Central limit theorem is also used to argue that the distribution of the mini-batch gradient is a Gaussian [236], which has been challenged only recently [188, 220]. The observation that the gradient noise is heavy tailed has been used to justify the superiority of the Adam optimizer in training attention models [231]. There also exists a link between the Fisher [3], Neural Tangent Kernel [88], and the gradient covariance matrix [131, 106, 200]. As such, any analysis of one [e.g., 97] could potentially be used to understand others.

Variance reduction as part of optimization methods for deep learning. Variance reduction is an important technique in gradient estimation at the core of many machine learning problems [137]. A variance reduced gradient estimator can then be used with a gradient-based optimization method. In such approaches, the performance of the optimizer depends on the gradient estimator but there is no feedback from the optimizer to improve the gradient estimator. Our work is related to variance reduction methods that directly modify the optimization method. [109] considered the difference between the covariance matrix of the gradients and the Fisher matrix and proposed incorporating the covariance matrix as a measure of model uncertainty in optimization. It has also been suggested that the division by the second moments of the gradient in Adam can be interpreted as variance adaptation [106]. Although we do not use Gradient Clustering for optimization, the formulation can be interpreted as a unifying approach that defines variance reduction as an objective.

Importance Sampling for Optimization. Our work is also closely related to importance sampling for stochastic optimization where data points are sampled according to a measure of importance such as the loss or the norm of the gradient [233, 99, 37, 96, 2, 148]. There are also myriad papers on ad-hoc sampling and re-weighting methods for reducing dataset imbalance and increasing data diversity [13, 94, 212, 93]. Based on empirical results,

[221] suggests that several sampling and ordering methods have only marginal benefits on standard datasets when training time is long enough. Our method can be viewed as an importance sampling method where the relative size of the cluster denotes the importance of its data points. Compared with using only gradient norm or the loss for importance sampling, we exploit the entire gradient vector for each data point that makes the method significantly more powerful.

Clustering gradients. Methods related to gradient clustering have been proposed in low-variance gradient estimation [85, 232, 27] supported by promising theory. However, these methods have either limited their experiments to linear models or treated a deep model as a linear one. Our proposed GC method performs efficient clustering in the gradient space with very few assumptions. GC is also related to works on model visualization where the entire training set is used to understand the behaviour of a model [160].

4.3 Mini-batch Gradient with Stratified Sampling

An important factor affecting optimization trade-offs is the diversity of training data. SGD entails a sampling process, often uniformly sampling from the training set. However, as illustrated in the following example, uniform sampling is not always ideal. Suppose there are duplicate data points in a training set. We can save computation time by removing all but one of the duplicates. To get the same gradient mean in expectation, it is sufficient to rescale the gradient of the remaining sample in proportion to the number of duplicates. In this example, mini-batch SGD will be inefficient because duplicates increase the variance of the average gradient mean.

Suppose we are given i.i.d. training data, $\{\mathbf{x}_i\}_{i=1}^N$, and a partitioning of their gradients, $\mathbf{g}_i = \frac{\partial}{\partial \boldsymbol{\theta}} \ell(\mathbf{x}_i; \boldsymbol{\theta})$, into K clusters, where N_k is the size of the k -th cluster. We can estimate the gradient mean on the training set, $\mathbf{g} = \frac{\partial}{\partial \boldsymbol{\theta}} L(\boldsymbol{\theta})$, by averaging K gradients, one from

each of K clusters, uniformly sampled:

$$\hat{\mathbf{g}}(\mathbf{a}) = \frac{1}{N} \sum_{k=1}^K N_k \mathbf{g}^{(k)}, \quad \mathbf{g}^{(k)} \sim \mathbb{U}(S_k), \quad (4.1)$$

where $\mathbf{g}^{(k)}$ is a uniformly sampled gradient from the k -th cluster $S_k = \{\mathbf{g}_i | a_i = k\}$, and $\mathbf{a} \in \{1, \dots, K\}^N$ where a_i is the index of the cluster to which i -th data point is assigned, so $N_k = \sum_{i=1}^N \mathbb{I}(a_i = k)$. Each sample is treated as a representative of its cluster and weighted by the size of that cluster. In the limit of $K = N$, we recover the batch gradient mean used in GD and for $K = 1$ we recover the single-sample stochastic gradient in SGD.

Proposition 4.3.1. (Bias/Variance of Mini-batch Gradient with Stratified Sampling).

For any partitioning of data, the estimator of the gradient mean using stratified sampling (Eq. (4.1)) is unbiased ($\mathbb{E}[\hat{\mathbf{g}}] = \mathbf{g}$) and $\mathbb{V}[\hat{\mathbf{g}}] = N^{-2} \sum_{k=1}^K N_k^2 \mathbb{V}[\mathbf{g}^{(k)}]$, where $\mathbb{V}[\cdot]$ is defined as the trace of the covariance matrix. (Proof in [Appendix A.1.1](#))

Remark. Under a stratified sampling scheme, in a dataset with duplicate samples, the gradients of duplicates do not contribute to the variance if assigned to the same partition with no other data points.

4.3.1 Weighted Gradient Clustering

Suppose, for a given number of clusters, K , we want to find the optimal partitioning, i.e., one that minimizes the variance of the gradient mean estimator, $\hat{\mathbf{g}}$. For d -dimensional gradient vectors, minimizing the variance in [Proposition 4.3.1](#), is equivalent to finding a weighted clustering of the gradients of data points,

$$\min_{\mathbf{a}} \mathbb{V}[\hat{\mathbf{g}}(a_i)] = \min_{\mathbf{a}} \sum_{k=1}^K N_k^2 \mathbb{V}[\mathbf{g}^{(k)}] = \min_{\mathbf{C}, \mathbf{a}} \sum_{k=1}^K \sum_{i=1}^N N_k \|\mathbf{C}_k - \mathbf{g}_i\|^2 \mathbb{I}(a_i = k), \quad (4.2)$$

where a cluster center, $\mathbf{C}_k \in \mathbb{R}^d$, is the average of the gradients in the k -th cluster, and $\mathbb{V}[\mathbf{g}^{(k)}] = \frac{1}{N_k} \sum_{i=1}^N \|\mathbf{C}_k - \mathbf{g}_i\|^2 \mathbb{I}(a_i = k)$. If we did not have the factor N_k , this objective

would be equivalent to the K-Means objective. The additional N_k factors encourage larger clusters to have lower variance, with smaller clusters comprising scattered data points.

If we could store the gradients for the entire training set, the clustering could be performed iteratively as a form of block coordinate descent, alternating between the following *Assignment* and *Update* steps, i.e., computing the cluster assignments and then the cluster centers:

$$\mathcal{A}: a_i = \arg \min_k N_k \|C_k - g_i\|^2 \quad \mathcal{U}: C_k = \frac{1}{N_k} \sum_{i=1}^N g_i \mathbb{I}(a_i = k) \quad (4.4)$$

The \mathcal{A} step is still too complex given the N_k multiplier. As such, we first solve it for fixed cluster sizes then update N_k before another \mathcal{U} step. These updates are similar to Lloyd’s algorithm for K-Means, but with the N_k multipliers, and to Expectation-Maximization for Gaussian Mixture Models, but here we use hard assignments. In contrast, the additional N_k multiplier makes the objective more complex in that performing \mathcal{AU} updates does not always guarantee a decrease in the clustering objective.

4.3.2 Efficient Gradient Clustering (GC)

Performing exact \mathcal{AU} updates (Eqs. (4.3) and (4.4)) is computationally expensive as they require the gradient of every data point. Deep learning libraries usually provide efficient methods that compute average mini-batch gradients without ever computing full individual gradients. We introduce Gradient Clustering (GC) for performing efficient \mathcal{AU} updates by breaking them into per-layer operations and introducing a low-rank approximation to cluster centers.

For any feed-forward network, we can decompose terms in \mathcal{AU} updates into independent per-layer operations as shown in Fig. 4.2. The main operations are computing $\|C_{kl} - g_{il}\|^2$ and cluster updates $C_{a_i,l} += g_{il}/N_{a_i}$ per layer l ; henceforth, we drop the layer index for simplicity.

Algorithm 1 \mathcal{A} step using Eq. (4.5)	Algorithm 2 N_k update	Algorithm 3 \mathcal{U} step using Eq. (4.6)
<pre> for $i = 1$ to N do for $k = 1$ to K do for $l = 1$ to L do $D_{kl} = \ \mathbf{C}_{kl} - \mathbf{g}_{il}\ ^2$ $\mathbf{S} = \sum_l D_{.l}$ $a_i = \arg \min_k N_k \mathbf{S}$ </pre>	<pre> $N_k = 0, \forall k = 1, \dots, K$ for $i = 1$ to N do $N_{a_i} += 1$ </pre>	<pre> $\mathbf{C}_k = 0, \forall k = 1, \dots, K$ for $i = 1$ to N do for $l = 1$ to L do $\mathbf{C}_{a_i, l} += \mathbf{g}_{il} / N_{a_i}$ </pre>

Figure 4.2: **Gradient Clustering Algorithm steps** applied on the gradients of a deep neural network with L layers. \mathbf{g}_{il} denotes the gradients of the i -th example w.r.t. the parameters of the l -th layer, \mathbf{C}_{kl} denotes k -th cluster center for the l -th layer, a_i denotes the assignment index for the i -th data point and N_k denotes the size of the k -th cluster.

For a single fully-connected layer, we denote the layer weights by $\boldsymbol{\theta} \in \mathbb{R}^{I \times O}$, where I and O denote the input and output dimensions for the layer. We denote the gradient with respect to $\boldsymbol{\theta}$ for the training set by $\mathbf{g} = \mathbf{A}\mathbf{D}^\top$, where $\mathbf{A} \in \mathbb{R}^{I \times N}$ comprises the input activations to the layer, and $\mathbf{D} \in \mathbb{R}^{O \times N}$ represents the gradients with respect to the layer outputs. The coordinates of cluster centers corresponding to this layer are denoted by $\mathbf{C} \in \mathbb{R}^{K \times I \times O}$. We index the clusters using k and the data by i . The k -th cluster center is approximated as $\mathbf{C}_k = \mathbf{c}_k \mathbf{d}_k^\top$, using vectors $\mathbf{c}_k \in \mathbb{R}^I$ and $\mathbf{d}_k \in \mathbb{R}^O$.

In the \mathcal{A} step we need to compute $\|\mathbf{C}_k - \mathbf{g}_i\|_F^2$ as part of the assignment cost, where $\|\cdot\|_F$ is the Frobenius-norm. We expand this term into three inner-products, and compute them separately. In particular, the term $\text{vec}\{\mathbf{C}_k\} \odot \text{vec}\{\mathbf{g}_i\}$ can be written as,

$$\text{vec}\{\mathbf{C}_k\} \odot \text{vec}\{\mathbf{A}_i \mathbf{D}_i^\top\} = (\mathbf{A}_i \odot \mathbf{c}_k)(\mathbf{D}_i \odot \mathbf{d}_k), \quad (4.5)$$

where \odot denotes inner product, and the RHS is the product of two scalars. Similarly, we compute the other two terms in the expansion of the assignment cost, i.e., $\text{vec}\{\mathbf{C}_k\} \odot \text{vec}\{\mathbf{C}_k\}$ and $\text{vec}\{\mathbf{g}_i\} \odot \text{vec}\{\mathbf{g}_i\}$ ([64] proposed a similar idea to compute the gradient norm).

The \mathcal{U} step in Eq. (4.4) is written as, $\mathbf{c}_k \mathbf{d}_k^\top = N_k^{-1} \sum_{i=1}^N \mathbf{A}_i \mathbf{D}_i^\top \mathbb{I}(a_i = k)$. This

equation might have no exact solution for \mathbf{c}_k and \mathbf{d}_k because the sum of rank-1 matrices is not necessarily rank-1. One approximation is the min-Frobenius-norm solution to $\mathbf{c}_k, \mathbf{d}_k$ using truncated SVD, where we use left and right singular-vectors corresponding to the largest singular-value of the RHS. However, the following updates are exact if activations and gradients of the outputs are uncorrelated, i.e., $\mathbb{E}_i[\mathbf{A}_i \mathbf{D}_i] = \mathbb{E}_i[\mathbf{A}_i] \mathbb{E}_i[\mathbf{D}_i]$ (similar to assumptions in K-FAC [133]),

$$\mathbf{c}_k = \frac{1}{N_k} \sum_{i=1}^N \mathbf{A}_i \mathbb{I}(a_i = k) \quad \mathbf{d}_k = \frac{1}{N_k} \sum_{i=1}^N \mathbf{D}_i \mathbb{I}(a_i = k). \quad (4.6)$$

In [Appendix A.2.1](#), we describe similar update rules for convolutional layers and in [Appendix A.2.2](#), we provide complexity analysis of GC. We can make the cost of GC negligible by making sparse incremental updates to cluster centers using mini-batch updates. The assignment step can also be made more efficient by processing only a portion of data as is common for training on large datasets. The rank-1 approximation can be extended to higher rank approximations with multiple independent cluster centers though with challenges in the implementation.

4.4 Experiments

In this section, we evaluate the accuracy of estimators of the gradient mean. This is a surrogate task for evaluating the performance of a model of the gradient distribution. We encourage the reader to predict the behaviour of gradient estimators before advancing in this section. In particular, does the reader expect the gradient variance to increase or decrease during the training? Surprisingly, we find that the gradient variance often increases in the majority of training.

We compare our proposed GC estimator to average mini-batch Stochastic Gradient (SG-B), and SG-B with double the mini-batch size (SG-2B). SG-2B is an important baseline for two reasons. First, it is a competitive baseline that always reduces the variance by a factor of 2 and requires at most twice the memory size and twice the run-time per mini-batch [181].

Second, the extra overhead of GC is approximately the same as keeping an extra mini-batch in the memory when the number of clusters is equal to the mini-batch size. We also include Stochastic Variance Reduced Gradient (SVRG) [95] as a method with the sole objective of estimating gradient mean with low variance.

We compare methods on a **single trajectory of mini-batch SGD** to decouple the optimization from gradient estimation. That is, we do not train with any of the estimators (hence no ‘D’ in SG-B and SG-2B). This allows us to continue analyzing a method even after it fails in reducing the variance. For training results using SG-B, SG-2B and, SVRG, we refer the reader to [181, 39]. For training with GC, it suffices to say that behaviours observed in this section are directly related to the performance of GC used for optimization.

As all estimators in this work are unbiased, the estimator with lowest variance is better estimating the gradient mean. We define *Average Variance* (variance in short) as the average over all coordinates of the variance of the gradient mean estimate for a fixed model snapshot. Average variance is the normalized trace of the covariance matrix and of particular interest in random matrix theory [198].

We also measure *Normalized Variance*, defined as $\mathbb{V}[g]/E[g^2]$ where the variance of a 1-dimensional random variable is divided by its second non-central moment. In signal processing, the inverse of this quantity is the signal to noise ratio (SNR). If SNR is less than one (normalized variance larger than one), the power of the noise is greater than the signal. Normalized variance also appears in standard convergence analysis of stochastic gradient descent [55]. As we show in [Appendix A.4](#), it can be shown that for Lipschitz continuous functions, variance reduction is only useful if the normalized variance is larger than constant 1. As such, it better correlates with the convergence speed compared with variance.

Additional details of the experimental setup can be found in [Appendix A.3](#).

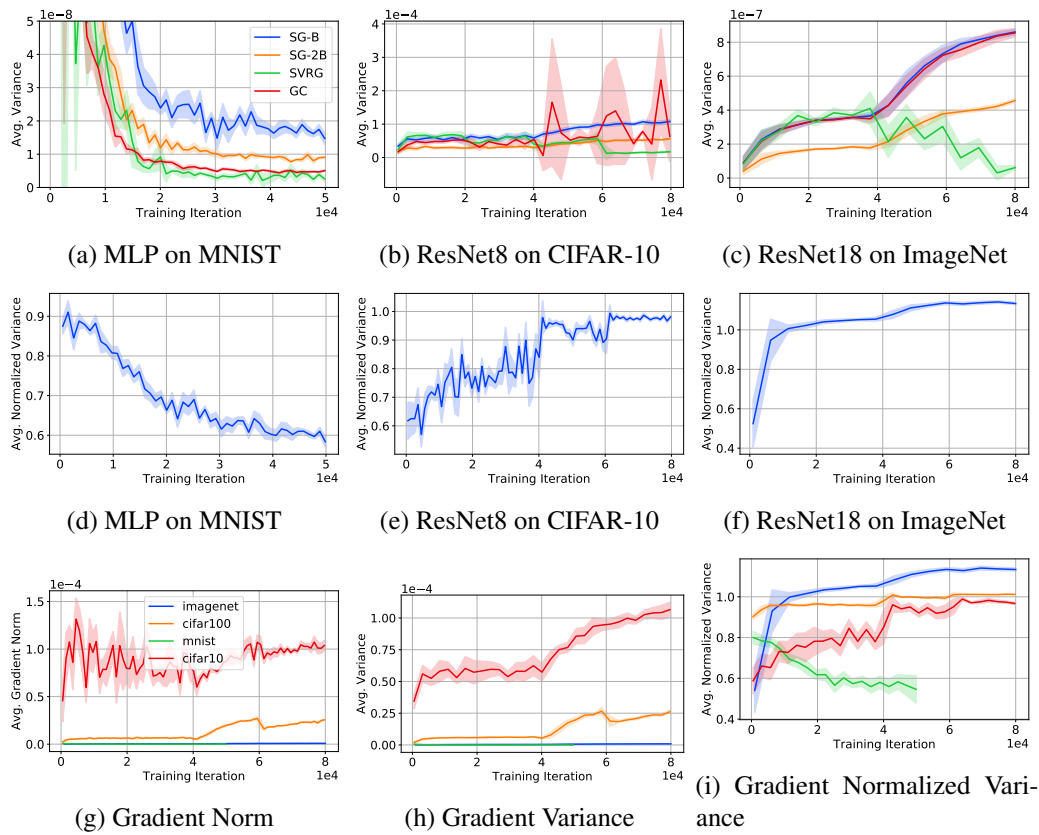


Figure 4.3: **Image classification models.** Variance (top) and normalized variance plots (middle). Bottom plots compare gradient statistics for SGD across datasets. We observe: normalized variance correlates with optimization difficulty, variance is decreasing on MNIST but increasing on CIFAR-10 and ImageNet, and variance fluctuates with GC on CIFAR-10.

4.4.1 MNIST: Low Variance, CIFAR-10: Noisy Estimates, ImageNet: No Structure

In this section, we study the evolution of gradient variance during training of an MLP on MNIST [111], ResNet8 [78] on CIFAR-10 [105], and ResNet18 on ImageNet [40]. Curves shown are from a single run and statistics are smoothed out over a rolling window. The standard deviation within the window is shown as a shaded area.

Normalized variance correlates with the time required to improve accuracy. In Figs. 4.3a to 4.3c, the variance of SG-2B is always half the variance of SG-B. A drawback of the variance is that it is not comparable across different problems. For example, on CIFAR-

10 the variance of all methods reaches 10^{-4} while on ImageNet where usually $10\times$ more iterations are needed, the variance is below 10^{-6} . In contrast, as we show by convergence analysis in [Appendix A.4](#), for Lipschitz continuous functions, variance reduction is only useful if the normalized variance is larger than constant 1. In [Figs. 4.3d to 4.3f](#), normalized variance better correlates with the convergence speed. Normalized variance on both MNIST and CIFAR-10 is always below 1 while on ImageNet it quickly goes above 1 (noise stronger than gradient). Notice that the denominator in the normalized variance is shared between all methods on the same trajectory of mini-batch SGD. As such, the normalized variance retains the relation of curves and is a scaled version of variance where the scaling varies during training as the norm of the gradient changes. For clarity, we only show the curve for SG-B.

How does the difficulty of optimization change during training? The variance on MNIST for all methods is constantly decreasing ([Fig. 4.3a](#)), i.e., the strength of noise decreases as we get closer to a local optima. These plots suggest that training an MLP on MNIST satisfies the Strong Growth Condition (SGC) [[177](#)] as the variance is numerically zero (below 10^{-8}). Normalized variance ([Fig. 4.3d](#)) decreases over time and is well below 1 (gradient mean has larger magnitude than the variance). SVRG performs particularly well by the end of the training because the training loss has converged to near zero (cross-entropy less than 0.005). Promising published results with SVRG are usually on datasets similar to MNIST where the loss reaches relatively small values. In contrast, on both CIFAR-10 ([Figs. 4.3b and 4.3e](#)) and ImageNet ([Figs. 4.3c and 4.3f](#)), the variance and normalized variance of all methods increase from the beginning for almost the entire training and especially after the learning rate drops. This means gradient variance depends on the distance to local optima. We hypothesize that the gradient of each training point becomes more unique as training progresses. Models we considered do not reach zero training loss within the given training time. If we increase the model size and train long enough and decrease the learning rate, eventually the gradient variance decreases to zero.

Variance can widely change during training but it happens only on particularly noisy data. On CIFAR-10, the variance of GC suddenly goes up but comes back down before

any updates to the cluster centers (Fig. 4.3b) while the variance of SVRG monotonically increases between updates. To explain these behaviours, notice that immediately after cluster updates, GC and SVRG should always have at most the same average variance as SG-B. We observed this behaviour consistently across different architectures such as other variations of ResNet and VGG on CIFAR-10. Fig. 4.6 shows the effect of adding noise on CIFAR-10. Label smoothing [197] reduces fluctuations but not completely. On the other hand, label corruption, where we randomly change the labels for 10% of the training data eliminates the fluctuations. We hypothesize that the model is oscillating between different states with significantly different gradient distributions. The experiments with corrupt labels suggest that mislabeled data might be the cause of fluctuations such that having more randomness in the labels forces the model to ignore originally mislabeled data.

Is the gradient distribution clustered in any dataset? The variance of GC on MNIST (Fig. 4.3a) is consistently lower than SG-2B which means it is exploiting clustering in the gradient space. On CIFAR-10 (Fig. 4.3b) the variance of GC is lower than SG-B but not lower than SG-2B except when fluctuating. The improved variance is more noticeable when training with corrupt labels. On ImageNet (Figs. 4.3c and 4.3f), the variance of GC is overlapping with SG-B. An example of a gradient distribution where GC is overlapping with SG-B is a uniform distribution.

Can GC speed-up training? Although on MNIST the variance is reduced using GC, there improvements on CIFAR-10 and ImageNet are inconsistent. As such, GC does not improve the convergence speed on CIFAR-10 and ImageNet. On CIFAR-10, we considered increasing the frequency of updates to the sampling until the fluctuations disappear. To remove all fluctuations, the frequency of updates after the first learning rate drop has to be less than every 100 optimization steps which increases the overall wall-clock time of the method unless the assignment step is performed fast in parallel with a distributed system.

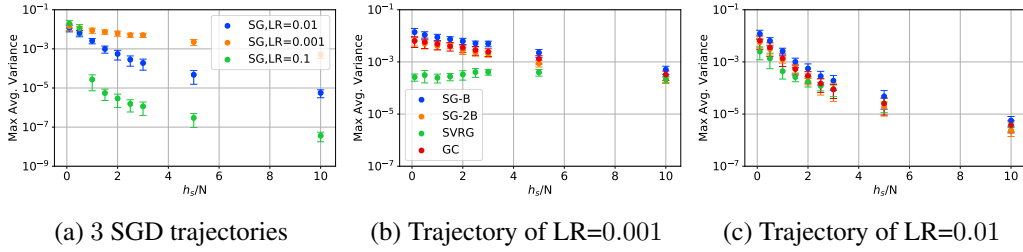


Figure 4.4: **Random Features models.** Variance (log-scale) versus the over-parametrization coefficient (student’s hidden divided by the training set size). We observe: teacher’s hidden is not influential, variance is low in overparametrized regime, and with larger learning rates. We aggregate results from hyper-parameters not shown.

4.4.2 Random Features Models: How Does Overparametrization Affect the Variance?

The Random Features (RF) model [162] provides an effective way to explore the behaviour of optimization methods across a family of learning problems. The RF model facilitates the discovery of optimization behaviours including the double-descent shape of the risk curve [77, 136]. We train a student RF model with hidden dimensions h_s on a fixed training set, $(\mathbf{x}_i, \mathbf{y}_i) \in \mathbb{R}^I \times \{\pm 1\}$, $i = 1, \dots, N$, sampled from a model, $\mathbf{x}_i \sim \mathcal{N}(0, \mathbb{I})$, $\mathbf{y}_i = \text{sign}(\sigma(\mathbf{x}_i^\top \hat{\boldsymbol{\theta}}_1)^\top \hat{\boldsymbol{\theta}}_2 + b)$ where σ is the ReLU activation function, and the teacher hidden features $\hat{\boldsymbol{\theta}}_1 \in \mathbb{R}^{I \times h_t}$, and second layer weights and bias, $\hat{\boldsymbol{\theta}}_2 \in \mathbb{R}^{h_t \times 1}$, $b \in \mathbb{R}$, are sampled from the standard normal distribution. Each I dimensional random feature of the teacher is scaled to ℓ_2 norm 1. We train a student RF model with random features $\boldsymbol{\theta}_1 \in \mathbb{R}^{I \times h_s}$ and second layer weights $\boldsymbol{\theta}_2 \in \mathbb{R}^{h_s \times 1}$ by minimizing the cross-entropy loss. In Fig. 4.4, we train hundreds of Random Features models and plot the average variance and normalized variance of gradient estimators. We show both maximum and mean of the statistics during training. The maximum better captures fluctuations of a gradient estimator and allows us to link our observations of variance to generalization using standard convergence bounds that rely on bounded noise [18].

Do models with small generalization gap converge faster? Based on small error bars, the only hyper-parameters that affect the variance are learning rate and the ratio of the size

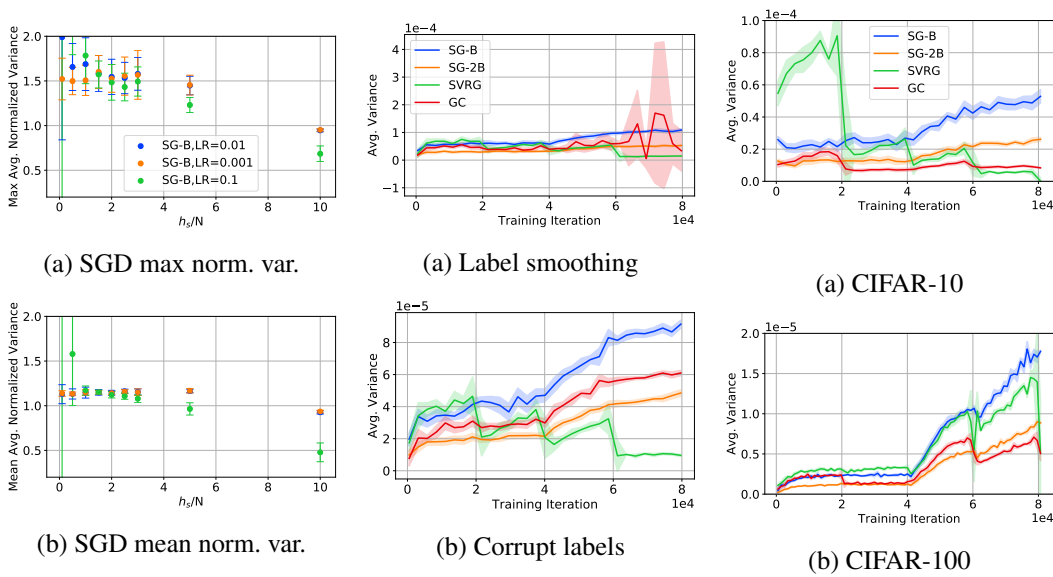


Figure 4.5: **Normalized variance on overparam. RF** is less than 1.

Figure 4.6: **CIFAR-10 Fluctuations** disappear with corrupt labels.

Figure 4.7: **Image classification with duplicates** exploited by GC.

of the student hidden layer over the training set size. In contrast, in analysis of risk and the double descent phenomena, we usually observe a dependence on ratio of the student hidden layer size to the teacher hidden layer size [136]. This suggests that models that generalize better are not necessarily ones that train faster.

Does “diminishing returns” happen because of overparametrization? Figs. 4.4b and 4.4c show that with the same learning rate, all methods achieve similar variance in the overparametrized regime. Note that due to the normalization of random features, the gradients in each coordinate are expected to decrease as overparametrization increases. We conjecture that the diminishing returns in increasing the mini-batch size should also be observed in overparametrized random features models similar to linear and deeper models [229, 181].

How does the variance change as learning rate varies? Fig. 4.4a shows that the variance is smaller for trajectories with larger learning rates and that the gap grows as overparametrization grows. This is a direct consequence of the dependence of the noise

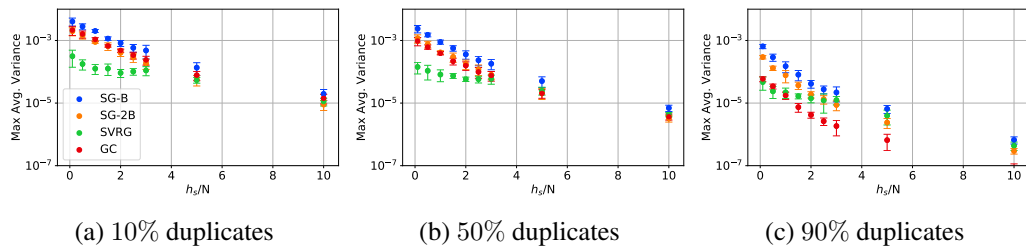


Figure 4.8: **Training RF Models with Duplicates.** GC identifies and exploits duplicates. Plots are similar to Fig. 4.4. Learning rate in all three is 0.01. In each training, there are 5 data points that are repeated equally to make up 10% (left), 50% (middle), and 90% (right) of the training set.

in the gradient on current parameters. In Section 4.4.1 we observe the opposite of this behaviour in deep models. In contrast, Fig. 4.5 shows that for overparametrization less than 5, all trajectories have similar normalized variance that is larger than one (noise is more powerful than the gradient).

4.4.3 Duplicates: Back to the Motivation for Gradient Clustering

In Fig. 4.8, we trained random features models with additional duplicated data points. We observe that as the ratio of duplicates to non-duplicates increases, the gap between the variance of GC and other methods improve. Without duplicate data, GC is always between SG-B and SG-2B. It is almost never worse than SG-B and never better than SG-2B. GC is as good as SG-2B at mild overparametrization (1 – 4). We need a degree of overparametrization for GC to reduce the variance but too much overparametrization leaves no room for improvement. When duplicates exist, GC performs well with a gap that does not decrease by overparametrization.

Similarly, experiments on CIFAR-10 and CIFAR-100 (Fig. 4.7) show that GC significantly reduces the variance when duplicate data points exist. In this experiment, 10 training points are selected randomly and duplicated 10000 times that dominate the training. As the training set size is 50000, the ratio of redundant points to the original data is $20\times$. Note that because of common data augmentations, duplicate data points are not exactly duplicate in

the input space and there is no guarantee that their gradients would be similar.

4.5 Conclusion

In this chapter, we introduced an efficient gradient clustering method and showed that stratified sampling based on the gradient clusters induces a low variance gradient estimator. We observed challenges in employing gradient clustering for optimization. To investigate, we studied the variance of the gradients for various optimization trajectories on standard benchmarks.

In the following, we summarize the hypotheses, results, and future work:

- We proved that stratified sampling based on a weighted clustering in the gradient space minimizes the variance of a mini-batch gradient estimator for a constant distribution of Gradients (Section 4.3). We designed an efficient gradient clustering method with a per-iteration computational cost comparable to a single back-prop.
- We demonstrated the success of gradient clustering in reducing the gradient variance on MNIST as well as in the presence of redundancy such as duplicate data (Sections 4.4.1 and 4.4.3). Future work could consider detecting and exploiting other types of redundancy and within-class imbalances using gradient clustering.
- We provided preliminary evidence and justification for the correlation between the normalized gradient variance and convergence speed of SGD (Section 4.4 and Appendix A.4). On MNIST, the normalized gradient variance decreases during training while it is increasing on CIFAR-10 and ImageNet for the models we tested. Future work could verify this correlation empirically for more model architectures and datasets. If verified, future work can study optimization methods such as stratified sampling with gradient clustering to minimize the normalized variance instead of the variance of gradients.
- We observed that the distribution of gradient changes significantly during the training

of CIFAR-10 models studied in this chapter. This observation does not challenge standard optimization methods but consistently impedes our proposed stratified sampling method. We hypothesized that a small subset of the training set such as a few mislabeled data might be responsible for the sudden changes in gradient clusters. In our follow-up work (not included in this thesis), we observed that the mean and variance of the normalized gradient do not change significantly during the training [49]. This observation aligns with our hypothesis. Future work can test our hypothesis by comparing the gradient cluster centers which can provide a method for detecting mislabeled or ambiguous data in the training set.

- We sought an answer for the question "Is there structure in the gradient space?" by applying weighted gradient clustering and measuring the objective, i.e., gradient variance. On MNIST and CIFAR-10, we successfully reduced the objective by performing the efficient but approximate clustering algorithm. This suggests that a clustered structure exists in the gradient space for the studied models on these datasets. In contrast, on ImageNet the variance is not reduced which implies a lack of clustered structure in the gradient space. This hypothesis is not fully tested and requires future work. For example, clustering with no weighting can be tried as well as whether the impact of the approximation error in efficient gradient clustering operations. It is also possible that alternative distance metrics to Euclidean distance would induce clusters that could be found by a modified gradient clustering method.

Chapter 5

Bridging the Gap Between Adversarial Robustness and Optimization Bias

The third and last problem studied in this thesis concerns adversarial robustness in deep learning. We hypothesize that robustness depends on the explicit training mechanisms and their implicit biases. The implication is that optimization choices not only impact the speed of training, computational resource requirements, and generalization performance but also indirectly affect the security and robustness of the models.

We demonstrate that the choice of optimizer, neural network architecture, and regularizer significantly affect the adversarial robustness of linear neural networks, providing guarantees without the need for adversarial training. To this end, we revisit a known result linking maximally robust classifiers and minimum norm solutions, and combine it with recent results on the implicit bias of optimizers. First, we show that, under certain conditions, it is possible to achieve both perfect standard accuracy and a certain degree of robustness, simply by training an overparametrized model using the implicit bias of the optimization. In that regime, there is a direct relationship between the type of the optimizer and the attack to

which the model is robust. To the best of our knowledge, this work is the first to study the impact of optimization methods such as sign gradient descent and proximal methods on adversarial robustness. Second, we characterize the robustness of linear convolutional models, showing that they resist attacks subject to a constraint on the Fourier- ℓ_∞ norm. To illustrate these findings we design a novel Fourier- ℓ_∞ attack that finds adversarial examples with controllable frequencies. We evaluate Fourier- ℓ_∞ robustness of adversarially-trained deep CIFAR-10 models from the standard RobustBench benchmark and visualize adversarial perturbations.

The content of this chapter have appeared in the following publication:

- **Faghri, Fartash** and Goyal, Sven and Vasconcelos, Cristina and Fleet, David J. and Pedregosa, Fabian and Le Roux, Nicolas, “*Bridging the Gap Between Adversarial Robustness and Optimization Bias*”, Workshop on Security and Safety in Machine Learning Systems, International Conference on Learning Representations (ICLR), 2021.

To ensure reproducibility, our code is publicly available ¹.

5.1 Introduction

Deep neural networks achieve high accuracy on standard test sets, yet [196] showed that any natural input correctly classified by a neural network can be modified with adversarial perturbations. Such perturbations fool the network into misclassification, even when they are constrained to be imperceptible to humans. Adversarial training improves model robustness by augmenting the training set with adversarial perturbations [67] and can be interpreted as approximately solving a saddle-point problem [126]. Adversarial training is the state-of-the-art approach to adversarial robustness [70, 36] and alternative approaches are more likely to exhibit spurious robustness [203]. Nevertheless, adversarial training is computationally expensive compared to standard training, as it involves an alternating

¹ https://github.com/fartashf/robust_bias

optimization. Adversarial training also exhibits a trade-off between standard generalization and adversarial robustness. That is, it achieves improved *robust accuracy*, on adversarially perturbed data, at the expense of *standard accuracy*, the probability of correct predictions on natural data [204]. This adversarial robustness trade-off has been shown to be intrinsic in a number of toy examples [52], independent of the learning algorithm in some cases [176]. Alternatives to adversarial training have been proposed to reduce this trade-off, but a gap remains in practice [230].

Here we consider connections between the adversarial robustness trade-off and optimization biases in training overparametrized models. Deep learning models can often achieve interpolation, i.e., they have the capacity to exactly fit the training data [227]. Their ability to generalize well in such cases has been attributed to an implicit bias toward simple solutions [72, 77].

Our main contribution is to connect two large bodies of work on adversarial robustness and optimization bias. Focusing on models that achieve interpolation, we use the formulation of a *Maximally Robust Classifier* from robust optimization [12]. We theoretically demonstrate that the choice of optimizer (Corollary 1), neural network architecture (Corollary 2), and regularizer (Corollary 3), significantly affect the adversarial robustness of linear neural networks. Even for linear models, the impact of these choices had not been characterized precisely prior to our work. We observe that, in contrast to adversarial training, under certain conditions we can find maximally robust classifiers at no additional computational cost.

Based on our theoretical results on the robustness of linear convolutional models to Fourier attacks, we introduce a new class of attacks in the Fourier domain. In particular, we design the Fourier- ℓ_∞ attack and illustrate our theoretical results. Extending to non-linear models, we attack adversarially-trained deep models on CIFAR-10 from the RobustBench benchmark [36] and find low and high frequency adversarial perturbations by directly controlling spectral properties through Fourier constraints. This example demonstrates how understanding maximal robustness of linear models is a stepping stone to understanding and guaranteeing robustness of non-linear models.

5.2 No Trade-offs with Maximally Robust Classifiers

We start by defining adversarial robustness and the robustness trade-off in adversarial training. Then, [Section 5.2.1](#) provides an alternative formulation to adversarial robustness that avoids the robustness trade-off. Let $\mathcal{D} = \{(\mathbf{x}_i, y_i)\}_{i=1}^n$ denote a training set sampled i.i.d. from a distribution, where $\mathbf{x}_i \in \mathbb{R}^d$ are features and $y_i \in \{-1, +1\}$ are binary labels.² A binary classifier is a function $\varphi : \mathbb{R}^d \rightarrow \mathbb{R}$, and its prediction on an input \mathbf{x} is given by $\text{sign}(\varphi(\mathbf{x})) \in \{-1, +1\}$. The aim in supervised learning is to find a classifier that accurately classifies the training data and generalizes to unseen test data. One standard framework for training a classifier is Empirical Risk Minimization (ERM), $\arg \min_{\varphi \in \Phi} \mathcal{L}(\varphi)$, where $\mathcal{L}(\varphi) := \mathbb{E}_{(\mathbf{x}, y) \sim \mathcal{D}} \zeta(y\varphi(\mathbf{x}))$, Φ is a family of classifiers, and $\zeta : \mathbb{R} \rightarrow \mathbb{R}^+$ is a loss function that we assume to be strictly monotonically decreasing to 0, i.e., $\zeta' < 0$. Examples are the exponential loss, $\exp(-\hat{y}y)$, and the logistic loss, $\log(1 + \exp(-\hat{y}y))$, where \hat{y} , y are the model prediction and the ground-truth label.

Given a classifier, an adversarial perturbation $\boldsymbol{\delta} \in \mathbb{R}^d$ is any small perturbation that changes the model prediction, i.e., $\text{sign}(\varphi(\mathbf{x} + \boldsymbol{\delta})) \neq \text{sign}(\varphi(\mathbf{x}))$, $\|\boldsymbol{\delta}\| \leq \varepsilon$, where $\|\cdot\|$ is a norm on \mathbb{R}^d , and ε is an arbitrarily chosen constant. It is common to use norm-ball constraints to ensure perturbations are small (e.g., imperceptible in images) but other constraints exist [\[20\]](#). Commonly used are the ℓ_p norms, $\|\mathbf{v}\|_p = \left(\sum_{i=0}^{d-1} [\mathbf{v}]_i^p\right)^{1/p}$, where $[\mathbf{v}]_i$ denotes the i -th element of a vector \mathbf{v} , for $i = 0, \dots, d-1$. In practice, an adversarial perturbation, $\boldsymbol{\delta}$, is found as an approximate solution to the following optimization problem,

$$\max_{\boldsymbol{\delta}: \|\boldsymbol{\delta}\| \leq \varepsilon} \zeta(y\varphi(\mathbf{x} + \boldsymbol{\delta})). \quad (5.1)$$

Under certain conditions, closed form solutions exist to the optimization problem in [\(5.1\)](#). For example, [\[67\]](#) observed that the maximal ℓ_∞ -bounded adversarial perturbation against a linear model (i.e., one causing the maximum change in the output) is the sign gradient

² We restrict our theoretical analysis to binary classification but we expect direct extensions to multi-class classification.

direction scaled by ε .

[126] defined an adversarially robust classifier as the solution to the saddle-point optimization problem,

$$\arg \min_{\varphi \in \Phi} \mathbb{E}_{(\mathbf{x}, y) \sim \mathcal{D}} \max_{\delta: \|\delta\| \leq \varepsilon} \zeta(y\varphi(\mathbf{x} + \delta)). \quad (5.2)$$

The saddle-point adversarial robustness problem is the robust counter-part to empirical risk minimization where the expected loss is minimized on worst-case adversarial samples defined as solutions to (5.1). Adversarial Training [67] refers to solving (5.2) using an alternated optimization. It is computationally expensive because it often requires solving (5.1) many times.

The main drawback of defining the adversarially robust classifier using (5.2), and a drawback of adversarial training, is that the parameter ε needs to be known or tuned. The choice of ε controls a trade-off between standard accuracy on samples of the dataset \mathcal{D} versus the robust accuracy, i.e., the accuracy on adversarial samples. At one extreme $\varepsilon = 0$, where (5.2) reduces to ERM. At the other, as $\varepsilon \rightarrow \infty$, all inputs in \mathbb{R}^d are within the ε -ball of every training point and can be an adversarial input. The value of the inner max in (5.2) for a training point \mathbf{x}, y is the loss of the most confident prediction over \mathbb{R}^d that is predicted as $-y$. For large enough ε , the solution to (5.2) is a classifier predicting the most frequent label, i.e., $\varphi(\cdot) = p^*$, where p^* is the solution to $\arg \min_p n_{-1}\zeta(-p) + n_{+1}\zeta(p)$, and n_{-1}, n_{+1} are the number of negative and positive training labels.

Robust accuracy is often a complementary generalization metric to standard test accuracy. In practice, we prefer a classifier that is accurate on the test set, and that additionally, achieves maximal robustness. The saddle-point formulation makes this challenging without the knowledge of the maximal ε . This trade-off has been studied in various works [204, 230, 51, 52, 176]. Regardless of the trade-off imposed by ε , adversarial training is considered to be the state-of-the-art for adversarial robustness. The evaluation is based on the robust accuracy achieved at fixed ε 's even though the standard accuracy is usually lower than a comparable non-robust model [36, 70].

5.2.1 Maximally Robust Classifier

In order to avoid the trade-off imposed by ε in adversarial robustness, we revisit a definition from robust optimization.

Definition 5.2.1. A **Maximally Robust Classifier** ([12]) is a solution to

$$\arg \max_{\varphi \in \Phi} \{ \varepsilon \mid y_i \varphi(\mathbf{x}_i + \boldsymbol{\delta}) > 0, \forall i, \|\boldsymbol{\delta}\| \leq \varepsilon \}. \quad (5.3)$$

Compared with the saddle-point formulation (5.2), ε in (5.3) is not an arbitrary constant. Rather, it is maximized as part of the optimization problem. Moreover, the maximal ε in this definition does not depend on a particular loss function. Note, a maximally robust classifier is not necessarily unique.

The downside of (5.3) is that the formulation requires the training data to be separable so that (5.3) is non-empty, i.e., there exists $\varphi \in \Phi$ such that $\forall i, y_i \varphi(\mathbf{x}_i) > 0$. In most deep learning settings, this is not a concern as models are large enough that they can interpolate the training data, i.e., for any dataset there exists φ such that $\varphi(\mathbf{x}_i) = y_i$. An alternative formulation is to modify the saddle-point problem and include an outer maximization on ε by allowing a non-zero slack loss. However, the new slack loss reimposes a trade-off between standard and robust accuracy (See Appendix B.1).

One can also show that adversarial training, i.e., solving the saddle-point problem (5.2), does not necessarily find a maximally robust classifier. To see this, suppose we are given the maximal ε in (5.3). Further assume the minimum of (5.2) is non-zero. Then the cost in the saddle-point problem does not distinguish between the following two models: 1) a model that makes no misclassification errors but has low confidence, i.e., $\forall i, 0 < \max_{\boldsymbol{\delta}} y_i \varphi(\mathbf{x}_i + \boldsymbol{\delta}) \leq c_1$ for some small c_1 2) a model that classifies a training point, \mathbf{x}_j , incorrectly but is highly confident on all other training data and adversarially perturbed ones, i.e., $\forall i \neq j, 0 < c_2 < \max_{\boldsymbol{\delta}} y_i \varphi(\mathbf{x}_i + \boldsymbol{\delta})$. The second model can incur a loss $n\zeta(c_1) - (n-1)\zeta(c_2)$ on \mathbf{x}_j while being no worse than the first model according to the cost of the saddle-point problem. The reason is another trade-off between standard and robust

accuracy caused by taking the expectation over data points.

5.2.2 Linear Models: Maximally Robust is the Minimum Norm Classifier

Given a dataset and a norm, what is the maximally robust linear classifier with respect to that norm? In this section, we revisit a result from [12] for classification.

Definition 5.2.2 (Dual norm). Let $\|\cdot\|$ be a norm on \mathbb{R}^n . The associated *dual norm*, denoted $\|\cdot\|_*$, is defined as $\|\delta\|_* = \sup_{\mathbf{x}} \{|\langle \delta, \mathbf{x} \rangle| \mid \|\mathbf{x}\| \leq 1\}$.

Definition 5.2.3 (Linear Separability). We say a dataset is linearly separable if there exists \mathbf{w}, b such that $y_i(\mathbf{w}^\top \mathbf{x}_i + b) > 0$ for all i .

Lemma 5.2.1 (Maximally Robust Linear Classifier ([12], §12)). *For linear models and linearly separable data, the following problems are equivalent; i.e., from a solution of one, a solution of the other is readily found.*

$$\text{Maximally robust classifier: } \arg \max_{\mathbf{w}, b} \{\varepsilon \mid y_i(\mathbf{w}^\top (\mathbf{x}_i + \delta) + b) > 0, \forall i, \|\delta\| \leq \varepsilon\}, \quad (5.4)$$

$$\text{Maximum margin classifier: } \arg \max_{\mathbf{w}, b: \|\mathbf{w}\|_* \leq 1} \{\varepsilon \mid y_i(\mathbf{w}^\top \mathbf{x}_i + b) \geq \varepsilon, \forall i\}, \quad (5.5)$$

$$\text{Minimum norm classifier: } \arg \min_{\mathbf{w}, b} \{\|\mathbf{w}\|_* \mid y_i(\mathbf{w}^\top \mathbf{x}_i + b) \geq 1, \forall i\}. \quad (5.6)$$

The expression $\min_i y_i(\mathbf{w}^\top \mathbf{x}_i + b) / \|\mathbf{w}\|$ is the margin of a classifier \mathbf{w} that is the distance of the nearest training point to the classification boundary, i.e., the line $\{\mathbf{v} : \mathbf{w}^\top \mathbf{v} = -b\}$.

We provide a proof for general norms based on [12] in [Appendix B.2.1](#). Each formulation in [Lemma 5.2.1](#) is connected to a wide array of results that can be transferred to other formulations. Maximally robust classification is one example of a problem in robust optimization that can be reduced and solved efficiently. Other problems such as robust regression as well as robustness to correlated input perturbations have been studied prior to deep learning [12].

On the other hand, maximum margin and minimum norm classification have long been popular because of their generalization guarantees. Recent theories for overparametrized models link the margin and the norm of a model to generalization [77]. Although the tools are different, connecting the margin and the norm of a model has also been the basis of generalization theories for Support Vector Machines and AdaBoost [184, 199]. Maximum margin classification does not require linear separability, because there can exist a classifier with $\varepsilon < 0$ that satisfies the margin constraints. Minimum norm classification is the easiest formulation to work with in practice as it does not rely on ε nor δ and minimizes a function of the weights subject to a set of constraints.

In what follows, we use [Lemma 5.2.1](#) to transfer recent results about minimum norm classification to maximally robust classification. These results have been the basis for explaining generalization properties of deep learning models [77, 145].

5.3 Implicit Robustness of Optimizers

The most common approach to empirical risk minimization (ERM) is through gradient-based optimization. As we will review shortly, [72] showed that gradient descent, and more generally steepest descent methods, have an implicit bias towards minimum norm solutions. From the infinitely many solutions that minimize the empirical risk, we can characterize the one found by steepest descent. Using [Lemma 5.2.1](#), we show that such a classifier is also maximally robust w.r.t. a specific norm.

Recall that ERM is defined as $\arg \min_{\varphi \in \Phi} \mathcal{L}(\varphi)$, where $\mathcal{L}(\varphi) = \mathbb{E}_{(\mathbf{x}, y) \sim \mathcal{D}} \zeta(y\varphi(\mathbf{x}))$. Here we assume \mathcal{D} is a finite dataset of size n . For the linear family of functions, we write $\mathcal{L}(\mathbf{w}, b)$. Hereafter, we rewrite the loss as $\mathcal{L}(\mathbf{w})$ and use an augmented representation with a constant 1 dimension. For linearly separable data and overparametrized models ($d > n$), there exist infinitely many linear classifiers that minimize the empirical risk [72]. We will find it convenient to ignore the scaling and focus on the normalized vector $\mathbf{w}/\|\mathbf{w}\|$, i.e., the direction of \mathbf{w} . We will say that the sequence $\mathbf{w}_1, \mathbf{w}_2, \dots$ converges in direction to a vector

\mathbf{v} if $\lim_{t \rightarrow \infty} \mathbf{w}_t / \|\mathbf{w}_t\| = \mathbf{v}$.

5.3.1 Steepest Descent on Fully-Connected Networks

Definition 5.3.1 (Steepest Descent). Let $\langle \cdot \rangle$ denote an inner product and $\|\cdot\|$ its associated norm, f a function to be minimized, and γ a step size. The steepest descent method associated with this norm finds

$$\begin{aligned} \mathbf{w}_{t+1} &= \mathbf{w}_t + \gamma \Delta \mathbf{w}_t, \\ \text{where } \Delta \mathbf{w}_t &\in \arg \min_{\mathbf{v}} \langle \nabla f(\mathbf{w}_t), \mathbf{v} \rangle + \frac{1}{2} \|\mathbf{v}\|^2. \end{aligned} \quad (5.7)$$

The steepest descent step, $\Delta \mathbf{w}_t$, can be equivalently written as $-\|\nabla f(\mathbf{w}_t)\|_* g_{\text{nst}}$, where $g_{\text{nst}} \in \arg \min \{ \langle \nabla f(\mathbf{w}_t), \mathbf{v} \rangle \mid \|\mathbf{v}\| = 1 \}$. A proof can be found in [19, §9.4].

Remark. For some p -norms, steepest descent steps have closed form expressions. Gradient Descent (GD) is steepest descent w.r.t. ℓ_2 norm where $-\nabla f(\mathbf{w}_t)$ is a steepest descent step. Sign gradient descent is steepest descent w.r.t. ℓ_∞ norm where $-\|\nabla f(\mathbf{w}_t)\|_1 \text{sign}(\nabla f(\mathbf{w}_t))$ is a steepest descent step. Coordinate Descent (CD) is steepest descent w.r.t. ℓ_1 norm where $-\nabla f(\mathbf{w}_t)_i \mathbf{e}_i$ is a steepest descent step (i is the coordinate for which the gradient has the largest absolute magnitude).

Theorem 5.3.1 (Implicit Bias of Steepest Descent ([72] (Theorem 5))). *For any separable dataset $\{\mathbf{x}_i, y_i\}$ and any norm $\|\cdot\|$, consider the steepest descent updates from (5.7) for minimizing the empirical risk $\mathcal{L}(\mathbf{w})$ (defined in Section 5.2) with the exponential loss, $\zeta(z) = \exp(-z)$. For all initializations \mathbf{w}_0 , and all bounded step-sizes satisfying a known upper bound, the iterates \mathbf{w}_t satisfy*

$$\lim_{t \rightarrow \infty} \min_i \frac{y_i \mathbf{w}_t^\top \mathbf{x}_i}{\|\mathbf{w}_t\|} = \max_{\mathbf{w}: \|\mathbf{w}\| \leq 1} \min_i y_i \mathbf{w}^\top \mathbf{x}_i. \quad (5.8)$$

In particular, if a unique maximum margin classifier $\mathbf{w}_{\|\cdot\|}^ = \arg \max_{\mathbf{w}: \|\mathbf{w}\| \leq 1} \min_i y_i \mathbf{w}^\top \mathbf{x}_i$ exists, the limit direction converges to it, i.e., $\lim_{t \rightarrow \infty} \frac{\mathbf{w}_t}{\|\mathbf{w}_t\|} = \mathbf{w}_{\|\cdot\|}^*$.*

In other words, the margin converges to the maximum margin and if the maximum margin classifier is unique, the iterates converge in direction to $\mathbf{w}_{\|\cdot\|}^*$. We use this result to derive our [Corollary 1](#).

Corollary 1 (Implicit Robustness of Steepest Descent). *For any linearly separable dataset and any norm $\|\cdot\|$, steepest descent iterates minimizing the empirical risk, $\mathcal{L}(\mathbf{w})$, satisfying the conditions of [Theorem 5.3.1](#), converge in direction to a maximally robust classifier,*

$$\arg \max_{\mathbf{w}} \{ \varepsilon \mid y_i \mathbf{w}^\top (\mathbf{x}_i + \boldsymbol{\delta}) > 0, \forall i, \|\boldsymbol{\delta}\|_* \leq \varepsilon \}.$$

In particular, a maximally robust classifier against ℓ_1 , ℓ_2 , and ℓ_∞ is reached, respectively, by sign gradient descent, gradient descent, and coordinate descent.

Proof. By [Theorem 5.3.1](#), the margin of the steepest descent iterates, $\min_i \frac{y_i \mathbf{w}_t^\top \mathbf{x}_i}{\|\mathbf{w}_t\|}$, converges as $t \rightarrow \infty$ to the maximum margin, $\max_{\mathbf{w}: \|\mathbf{w}\| \leq 1} \min_i y_i \mathbf{w}^\top \mathbf{x}_i$. By [Lemma 5.2.1](#), any maximum margin classifier w.r.t. $\|\cdot\|$ gives a maximally robust classifier w.r.t. $\|\cdot\|_*$. \square

[Corollary 1](#) implies that for overparametrized linear models, we obtain guaranteed robustness by an appropriate choice of optimizer without the additional cost and trade-off of adversarial training. We note that [Theorem 5.3.1](#) and [Corollary 1](#), characterize linear models, but do not account for the bias b . We can close the gap with an augmented input representation, to include the bias explicitly. Or one could preprocess the data, removing the mean before training.

To extend [Corollary 1](#) to deep learning models one can use generalizations of [Theorem 5.3.1](#). For the special case of gradient descent, [Theorem 5.3.1](#) has been generalized to multi-layer fully-connected linear networks and a larger family of strictly monotonically decreasing loss functions including the logistic loss [[143](#), Theorem 2].

5.3.2 Gradient Descent on Linear Convolutional Networks

In this section, we show that even for linear models, the choice of the architecture affects implicit robustness, which gives another alternative for achieving maximal robustness. We

use a generalization of [Theorem 5.3.1](#) to linear convolutional models.

Definition 5.3.2 (Linear convolutional network). An L -layer convolutional network with 1-D circular convolution is parameterized using weights of $L - 1$ convolution layers, $\mathbf{w}_1, \dots, \mathbf{w}_{L-1} \in \mathbb{R}^d$, and weights of a final linear layer, $\mathbf{w}_L \in \mathbb{R}^d$, such that the linear mapping of the network is

$$\varphi_{\text{conv}}(\mathbf{x}; \mathbf{w}_1, \dots, \mathbf{w}_L) := \mathbf{w}_L^\top (\mathbf{w}_{L-1} \star \dots (\mathbf{w}_1 \star \mathbf{x})).$$

Here, circular convolution is defined as $[\mathbf{w} \star \mathbf{x}]_i := \frac{1}{\sqrt{d}} \sum_{k=0}^{d-1} [\mathbf{w}]_{\overline{-k}} [\mathbf{x}]_{\overline{i+k}}$, where $[v]_i$ denotes the i -th element of a vector \mathbf{v} for $i = 0, \dots, d-1$, and $\overline{i} = i \bmod d$.³

A linear convolutional network is equivalent to a linear model with weights $\mathbf{w} = \mathbf{w}_L \star (\dots \star (\mathbf{w}_2 \star \mathbf{w}_1))$ because of the associative property of convolution. In particular, for two-layer linear convolutional networks $\mathbf{w} = \mathbf{w}_2 \star \mathbf{w}_1$.

Definition 5.3.3 (Discrete Fourier Transform). $\mathcal{F}(\mathbf{w}) \in \mathbb{C}^d$ denotes the Fourier coefficients of \mathbf{w} where $[\mathcal{F}(\mathbf{w})]_d = \frac{1}{\sqrt{d}} \sum_{k=0}^{d-1} [\mathbf{w}]_k \exp(-\frac{2\pi j}{d} kd)$ and $j^2 = -1$.

Theorem 5.3.2 (Implicit Bias towards Fourier Sparsity ([\[73\]](#), Theorem 2, 2.a)). *Consider the family of L -layer linear convolutional networks and the sequence of gradient descent iterates, \mathbf{w}_t , minimizing the empirical risk, $\mathcal{L}(\mathbf{w})$, with the exponential loss, $\exp(-z)$. For almost all linearly separable datasets under known conditions on the step size and convergence of iterates, \mathbf{w}_t converges in direction to the classifier minimizing the norm of the Fourier coefficients given by*

$$\arg \min_{\mathbf{w}_1, \dots, \mathbf{w}_L} \{ \|\mathcal{F}(\mathbf{w})\|_{2/L} \mid y_i \langle \mathbf{w}, \mathbf{x}_i \rangle \geq 1, \forall i \}. \quad (5.9)$$

In particular, for two-layer linear convolutional networks the implicit bias is towards the solution with minimum ℓ_1 norm of the Fourier coefficients, $\|\mathcal{F}(\mathbf{w})\|_1$. For $L > 2$, the convergence is to a first-order stationary point.

³ We use the usual definition of circular convolution in signal processing, rather than cross-correlation, $\mathbf{w}^\dagger \star \mathbf{x}$ with $[v^\dagger]_i = [v]_{\overline{-i}}$, which is used in deep learning literature, but not associative.

Algorithm 4 Fourier- ℓ_∞ Attack (see [Appendix B.3](#))

Input: data \mathbf{x} , label y , loss function ζ , classifier φ , perturbation size ε , number of attack steps m , dimensions d , Fourier transform \mathcal{F}

for $k = 1$ **to** m **do**

$$\hat{\mathbf{g}} = \mathcal{F}(\nabla_{\mathbf{x}} \zeta(y\varphi(\mathbf{x})))$$

$$[\delta]_i = \varepsilon \frac{[\hat{\mathbf{g}}]_i}{|[\hat{\mathbf{g}}]_i|}, \forall i \in \{0, \dots, d-1\}$$

$$\mathbf{x} = \mathbf{x} + \mathcal{F}^{-1}(\delta)$$

We use this result to derive our [Corollary 2](#).

Corollary 2 (Maximally Robust to Perturbations with Bounded Fourier Coefficients). *Consider the family of two-layer linear convolutional networks and the gradient descent iterates, \mathbf{w}_t , minimizing the empirical risk. For almost all linearly separable datasets under conditions of [Theorem 5.3.2](#), \mathbf{w}_t converges in direction to a maximally robust classifier,*

$$\arg \max_{\mathbf{w}_1, \dots, \mathbf{w}_L} \{\varepsilon \mid y_i \varphi_{conv}(\mathbf{x}_i + \delta; \{\mathbf{w}_l\}_{l=1}^L) > 0, \forall i, \|\mathcal{F}(\delta)\|_\infty \leq \varepsilon\}.$$

Proof in [Appendix B.2.2](#). [Corollary 2](#) implies that, at no additional cost, linear convolutional models are already maximally robust, but w.r.t. perturbations in the Fourier domain. We call attacks with ℓ_p constraints in the Fourier domain *Fourier- ℓ_p* attacks. [Appendix B.6](#) depicts various norm-balls in 3D to illustrate the significant geometrical difference between the Fourier- ℓ_∞ and other commonly used norm-balls for adversarial robustness. One way to understand [Corollary 2](#) is to think of perturbations that succeed in fooling a linear convolutional network. Any such adversarial perturbation must have at least one frequency beyond the maximal robustness of the model. This condition is satisfied for perturbations with small ℓ_0 norm in the spatial domain, i.e., only a few pixels are perturbed and similarly by ℓ_1 norm perturbations as they are constrained to be more sparse than other ℓ_p norm perturbations. Sparse perturbations in the spatial domain can be dense in the Fourier domain.

5.3.3 Fourier Attacks

The predominant motivation for designing new attacks is to *fool* existing models. In contrast, our results characterize the attacks that existing models *perform best* against, as measured by maximal robustness. Based on [Corollary 2](#) we design the Fourier- ℓ_p attack to verify our results. Some adversarial attacks exist with Fourier constraints [\[206, 74\]](#). [\[183\]](#) proposed a Fourier- ℓ_p attack that includes Fourier constraints in addition to ℓ_p constraints in the spatial domain. Our theoretical results suggest a more general class of attacks with only Fourier constraints.

The maximal ℓ_p -bounded adversarial perturbation against a linear model in [\(5.1\)](#) consists of real-valued constraints with a closed form solution. In contrast, maximal Fourier- ℓ_p has complex-valued constraints. In [Appendix B.3](#) we derive the Fourier- ℓ_∞ attack in closed form for linear models and provide the pseudo-code in [Algorithm 4](#). To find perturbations as close as possible to natural corruptions such as blur, ε can be a matrix of constraints that is multiplied elementwise by δ . As our visualizations in [Fig. 5.1](#) show, adversarial perturbations under bounded Fourier- ℓ_∞ can be controlled to be high frequency and concentrated on subtle details of the image, or low frequency and global. We observe that high frequency Fourier- ℓ_∞ attacks succeed more easily with smaller perturbations compared with low frequency attacks. The relative success of our band-limited Fourier attacks matches the empirical observation that the amplitude spectra of common ℓ_p attacks are largely band-limited as such attacks succeed more easily [\[223\]](#).

5.4 Explicit Regularization

Above we discussed the impact of optimization method and model architecture on robustness. Here, we discuss explicit regularization as another choice that affects robustness.

Definition 5.4.1 (Regularized Classification). The regularized empirical risk minimization problem for linear classification is defined as

$$\hat{\mathbf{w}}(\lambda) = \arg \min_{\mathbf{w}} \mathbb{E}_{(x,y) \sim \mathcal{D}} \zeta(y\mathbf{w}^\top \mathbf{x}) + \lambda \|\mathbf{w}\|,$$

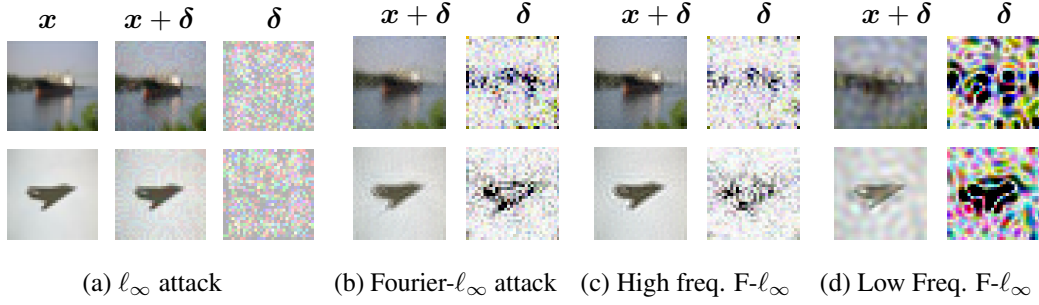


Figure 5.1: **Adversarial attacks (ℓ_∞ and Fourier- ℓ_∞) against CIFAR-10 classification models.** Fourier- ℓ_∞ perturbations (b) in the spatial domain are concentrated around subtle details of the object (darker means stronger perturbation). In contrast, ℓ_∞ perturbations (a) are perceived by people as random noise. Fourier- ℓ_∞ can also be controlled to be high or low frequency (c, d). It is more difficult to attack a standard model with only low frequency perturbations (for all attacks $\varepsilon = 8/255$ but for low frequency Fourier- ℓ_∞ $\varepsilon = 50/255$, otherwise attack fails). Appendix B.5.4 shows visualizations for variety of models in RobustBench.

where λ denotes a regularization constant, ζ is a monotone loss function, and \mathcal{D} is a dataset. For simplicity we assume this problem has a unique solution while the original ERM can have multiple solutions.

Theorem 5.4.1 (Maximum Margin Classifier using Regularization ([169], Theorem 2.1)). *Consider linearly separable finite datasets and monotonically non-increasing loss functions. Then as $\lambda \rightarrow 0$, the sequence of solutions, $\hat{w}(\lambda)$, to the regularized problem in Definition 5.4.1, converges in direction to a maximum margin classifier as defined in (5.5). Moreover, if the maximum margin classifier is unique,*

$$\lim_{\lambda \rightarrow 0} \frac{\hat{w}(\lambda)}{\|\hat{w}(\lambda)\|} = \arg \max_{w: \|w\| \leq 1} \min_i y_i w^\top x_i. \quad (5.10)$$

The original proof in [169] was given specifically for ℓ_p norms, however we observe that their proof only requires convexity of the norm, so we state it more generally. Quasi-norms such as ℓ_p for $p < 1$ are not covered by this theorem. In addition, the condition on the loss function is weaker than our strict monotonic decreasing condition as shown in [143, Appendix A].

We use this result to derive our [Corollary 3](#).

Corollary 3 (Maximally Robust Classifier via Infinitesimal Regularization). *For linearly separable data, under conditions of [Theorem 5.4.1](#), the sequence of solutions to regularized classification problems converges in direction to a maximally robust classifier. That is, $\lim_{\lambda \rightarrow 0} \hat{\mathbf{w}}(\lambda) / \|\hat{\mathbf{w}}(\lambda)\|$ converges to a solution of $\arg \max_{\mathbf{w}} \{\varepsilon \mid y_i \mathbf{w}^\top (\mathbf{x}_i + \boldsymbol{\delta}) > 0, \forall i, \|\boldsymbol{\delta}\|_* \leq \varepsilon\}$.*

Proof. By [Theorem 5.4.1](#), the margin of the sequence of regularized classifiers, $\min_i y_i \frac{\hat{\mathbf{w}}(\lambda)^\top \mathbf{x}_i}{\|\hat{\mathbf{w}}(\lambda)\|}$, converges to the maximum margin, $\max_{\mathbf{w}: \|\mathbf{w}\| \leq 1} \min_i y_i \mathbf{w}^\top \mathbf{x}_i$. By [Lemma 5.2.1](#), any maximum margin classifier w.r.t. $\|\cdot\|$ gives a maximally robust classifier w.r.t. $\|\cdot\|_*$. \square

Assuming the solution to the regularized problem is unique, the regularization term replaces other implicit biases in minimizing the empirical risk. The regularization coefficient controls the trade-off between robustness and standard accuracy. The advantage of this formulation compared with adversarial training is that we do not need the knowledge of the maximally robust ε to find a maximally robust classifier. It suffices to choose an infinitesimal regularization coefficient. [\[215, Theorem 4.1\]](#) generalized [Theorem 5.4.1](#) for a family of classifiers that includes fully-connected networks with ReLU non-linearities, which allows for potential extension of [Corollary 3](#) to non-linear models. There remain gaps in this extension (see [Appendix B.4](#)).

Explicit regularization has been explored as an alternative approach to adversarial training [\[81, 190, 230, 158, 75\]](#). To be clear, we do not propose a new regularization method but rather, we provide a framework for deriving and guaranteeing the robustness of existing and future regularization methods.

5.5 Experiments

This section empirically compares approaches to finding maximally robust classifiers. [Section 5.5.3](#) evaluates the robustness of CIFAR-10 [\[105\]](#) image classifiers against our Fourier- ℓ_∞ attack. We implement our attack in AutoAttack [\[35\]](#) and evaluate the robustness of

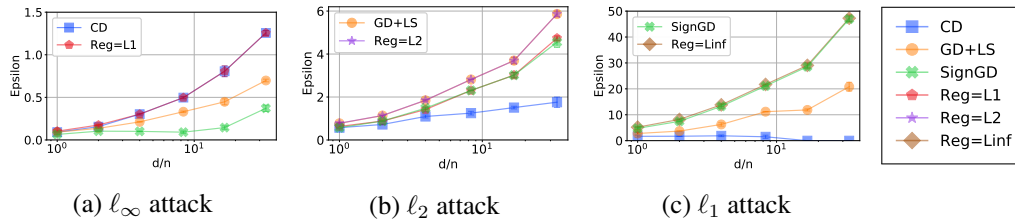


Figure 5.2: **Maximally robust perturbation size (ε) for linear models against ℓ_∞ , ℓ_2 , and ℓ_1 attacks.** For each attack, there exists one optimizer and one regularization method that finds a maximally robust classifier (inner legends). We compare Coordinate Descent (CD), Gradient Descent with Line Search (GD+LS), Sign Gradient Descent (SignGD), and explicit ℓ_1 , ℓ_2 , and ℓ_∞ regularization. The gap between methods grows with the overparametrization ratio (d/n). (More figures in [Appendix B.5.3](#))

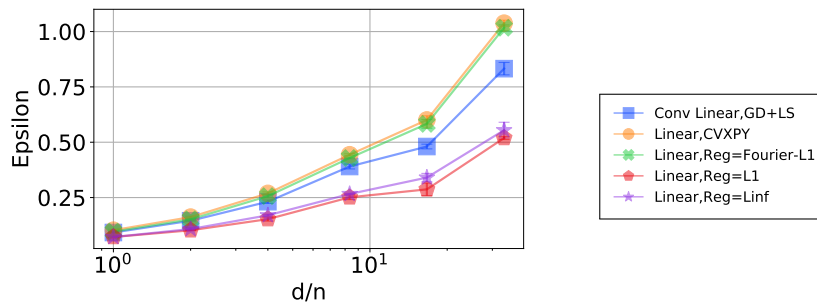


Figure 5.3: **Maximally robust ε against Fourier- ℓ_∞ attack.** Explicit Fourier- ℓ_1 regularization finds a maximally robust classifier as it achieves similar robustness as CVXPY’s solution. A linear convolutional model converges to a solution but a small gap exists.

recent defenses available in RobustBench [36]. Details of the experiments and additional visualizations are in [Appendix B.5](#).

5.5.1 Maximally Robust to ℓ_∞ , ℓ_2 , ℓ_1 , and Fourier- ℓ_∞ Bounded Attacks

[Fig. 5.2](#) and [5.3](#) plot the maximally robust ε as a function of the overparametrization ratio d/n , where d is the model dimension and n is the number of data points. [Fig. 5.2](#) shows robustness against ℓ_∞ , ℓ_2 , and ℓ_1 attacks for linear models. Coordinate descent and explicit ℓ_1 regularization find a maximally robust ℓ_∞ classifier. Gradient descent and ℓ_2 regularization find a maximally robust ℓ_2 classifier. Sign gradient descent and ℓ_∞ regularization find a maximally robust ℓ_1 classifier. The gap between margins grows as d/n increases. [Fig. 5.3](#)

shows robustness against Fourier- ℓ_∞ attack; training a 2-layer linear convolutional network with gradient descent converges to a maximally robust classifier. A gap exists between the linear convolutional network and the maximally robust classifier that should theoretically disappear with training budget greater than what we have used.

For these plots we synthesized linearly separable data focusing on overparametrized classification problems (i.e., $d > n$). Plotting the overparametrization ratio shows how robustness changes as models become more complex. We compare models by computing the maximal ε against which they are robust, or equivalently, the margin for linear models, $\min_i y_i \mathbf{w}^\top \mathbf{x}_i / \|\mathbf{w}\|$. As an alternative to the margin, we estimate the maximal ε for a model by choosing a range of potential values, generating adversarial samples, and finding the largest value against which the classification error is zero. Generating adversarial samples involves optimization, and requires more implementation detail compared with computing the margin. Plots in this section are based on generating adversarial samples to match common practice in the evaluation of non-linear models. Matching margin plots are presented in [Appendix B.5.3](#), which compare against the solution found using CVXPY [42] and adversarial training given the maximal ε . Our plots depict mean and error bars for 3 random seeds.

5.5.2 Plotting the Trade-offs

[Fig. 5.4](#) illustrates the trade-off between standard accuracy and adversarial robustness. Adversarial training finds the maximally robust classifier only if it is trained with the knowledge of the maximally robust ε ([Fig. 5.4a](#)). Without this knowledge, we have to search for the maximal ε by training multiple models. This adds further computational complexity to adversarial training which performs an alternated optimization. In contrast, explicit regularization converges to a maximally robust classifier for a small enough regularization constant ([Fig. 5.4b](#)).

On CIFAR-10, we compare adversarial training with the regularization method TRADEs [230] following the state-of-the-art best practices [70]. Both methods depend on a constant ε

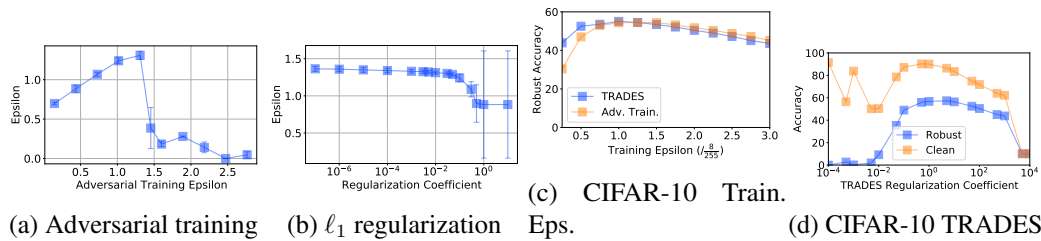


Figure 5.4: **Trade-off in robustness against ℓ_∞ attack in linear models and CIFAR-10.** We plot the maximally robust ε for adversarial training and explicit regularization. Robustness is controlled using ε in adversarial training (a) and regularization coefficient in explicit regularization (b). Using adversarial training we have to search for the maximal ε but for explicit regularization it suffices to choose a small regularization coefficient. Similarly, on CIFAR-10, the highest robustness at a fixed test ε is achieved for ε used during training (c). In contrast to optimal linear regularizations, TRADES shows degradation as the regularization coefficient decreases (d). Discussion in [Section 5.5.2](#)

during training. [Fig. 5.4c](#) shows optimal robustness is achieved for a model trained and tested with the same ε . When the test ε is unknown, both methods need to search for the optimal ε . Given the optimal training ε , [Fig. 5.4d](#) investigates whether TRADES performs similar to an optimal linear regularization (observed in [Fig. 5.4b](#)), that is the optimal robustness is achieved with infinitesimal regularization. In contrast to the linear regime, the robustness degrades with smaller regularization. We hypothesize that with enough model capacity, using the optimal ε , and sufficient training iterations, smaller regularization should improve robustness. That suggests that there is potential for improvement in TRADES and better understanding of robustness in non-linear models.

5.5.3 CIFAR-10 Fourier- ℓ_∞ Robustness

[Fig. 5.5](#) reports the maximally robust ε of image classification models on CIFAR-10. We evaluate top defenses on the leaderboard of RobustBench [\[36\]](#). The attack methods are APGD-CE and APGD-DLR with default hyper-parameters in RobustBench and $\varepsilon = 8/255$. Theoretical results do not provide guarantees beyond the maximally robust ε . Even robust models against corruptions with no adversarial training achieve similar robustness to ℓ_2/ℓ_∞ models. The maximal ε is the largest at which adversarial accuracy is no more than 1%

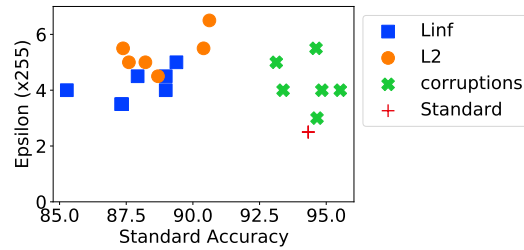


Figure 5.5: **Maximally robust ε against Fourier- ℓ_∞ for recent defenses.** Color and shape denote the type of robust training: adversarial (ℓ_2 or ℓ_∞), corruptions, or standard training. Fourier- ℓ_∞ is a strong attack against current robust models.

worse than the standard accuracy. All models have almost zero accuracy against larger, but still perceptually small, perturbations ($\varepsilon = 20/255$). [Appendix B.5.4](#) gives more examples of Fourier- ℓ_∞ attacks and band-limited variations similar to [Fig. 5.1](#) for robustly trained models, showing that perturbations are qualitatively different from those against the standard model.

5.6 Related work

This paper bridges two bodies of work on adversarial robustness and optimization bias. As such there are many related works, the most relevant of which we discuss here. Prior works either did not connect optimization bias to adversarial robustness beyond margin-maximization [[124](#), [43](#), [47](#)] or only considered adversarial training with a given perturbation size [[114](#)].

Robustness Trade-offs Most prior work defines the metric for robustness and generalization using an expectation over the loss. Instead, we define robustness as a set of classification constraints. Our approach better matches the security perspective that even a single inaccurate prediction is a vulnerability. The limitation is explicit constraints only ensure perfect accuracy near the training set. Standard generalization remains to be studied using other approaches such as those with assumptions on the data distribution. Existing work has used assumptions about the data distribution to achieve explicit trade-offs between robustness and

standard generalization [44, 89, 90, 161, 204, 230, 176, 51, 52].

Fourier Analysis of Robustness. Various observations have been made about Fourier properties of adversarial perturbations against deep non-linear models [87, 206, 183]. [223] showed that adversarial training increases robustness to perturbations concentrated at high frequencies and reduces robustness to perturbations concentrated at low frequencies. [153] also observed that the measured margin of classifiers at high frequencies is larger than the margin at low frequencies. Our **Corollary 2** does not distinguish between low and high frequencies but we establish an exact characterization of robustness. [24] hypothesized about the implicit robustness to ℓ_1 perturbations in the Fourier domain while we prove maximal robustness to Fourier- ℓ_∞ perturbations.

Architectural Robustness. An implication of our results is that robustness can be achieved at a lower computational cost compared with adversarial training by various architectural choices as recently explored [222, 58, 9]. Moreover, for architectural choices that align with human biases, standard generalization can also improve [208]. Another potential future direction is to rethink ℓ_p robustness as an architectural bias and find inspiration in the human visual system for appropriate architectural choices.

Robust Optimization A robust counterpart to an optimization problem considers uncertainty in the data and optimizes for the worst-case. [12] provided extensive formulations and discussions on robust counterparts to various convex optimization problems. Adversarial robustness is one such robust counterpart and many other robust counterparts could also be considered in deep learning. An example is adversarial perturbations with different norm-ball constraints at different training inputs. [126] observed the link between robust optimization and adversarial robustness where the objective is a min-max problem that minimizes the worst-case loss. However, they did not consider the more challenging problem of maximally robust optimization that we revisit.

Implicit bias of optimization methods. In [Section 2.1.7](#) we discussed prior work on the implicit bias of optimization methods. Here we revisit prominent works and explain the connection to this chapter.

Minimizing the empirical risk for an overparametrized model with more parameters than the training data has multiple solutions. [\[228\]](#) observed that overparametrized deep models can even fit to randomly labeled training data, yet given correct labels they consistently generalize to test data. This behavior has been explained using the implicit bias of optimization methods towards particular solutions. [\[72\]](#) proved that minimizing the empirical risk using steepest descent and mirror descent have an implicit bias towards minimum norm solutions in overparametrized linear classification. [\[73\]](#) proved the implicit bias of gradient descent in training linear convolutional classifiers is towards minimum norm solutions in the Fourier domain that depends on the number of layers.

Recent theory of generalization in deep learning, in particular the double descent phenomenon, studies the generalization properties of minimum norm solutions for finite and noisy training sets [\[77\]](#). Characterization of the double descent phenomenon relies on the implicit bias of optimization methods while using additional assumptions about the data distribution. In contrast, our results only rely on the implicit bias of optimization and hence are independent of the data distribution.

Hypotheses. [\[67\]](#) proposed the linearity hypothesis that informally suggests ℓ_p adversarial samples exist because deep learning models converge to functions similar to linear models. To improve robustness, they argued models have to be more non-linear. Based on our framework, linear models are not inherently weak. When trained, regularized, and parametrized appropriately they can be robust to some degree, the extent of which depends on the dataset. [\[60\]](#) proposed adversarial spheres as a toy example where a two layer neural network exists with perfect standard and robust accuracy for non-zero perturbations. Yet, training a randomly initialized model with gradient descent and finite data does not converge to a robust model. Based on our framework, we interpret this as an example where the

implicit bias of gradient descent is not towards the ground-truth model, even though there is no misalignment in the architecture. It would be interesting to understand this implicit bias in future work.

Robustness to ℓ_p -bounded attacks. Robustness is achieved when any perturbation to natural inputs that changes a classifier’s prediction also confuses a human. ℓ_p -bounded attacks are the first step in achieving adversarial robustness. [203] have recently shown many recent robust models only achieve spurious robustness against ℓ_∞ and ℓ_1 attacks. [35] showed that on image classification datasets there is still a large gap in adversarial robustness to ℓ_p -bounded attacks and standard accuracy. Robustness to multiple ℓ_p -bounded perturbations through adversarial training and its trade-offs has also been analyzed [202, 127]. [182, 180] argue that none of ℓ_0 , ℓ_1 , ℓ_∞ , or SSIM are a perfect match for human perception of similarity. That is for any such norm, for any ε , there exists a perturbation such that humans classify it differently. Attacks based on other perceptual similarity metrics exist [234, 119]. This shows that the quest for adversarial robustness should also be seen as a quest for understanding human perception.

Robustness through Regularization Various regularization methods have been proposed for adversarial robustness that penalize the gradient norm and can be studied using the framework of maximally robust classification. [121] proposed general ℓ_p norm regularization of gradients. [81] proposed the Cross-Lipschitz penalty by regularizing the norm of the difference between two gradient vectors of the function. [168] proposed ℓ_2 regularization of the norm of the gradients. [190] performed regularization of Frobenius norm of the per-layer Jacobian. [139] proposed penalizing the curvature of the loss function. [158] proposed encouraging local linearity by penalizing the error of local linearity. [186] proposed regularization of the gradient norm where the dual norm of the attack norm is used. [123] proposed Hessian regularization. [75] showed that some regularization methods are equivalent or perform similarly in practice. Strong gradient or curvature regularization methods can suffer from gradient masking [123].

Certified Robustness. Adversarially trained models are empirically harder to attack than standard models. But their robustness is not often provable. Certifiably robust models seek to close this gap [81, 218, 34, 69, 173]. A model is certifiably robust if for any input, it also provides an ε -certificate that guarantees robustness to any perturbation within the ε -ball of the input. In contrast, a maximally robust classifier finds a classifier that is guaranteed to be robust to maximal ε while classifying all training data correctly. That allows for data dependent robustness guarantees at test time. In this work, we have not explored standard generalization guarantees.

5.6.1 Investigating the Gap in the Convergence of Linear Convolutional Networks

We further investigated the gap between theory and experiment in Fig. 5.3, and our results are consistent with the observations of [226, Section 6]. The gap appears to be due to finite training time and it depends on the scale of the initialization and the learning rate. We were able to eliminate the gap for low dimensional problems (e.g., $d = 2$) by tuning the initialization scale. For high-dimensional problems (e.g., $d = 100$), it is more challenging to find the optimal initialization scale. As suggested by [226], this is an important problem for future work of implicit optimization bias literature.

For completeness, we did test different aspects of our implementation to rule out other causes. Here is a list of potential causes we eliminated:

- The scaling of the DFT matrix is accurate for comparison with the minimum-norm Fourier- ℓ_1 solution.
- Numerical error does not seem to contribute to the gap as we do not see an improvement by switching from Float32 to Float64.
- We thoroughly tested our implementation of the convolution operation and linearization operation.

5.7 Conclusion

We demonstrated that the choice of optimizer, neural network architecture, and regularizer, significantly affect the adversarial robustness of linear neural networks. These results lead us to a novel Fourier- ℓ_∞ attack with controllable spectral properties applied against deep non-linear CIFAR-10 models. Our results provide a framework, insights, and directions for improving robustness of non-linear models through approaches other than adversarial training.

In the following, we summarize the hypotheses, results, and future work:

- We revisited the definition of Maximally Robust Classification and justified as a formulation of the problem of finding adversarially robust models. We argue that Maximally Robust Classification is an alternative problem formulation possibly more challenging to solve than standard min-max formulation of adversarial robustness. There is also no ambiguity in the choice of hyper-parameters in the formulation of the Maximally Robust Classifier.
- For linear models, we prove guaranteed maximal robustness achieved only by the choice of the optimizer, regularization, or architecture. We have achieved this through our Corollaries. For example, because of our results, it can no longer be claimed that “A regularization method alone cannot achieve maximal robustness”. At least in the linear case we showed that such a regularizer exists.
- We rigorously established the adversarial robustness of linear convolutional neural networks in the Fourier domain. In that direction our novel Fourier attack creates one potential direction for understanding the robustness of non-linear models.
- We prove that under certain conditions no additional per-iteration cost of solving an optimization problem is needed, yet such a solution might take many iterations to find. We have not done computational analysis of the methods studied in this chapter which can be done with additional assumptions on the data distribution. Our results only

require linear separability of the data.

- We have not proposed a novel defense for non-linear models. We discuss future directions and challenges in [Section 5.6](#) and [Appendix B.4](#). In particular, there is a growing literature on the implicit bias of non-linear networks that can be used to extend our results [[32](#), [122](#), [151](#)]. Non-linear solutions might require significantly different mathematical tools and efforts from a wider community and take years to find.
- We do not claim that robustness guarantees achieved through the choice of the optimizer, architecture, or regularization are sufficient for any given model family, task or domain of application. For example, if the data is not linearly separable, additional sacrifices need to be made (See [Appendix B.1](#)). Having said that, efficiently finding the maximally robust classifier for deep non-linear models might be achievable by appropriate choices of all these in addition to adversarial training with an appropriate epsilon.
- There is a small gap in [Fig. 5.3](#) between theory and experiment that might be due to a missing condition in the original theory of [[73](#)]. We have provided additional discussion in [Section 5.6.1](#).

Chapter 6

Conclusion and Future Work

In this thesis we discussed ideas for improving training efficiency and connections to robustness in deep learning. [Chapter 3](#) showed that hard negatives are better than uniformly sampled negatives; they result in faster training and better generalization. [Chapter 4](#) proposed gradient clustering to reduce the gradient variance by automatically discovering and exploiting data diversity. The mixed results revealed gaps in our understanding of training deep learning models. Finally, [Chapter 5](#) establishes a connection between robustness and optimization choices and shows that the two challenges are closely related.

What is the most efficient and robust training method in deep learning? This remains an open question for us. Various approaches focus on improving training efficiency and standard generalization but lack attention to adversarial robustness and biased data distributions. Interesting and vibrant approaches include few-shot learning, transfer learning, and meta learning [[83](#), [211](#), [54](#)]. On the other hand, contrastive learning and adversarial learning [[76](#), [66](#)] are designed with only the objective of robustness to adversarial inputs or preset data transformations.

Our observations in [Chapter 3](#) are in favor of adversarial and robust representation learning approaches. Hard negatives in triplet losses are examples are adversarial inputs where only inputs in the training set define the natural data distribution. Adversarial learning and contrastive learning methods might also benefit from a similar observation that semi-

hard negatives provide superior generalization than absolute hard negatives. Curriculum learning [14] might provide more adjustable contrastive and adversarial samples. Learning multi-modal embeddings remain particularly propitious for efficient hard negative-based methods with no need for curriculum learning or generative adversarial networks [29, 213, 8].

Our results in Chapter 5 suggest an alternative or complementary approach by design. Instead of adversarial learning, under certain conditions, similar solutions can be found by appropriate architecture, optimizer and regularizer. The right architecture, e.g., convolution versus fully-connected neural networks, would significantly reduce the amount of adversarial training required. In some cases, adversarial training may become unnecessary.

In conclusion, this thesis raises more questions than it answers. What follows are some possible directions for further research on related problems.

In Chapter 5 we discuss the problem of maximally robust classification through which we transferred results on implicit and explicit bias of optimization methods to adversarial robustness. There is potential in extending this connection to transfer results in both directions. One example is to transfer provable guarantees for deep non-linear models to infer the implicit bias of various optimization methods that have not yet been derived. Exploiting the connection in the opposite direction, there have been recent results on the implicit bias of ReLU networks and the directional convergence of deep linear networks that imply further maximal robustness results.

In Chapter 4 we designed an efficient gradient clustering method. An application of gradient clustering is in automatically detecting imbalanced data according to gradient information and modifying the sampling to adjust and calibrate training. For example, by changing the learning paradigm from Empirical Risk Minimization to Distributionally Robust Optimization we should be able to formalize the design of distributionally robust sampling methods. Worst-group error is an evaluation metric commonly used in distributionally robust optimization that is a robust counterpart to the average error in expected risk minimization. In SGD with gradient clustering we used a reweighting to achieve unbiased gradient estimates

that would guarantee convergence to the same optimum as SGD with uniform sampling. Recently it has been shown that upweighting the minority class negatively impacts the minority error while subsampling the majority class improves it [171]. Inspired by this observation one might consider gradient clustering for distributionally robust optimization without reweighting samples. The gradient clustering sampler would then intrinsically find majority groups of data and sample the same number for all majority and minority groups.

An extension to both Chapters 4 and 5 is to understand the implications of implicit bias in continual and lifelong learning. Continual learning is a challenging task in machine learning restricted by catastrophic forgetting in training and lack of backward and forward transfer. In continual learning and for memoryless methods, we can describe the impact of prior learning tasks as a change in the initialization of the future learnings. Based on the prior work discussed in Chapter 5, we know in certain problems, the initialization changes the solution found. It is possible to connect the implicit bias and initialization for sequential linear regression tasks and design an optimal method of initialization depending on the similarity of tasks. Extending this idea to continual learning benchmarks is an interesting future direction.

Another extension to Chapter 5 is to characterize the implicit robustness of preconditioned optimization methods [4]. The implicit bias of preconditioned methods is different from gradient descent and depends on how the preconditioning is estimated. The alternative implicit bias results in an alternative implicit robustness that may be allow robustness to a new family of practical adversarial perturbations.

Finally, in adversarial learning and contrastive learning, the performance depends on the strength of adversarial inputs and data augmentations [31]. One possible direction for future work is the exact characterization of the dependence on adversarial strength in simple learning settings that would allow better justifications and recipes for curriculum learning. Gradient-aware methods such as variations of gradient clustering proposed in Chapter 4 should be useful in the direction of adversarial and contrastive learning as recent work corroborates [125].

Appendix A

Appendices to the Chapter on Gradient Clustering

A.1 Additional Details of Gradient Clustering

A.1.1 Proof of **Proposition 4.3.1**

The gradient estimator, $\hat{\mathbf{g}}$, is unbiased for any partitioning of data, i.e., equal to the average gradient of the training set,

$$\mathbb{E}[\hat{\mathbf{g}}] = \frac{1}{N} \sum_{k=1}^K N_k \mathbb{E}[\mathbf{g}^{(k)}] = \frac{1}{N} \sum_{k=1}^K N_k \left(\frac{1}{N_k} \sum_{j=1}^{N_k} \mathbf{g}_j^{(k)} \right) = \frac{1}{N} \underbrace{\sum_{k=1}^K \sum_{j=1}^{N_k} \mathbf{g}_j^{(k)}}_{(*)} = \frac{1}{N} \sum_{i=1}^N \mathbf{g}_i = \mathbf{g},$$

where we use the fact that the expectation of a random sample drawn uniformly from a subset is equal to the expectation of the average of samples from that subset. Also note that the gradient of every training example appears once in (*).

Although partitioning does not affect the bias of $\hat{\mathbf{g}}$, it does affect the variance,

$$\mathbb{V}[\hat{\mathbf{g}}] = \frac{1}{N^2} \left(\sum_{i=1}^N N_k^2 \mathbb{V}[\mathbf{g}^{(k)}] + 2 \sum_{k=1}^K \sum_{\hat{k}=1}^{N_{\hat{k}}} N_k N_{\hat{k}} \mathbb{C}[\mathbf{g}^{(k)}, \mathbf{g}^{(\hat{k})}] \right) = \frac{1}{N^2} \sum_{k=1}^K N_k^2 \mathbb{V}[\mathbf{g}^{(k)}] \quad (\text{A.1})$$

where the variance is defined as the trace of the covariance matrix. Since we assume the training set is sampled i.i.d., the covariance between gradients of any two samples is zero. In a dataset with duplicate samples, the gradients of duplicates will be clustered into one cluster with zero variance if mingled with no other data points.

A.2 Additional Details of Efficient GC

A.2.1 Convolutional Layers

In neural networks, the convolution operation is performed as an inner product between a set of weights $\boldsymbol{\theta} \in \mathbb{R}^{h \times w \times \hat{I} \times O}$, namely kernels, by patches of size $h \times w$ in the input. Assuming that we have preprocessed the input by extracting patches, the gradient w.r.t. $\boldsymbol{\theta}$ is $\mathbf{g}_i = \sum_t \mathbf{g}_{b,t}$, $\mathbf{g}_{b,t} \in \mathbb{R}^{I \times O}$ is the gradient at the spatial location $t \in T$ and $I = h \times w \times \hat{I}$ is the flattened dimension of a patch. The gradient at spatial location t is computed as $\mathbf{g}_{b,t} = \mathbf{A}_{b,t} \mathbf{D}_{b,t}^\top$.

Like the fully-connected case, we use a rank-1 approximation to the cluster centers in a convolution layer, defining $\mathbf{C}_k = \mathbf{c}_k \mathbf{d}_k^\top$. As such, \mathcal{AU} steps are performed efficiently. For the \mathcal{A} step we rewrite $\text{vec}\{\mathbf{C}_k\} \odot \text{vec}\{\mathbf{g}_i\}$,

$$\text{vec}\{\mathbf{C}_k\} \odot \text{vec}\left\{\sum_t \mathbf{A}_{b,t} \mathbf{D}_{b,t}^\top\right\} = \sum_{u,v} (\mathbf{c}_{ku} \mathbf{d}_{kv}) \left(\sum_t \mathbf{A}_{btu} \mathbf{D}_{btv}\right) \quad (\text{A.2})$$

$$= \sum_t \left(\sum_u \mathbf{c}_{ku} \mathbf{A}_{btu}\right) \left(\sum_v \mathbf{d}_{kv} \mathbf{D}_{btv}\right), \quad (\text{A.3})$$

where the input dimension is indexed by u and the output dimension is indexed by v . Eqs. [A.2](#) and [A.3](#) provide two ways of computing the inner-product, where we first compute the inner

Operation	FC Complexity	Conv Complexity
$\mathbf{C} \odot \mathbf{g}$	$KB(I + O)$	Eq. A.2: $B(T + K)IO$ Eq. A.3: $BTK(I + O)$
$\mathbf{C} \odot \mathbf{C}$	$K(I + O)$	$K(I + O)$
$\mathbf{g} \odot \mathbf{g}$	$B(I + O)$	Eq. A.2: $BTIO$, Eq. A.3: $BT^2(I + O)$
Back-prop	BIO	$BTIO$
\mathcal{A} step	$KB(I + O)$	See Sec. A.2.2
\mathcal{U} step	$B(I + O)$	$B(I + O)$

Table A.1: Complexity of GC compared to the cost of back-prop.

sums, then the outer sum. The efficiency of each formulation depends on the size of the kernel and layer’s input and output dimensions.

A.2.2 Complexity Analysis

GC, described in Fig. 4.2, performs two sets of operations, namely, the cluster center updates (\mathcal{U} step), and the assignment update of data to clusters (\mathcal{A} step). \mathcal{A} steps instantly affect the optimization by changing the sampling process. As such, we perform an \mathcal{A} step every few epochs and change the sampling right after. In contrast, the \mathcal{U} step can be done in parallel and more frequently than the \mathcal{A} step, or online using mini-batch updates. The cost of both steps is amortized over optimization steps.

Table A.1 summarizes the run-time complexity of GC compared to the cost of single SGD step. The \mathcal{U} step is always cheaper than a single back-prop step. The \mathcal{A} step is cheaper for fully-connected layers if $K < \min(I, O)$.

For convolutional layers, we have two ways to compute the terms in the \mathcal{A} step (Eqs. A.2 and A.3). For $\mathbf{C} \odot \mathbf{g}$, if $\min(T, K) < K < \min(I, O)$, Eq. A.3 is more efficient. For $\mathbf{g} \odot \mathbf{g}$, Eq. A.3 is more efficient if $T < \min(I, O)$. If $K < T$, both methods have lower complexity than a single back-prop step. If we did not have the N_k multiplier in the \mathcal{A} step, we could ignore the computation of the norm of the gradients, and hence further reduce the cost.

In common neural network architectures, the condition $K < T$ is easily satisfied as T in all layers is almost always more than 10 and usually greater than 100, while 10-100 clusters provides significant variance reduction. As such, the total overhead cost with an efficient implementation is at most $2\times$ the cost of a normal back-prop step. We can further reduce this cost by performing GC on a subset of the layers, e.g., one might exclude the lowest convolutional layers.

The total memory overhead is equivalent to increasing the mini-batch size by K samples as we only need to store rank-1 approximations to the cluster centers.

A.3 Additional Details for Experiments

The mini-batch size in GC and SVRG and the number of clusters in GC are the same as the mini-batch size in SG-B and the same as the mini-batch size used for training using SGD. To measure the gradient variance, we take snapshots of the model during training, sample tens of mini-batches from the training set (in case of GC, with stratified sampling), and measure the average variance of the gradients.

We measure the performance metrics (e.g., loss, accuracy and variance) as functions of the number of training iterations rather than wall-clock time. In other words, we do not consider computational overhead of different methods. In practice, such analysis is valid as long as the additional operations could be parallelized with negligible cost.

A.3.1 Experimental Details for Image Classification Models

On MNIST, our MLP model consists of three fully connected layers: layer1: $28 * 28 \times 1024$, layer2: 1024×1024 , layer3: 1024, 10. We use ReLU activations and no dropout in this MLP. We train all methods with learning rate 0.02, weight decay 5×10^{-4} , and momentum 0.5. On CIFAR-10, we train ResNet8 with no batch normalization layer and learning rate 0.01, weight decay 5×10^{-4} , and momentum 0.9 for 80000 iterations. We decay the learning rate at 40000 and 60000 iterations by a factor of 0.1. On CIFAR-100, we train ResNet32 starting

Dataset	Model	B	T	Log T	Estim T	U	GC T
MNIST	MLP	128	50000	500	50	2000	10
CIFAR-10	ResNet8	128	80000	500	50	20000	3
CIFAR-100	ResNet32	128	80000	500	50	20000	3
ImageNet	ResNet18	128	80000	1000	10	10000	3

Table A.2: Hyperparameters.

with learning rate 0.1. Other hyper-parameters are the same as in CIFAR-10. On ImageNet, we train ResNet18 starting with learning rate 0.1, weight decay 1×10^{-4} , and momentum 0.9. We use a similar learning rate schedule to CIFAR-10.

In [Appendix A.3.1](#) we list the following hyper-parameters: the interval of measuring gradient variance and normalized variance (Log T), number of gradient estimates used on measuring variance (Estim T), the interval of updating the control variate in SVRG and the clustering in GC (U), and the number of GC update iterations (GC T).

In plots for random features models, each point is generated by keeping h_s fixed at 1000 and varying N in the range $[0.1, 10]$. We average over 3 random seeds, 2 teacher hidden dimensions and 2 input dimensions (both $\times 0.1$ and $\times 10$ student hidden). We use mini-batch size 10 for SG-B, SVRG, and GC.

A rough estimate of the overparametrization coefficient (discussed in [Section 4.4.2](#)) for deep models is to divide the total number of parameters by the number of training data. On MNIST the coefficient is approximately 37 for CNN and 31 for MLP. On CIFAR-10 it is approximately 3 for ResNet8 and 9 for ResNet32. Common data augmentations increase the effective training set size by $10\times$. On the other hand, the depth potentially increases the capacity of models exponentially (cite the paper that theoretically says how many data points a model can memorize). As such, it is difficult to directly relate these numbers to the behaviours observed in RF models.

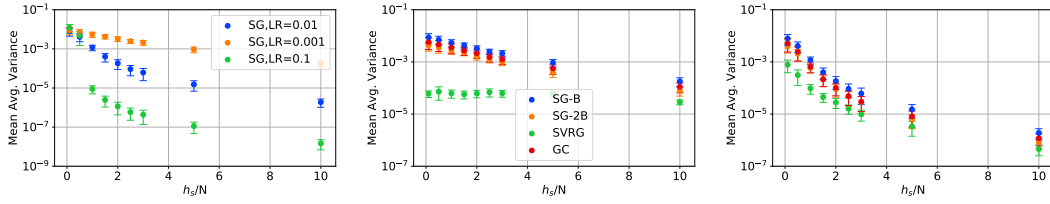


Figure A.1: Mean variance plots for Fig. 4.4

A.3.2 Experimental Details for Random Features Models

The number of training iterations is chosen such that the training loss has flattened. The maximum is taken over the last 70% of iterations (the variance is usually high for all methods in the first 30%). Mean variance plots for random features models are similar to max variance plots presented in Section 4.4.2.

We aggregate results from multiple experiments with the following range of hyperparameters. Each point is generated by keeping h_s fixed at 1000 and varying N in the range $[0.1, 10]$. We average over 3 random seeds, 2 teacher hidden dimensions and 2 input dimensions (both $\times 0.1$ and $\times 10$ student hidden).

A.4 Normalized Variance and Convergence Analysis

Normalized variance appears in standard convergence analysis of stochastic gradient descent [55]. To understand the connection, we briefly review a standard result. Let $f : \mathbb{R}^n \rightarrow \mathbb{R}$ be a L -Lipschitz continuous function, i.e.,

$$\|\nabla f(\mathbf{x}) - \nabla f(\mathbf{y})\| \leq L\|\mathbf{x} - \mathbf{y}\|, \forall \mathbf{x}, \mathbf{y} \in \mathbb{R}^n. \quad (\text{A.4})$$

Consider the stochastic gradient descent method with updates,

$$\mathbf{x}_{k+1} = \mathbf{x}_k - \alpha_k \mathbf{g}_k \quad (\text{A.5})$$

where α_k is the step size and

$$\mathbf{g}_k := \nabla f(\mathbf{x}_k) + \mathbf{e}_k \quad (\text{A.6})$$

is an estimate of the gradient with the residual \mathbf{e}_k .

For $\alpha_k = 1/L$, the iterates of stochastic gradient descent satisfy the inequality [55, Eq. 2.3]

$$f(\mathbf{x}_{k+1}) \leq f(\mathbf{x}_k) - \frac{1}{2L} \|\nabla f(\mathbf{x}_k)\|^2 + \frac{1}{2L} \|\mathbf{e}_k\|^2, \quad (\text{A.7})$$

Let $E[\mathbf{e}_k] = 0$, by subtracting $f(x_*)$ from both sides and taking expectations we have

$$\mathbb{E}[f(\mathbf{x}_{k+1}) - f(x_*)] \leq \mathbb{E}[f(\mathbf{x}_k) - f(x_*)] - \frac{1}{2L} \mathbb{E}[\|\nabla f(\mathbf{x}_k)\|^2] + \frac{1}{2L} \mathbb{E}[\|\mathbf{e}_k\|^2] \quad (\text{A.8})$$

$$\mathbb{E}[f(\mathbf{x}_{k+1}) - f(x_*)] \leq \mathbb{E}[f(\mathbf{x}_k) - f(x_*)] - \frac{1}{2L} \mathbb{E}[\|\nabla f(\mathbf{x}_k)\|^2] (1 - \zeta), \quad (\text{A.9})$$

where $\zeta = \mathbb{E}[\|\mathbf{e}_k\|^2] / \mathbb{E}[\|\nabla f(\mathbf{x}_k)\|^2]$ is the normalized variance of the residual and the gradient as defined in [Section 4.4](#).

If the normalized variance is small, i.e. $\zeta \ll 1$, the noise error is dominated by the non-stochastic error. As such, reducing the gradient variance would not speed up the training while for $1 \ll \zeta$, reducing the variance improves the convergence speed. This matches the diminishing returns observations in practice as we discuss in [Section 4.4](#).

Appendix B

Appendices to the Chapter on Bridging the Gap Chapter

B.1 Generalization of the Maximally Robust Classifier

Definition B.1.1 (Maximally Robust Classifier with Slack Loss). Let $\xi \geq 0$ denote a given slack variable. A maximally robust classifier with slack loss is the solution to

$$\arg \max_{\varphi \in \Phi} \left\{ \varepsilon \mid \mathbb{E}_{(\mathbf{x}, y)} \max_{\|\boldsymbol{\delta}\| \leq \varepsilon} \zeta(y\varphi(\mathbf{x} + \boldsymbol{\delta})) \leq \xi \right\}. \quad (\text{B.1})$$

This formulation is similar to the saddle-point problem in that we seek to minimize the expectation of the worst case loss. The difference is that we also seek to maximize ε . However, we have introduced another arbitrary variable ξ that is not optimized as part of the problem. For linear classifiers and the hinge loss, $\zeta(z) = [1 - z]_+$, [Eq. \(B.1\)](#) can be written as,

$$\arg \max_{\mathbf{w}} \left\{ \varepsilon \mid \mathbb{E}_{(\mathbf{x}, y)} [1 - y\mathbf{w}^\top \mathbf{x} + \varepsilon \|\mathbf{w}\|_*]_+ \leq \xi \right\}, \quad (\text{B.2})$$

where $[\cdot]_+$ is the hinge loss, and the weight penalty term $\|\mathbf{w}\|_*$ is inside the hinge loss. This subtle difference makes solving the problem more challenging than weight penalty outside

the loss.

Because of the two challenges we noted, we do not study the maximal robustness with slack loss.

B.2 Proofs

B.2.1 Proof of Lemma 5.2.1

Proof. We first show that the maximally robust classifier is equivalent to a robust counterpart by removing δ from the problem,

$$\begin{aligned}
& \arg \max_{\mathbf{w}, b} \{ \varepsilon \mid y_i(\mathbf{w}^\top(\mathbf{x}_i + \boldsymbol{\delta}) + b) > 0, \forall i, \|\boldsymbol{\delta}\| \leq \varepsilon \} \\
& \quad \text{(homogeneity of } p\text{-norm)} \\
& = \arg \max_{\mathbf{w}, b} \{ \varepsilon \mid y_i(\mathbf{w}^\top(\mathbf{x}_i + \varepsilon\boldsymbol{\delta}) + b) > 0, \forall i, \|\boldsymbol{\delta}\| \leq 1 \} \\
& \quad \text{(if it is true for all } \boldsymbol{\delta} \text{ it is true for the worst of them)} \\
& = \arg \max_{\mathbf{w}, b} \{ \varepsilon \mid \inf_{\|\boldsymbol{\delta}\| \leq 1} y_i(\mathbf{w}^\top(\mathbf{x}_i + \varepsilon\boldsymbol{\delta}) + b) > 0, \forall i \} \\
& = \arg \max_{\mathbf{w}, b} \{ \varepsilon \mid y_i(\mathbf{w}^\top \mathbf{x}_i + b) + \varepsilon \inf_{\|\boldsymbol{\delta}\| \leq 1} \mathbf{w}^\top \boldsymbol{\delta} > 0, \forall i \} \\
& \quad \text{(definition of dual norm)} \\
& = \arg \max_{\mathbf{w}, b} \{ \varepsilon \mid y_i(\mathbf{w}^\top \mathbf{x}_i + b) > \varepsilon \|\mathbf{w}\|_*, \forall i \}
\end{aligned}$$

Assuming $\mathbf{w} \neq 0$, which is a result of linear separability assumption, we can divide both sides by $\|\mathbf{w}\|_*$ and change variables,

$$= \arg \max_{\mathbf{w}, b} \{ \varepsilon \mid y_i(\mathbf{w}^\top \mathbf{x}_i + b) \geq \varepsilon, \forall i, \|\mathbf{w}\|_* \leq 1 \},$$

where we are also allowed to change $>$ to \geq because any solution to one problem gives an

equivalent solution to the other given $\mathbf{w} \neq 0$.

Now we show that the robust counterpart is equivalent to the minimum norm classification problem by removing ε . When the data is linearly separable there exists a solution with $\varepsilon > 0$,

$$\begin{aligned} & \arg \max_{\mathbf{w}, b} \{ \varepsilon \mid y_i(\mathbf{w}^\top \mathbf{x}_i + b) > \varepsilon \|\mathbf{w}\|_*, \forall i \} \\ &= \arg \max_{\mathbf{w}, b} \left\{ \varepsilon \mid y_i \left(\frac{\mathbf{w}^\top}{\varepsilon \|\mathbf{w}\|_*} \mathbf{x}_i + \frac{b}{\varepsilon \|\mathbf{w}\|_*} \right) \geq 1, \forall i \right\} \end{aligned}$$

This problem is invariant to any non-zero scaling of (\mathbf{w}, b) , so with no loss of generality we set $\|\mathbf{w}\|_* = 1$.

$$= \arg \max_{\mathbf{w}, b} \left\{ \varepsilon \mid y_i \left(\frac{\mathbf{w}^\top}{\varepsilon} \mathbf{x}_i + b \right) \geq 1, \forall i, \|\mathbf{w}\|_* = 1 \right\}$$

Let $\mathbf{w}' = \mathbf{w}/\varepsilon$, then the solution to the following problem gives a solution for \mathbf{w} ,

$$\begin{aligned} & \arg \max_{\mathbf{w}', b} \left\{ \frac{1}{\|\mathbf{w}'\|_*} \mid y_i(\mathbf{w}'^\top \mathbf{x}_i + b) \geq 1, \forall i \right\} \\ &= \arg \min_{\mathbf{w}', b} \left\{ \|\mathbf{w}'\|_* \mid y_i(\mathbf{w}'^\top \mathbf{x}_i + b) \geq 1, \forall i \right\}. \end{aligned}$$

□

B.2.2 Proof of Maximally Robust to Perturbations Bounded in Fourier Domain (Corollary 2)

The proof mostly follows from the equivalence for linear models in [Appendix B.2.1](#) by substituting the dual norm of Fourier- ℓ_1 . Here, \mathbf{A}^* denotes the complex conjugate transpose, $\langle \mathbf{u}, \mathbf{v} \rangle = \mathbf{u}^\top \mathbf{v}^*$ is the complex inner product, $[\mathbf{F}]_{ik} = \frac{1}{\sqrt{D}} \omega_D^{ik}$ the DFT matrix where $\omega_D = e^{-j2\pi/D}$, $j = \sqrt{-1}$.

Let $\|\cdot\|$ be a norm on \mathbb{C}^n and $\langle \cdot, \cdot \rangle$ be the complex inner product. Similar to \mathbb{R}^n , the associated dual norm is defined as $\|\delta\|_* = \sup_{\mathbf{x}} \{ |\langle \delta, \mathbf{x} \rangle| \mid \|\mathbf{x}\| \leq 1 \}$.

$$\begin{aligned}
& \|\mathcal{F}(\mathbf{w})\|_1 \\
&= \sup_{\|\boldsymbol{\delta}\|_\infty \leq 1} |\langle \mathcal{F}(\mathbf{w}), \boldsymbol{\delta} \rangle| \\
&\quad \text{(Expressing DFT as a linear transformation.)} \\
&= \sup_{\|\boldsymbol{\delta}\|_\infty \leq 1} |\langle \mathbf{F}\mathbf{w}, \boldsymbol{\delta} \rangle| \\
&= \sup_{\|\boldsymbol{\delta}\|_\infty \leq 1} |\langle \mathbf{w}, \mathbf{F}^* \boldsymbol{\delta} \rangle| \\
&\quad \text{(Change of variables and } \mathbf{F}^{-1} = \mathbf{F}^* \text{.)} \\
&= \sup_{\|\mathbf{F}\boldsymbol{\delta}\|_\infty \leq 1} |\langle \mathbf{w}, \boldsymbol{\delta} \rangle| \\
&= \sup_{\|\mathcal{F}(\boldsymbol{\delta})\|_\infty \leq 1} |\langle \mathbf{w}, \boldsymbol{\delta} \rangle|.
\end{aligned}$$

B.3 Linear Operations in Discrete Fourier Domain

Finding an adversarial sample with bounded Fourier- ℓ_∞ involves ℓ_∞ complex projection to ensure adversarial samples are bounded, as well as the steepest ascent direction w.r.t the Fourier- ℓ_∞ norm. We also use the complex projection onto ℓ_∞ simplex for proximal gradient method that minimizes the regularized empirical risk.

B.3.1 ℓ_∞ Complex Projection

Let \mathbf{v} denote the ℓ_2 projection of $\mathbf{x} \in \mathbb{C}^d$ onto the ℓ_∞ unit ball. It can be computed as,

$$\arg \min_{\|\mathbf{v}\|_\infty \leq 1} \frac{1}{2} \|\mathbf{v} - \mathbf{x}\|_2^2 \tag{B.3}$$

$$= \{\mathbf{v} : \forall i, \mathbf{v}_i = \arg \min_{|\mathbf{v}_i| \leq 1} \frac{1}{2} |\mathbf{v}_i - \mathbf{x}_i|^2\}, \tag{B.4}$$

that is independent projection per coordinate which can be solved by 2D projections onto ℓ_2 the unit ball in the complex plane.

B.3.2 Steepest Ascent Direction w.r.t. Fourier- ℓ_∞

Consider the following optimization problem,

$$\arg \max_{\mathbf{v}: \|\mathbf{F}\mathbf{v}\|_\infty \leq 1} f(\mathbf{v}), \quad (\text{B.5})$$

where $\mathbf{F} \in \mathbb{C}^{d \times d}$ is the Discrete Fourier Transform (DFT) matrix and $\mathbf{F}^* = \mathbf{F}^{-1}$ and \mathbf{F}^* is the conjugate transpose.

Normalized steepest descent direction is defined as (See [19, Section 9.4]),

$$\arg \min_{\mathbf{v}} \{ \langle \nabla f(\mathbf{w}), \mathbf{v} \rangle : \|\mathbf{v}\| = 1 \}. \quad (\text{B.6})$$

Similarly, we can define the steepest ascent direction,

$$\arg \max_{\mathbf{v} \in \mathbb{R}^d} \{ |\langle \nabla f(\mathbf{w}), \mathbf{v} \rangle| : \|\mathbf{F}\mathbf{v}\|_\infty = 1 \} \quad (\text{B.7})$$

$$(\text{Assuming } f \text{ is linear.}) \quad (\text{B.8})$$

$$\arg \max_{\mathbf{v} \in \mathbb{R}^d} \{ |\langle \mathbf{g}, \mathbf{F}^* \mathbf{F}\mathbf{v} \rangle| : \|\mathbf{F}\mathbf{v}\|_\infty = 1 \} \quad (\text{B.9})$$

$$\arg \max_{\mathbf{v} \in \mathbb{R}^d} \{ |\langle \mathbf{F}\mathbf{g}, \mathbf{F}\mathbf{v} \rangle| : \|\mathbf{F}\mathbf{v}\|_\infty = 1 \} \quad (\text{B.10})$$

where $\mathbf{g} = \nabla f(\mathbf{w})$.

Consider the change of variable $\mathbf{u} = \mathbf{F}\mathbf{v} \in \mathbb{C}^{d \times d}$. Since \mathbf{v} is a real vector its DFT is Hermitian, i.e., $\mathbf{u}_i^* = [\mathbf{u}]_{\bar{i}}$ for all coordinates i where $\bar{j} = j \pmod{d}$. Similarly, $\mathbf{F}\mathbf{g}$ is

Hermitian.

$$\arg \max_{\mathbf{u} \in \mathbb{C}^d: \|\mathbf{u}\|_\infty=1} \{|\langle \mathbf{F}\mathbf{g}, \mathbf{u} \rangle| : \mathbf{u}_i^* = [\mathbf{u}]_{-i}\} \quad (\text{B.11})$$

$$\arg \max_{\mathbf{u} \in \mathbb{C}^d: \forall i, |\mathbf{u}_i|=1} \{[|\mathbf{F}\mathbf{g}]_i \mathbf{u}_i| + |[\mathbf{F}\mathbf{g}]_{-i} \mathbf{u}_i^*| : \mathbf{u}_i^* = [\mathbf{u}]_{-i}\} \quad (\text{B.12})$$

$$\arg \max_{\mathbf{u} \in \mathbb{C}^d: \forall i, |\mathbf{u}_i|=1} \{[|\mathbf{F}\mathbf{g}]_i \mathbf{u}_i| + |[\mathbf{F}\mathbf{g}]_i^* \mathbf{u}_i^*| : \mathbf{u}_i^* = [\mathbf{u}]_{-i}\} \quad (\text{B.13})$$

$$\arg \max_{\mathbf{u} \in \mathbb{C}^d: \forall i, |\mathbf{u}_i|=1} \{[|\mathbf{F}\mathbf{g}]_i \mathbf{u}_i| : \mathbf{u}_i^* = [\mathbf{u}]_{-i}\} \quad (\text{B.14})$$

$$\mathbf{u}_i = [\mathbf{F}\mathbf{g}]_i / |[\mathbf{F}\mathbf{g}]_i|. \quad (\text{B.15})$$

and the steepest ascent direction is $\mathbf{v}_i = \mathbf{F}^{-1} \mathbf{u}_i$ which is a real vector. In practice, there can be non-zero small imaginary parts as numerical errors which we remove.

B.4 Non-linear Maximally Robust Classifiers

Recall that the definition of a maximally robust classifier ([Definition 5.2.1](#)) handles non-linear families of functions, Φ :

$$\arg \max_{\varphi \in \Phi} \{\varepsilon \mid y_i \varphi(\mathbf{x}_i + \boldsymbol{\delta}) > 0, \forall i, \|\boldsymbol{\delta}\| \leq \varepsilon\}.$$

Here we extend the proof in [Lemma 5.2.1](#) that made the maximally robust classification tractable by removing $\boldsymbol{\delta}$ and ε from the problem. In linking a maximally robust classifier to a minimum norm classifier when there exists a non-linear transformation, the first step that requires attention is the following,

$$\begin{aligned} & \arg \max_{\varphi \in \Phi} \{\varepsilon : \inf_{\|\boldsymbol{\delta}\| \leq 1} y_i \varphi(\mathbf{x}_i + \varepsilon \boldsymbol{\delta}) > 0, \forall i\} \\ & \neq \arg \max_{\varphi \in \Phi} \{\varepsilon : y_i \varphi(\mathbf{x}_i) + \varepsilon \inf_{\|\boldsymbol{\delta}\| \leq 1} \varphi(\boldsymbol{\delta}) > 0, \forall i\} \end{aligned}$$

Lemma B.4.1 (Gradient Norm Weighted Maximum Margin). *Let Φ be a family of locally*

linear classifiers near training data, i.e.,

$$\begin{aligned} \Phi &= \{\varphi : \exists \xi > 0, \forall i, \|\boldsymbol{\delta}\| \leq 1, \varepsilon \in [0, \xi), \\ &\quad \varphi(\mathbf{x}_i + \varepsilon \boldsymbol{\delta}) = \varphi(\mathbf{x}_i) + \varepsilon \boldsymbol{\delta}^\top \frac{\partial}{\partial \mathbf{x}} \varphi(\mathbf{x}_i)\}. \end{aligned}$$

Then a maximally robust classifier is a solution to the following problem,

$$\arg \max_{\varphi \in \Phi, \varepsilon \leq \xi} \{\varepsilon : y_i \varphi(\mathbf{x}_i) > \varepsilon \|\frac{\partial}{\partial \mathbf{x}} \varphi(\mathbf{x}_i)\|_*, \forall i\}.$$

Proof.

$$\begin{aligned} &\arg \max_{\varphi} \{\varepsilon : \inf_{\|\boldsymbol{\delta}\| \leq 1} y_i \varphi(\mathbf{x}_i + \varepsilon \boldsymbol{\delta}) \geq 0, \forall i\} \\ &\quad \text{(Taylor approx.)} \\ &= \arg \max_{\varphi} \{\varepsilon : \inf_{\|\boldsymbol{\delta}\| \leq 1} y_i \varphi(\mathbf{x}_i) + y_i \varepsilon \boldsymbol{\delta}^\top \frac{\partial}{\partial \mathbf{x}} \varphi(\mathbf{x}_i) \geq 0, \forall i\} \\ &= \arg \max_{\varphi} \{\varepsilon : y_i \varphi(\mathbf{x}_i) + \varepsilon \inf_{\|\boldsymbol{\delta}\| \leq 1} \boldsymbol{\delta}^\top \frac{\partial}{\partial \mathbf{x}} \varphi(\mathbf{x}_i) \geq 0, \forall i\} \\ &\quad \text{(Dual to the local derivative.)} \\ &= \arg \max_{\varphi} \{\varepsilon : y_i \varphi(\mathbf{x}_i) \geq \varepsilon \|\frac{\partial}{\partial \mathbf{x}} \varphi(\mathbf{x}_i)\|_*, \forall i\} \\ &\quad \text{(Assuming constant gradient norm near data.)} \\ &= \arg \max_{\varphi : \|\frac{\partial}{\partial \mathbf{x}} \varphi(\mathbf{x})\|_* \leq 1} \{\varepsilon : y_i \varphi(\mathbf{x}_i) \geq \varepsilon, \forall i\}. \end{aligned}$$

□

The equivalence in [Lemma B.4.1](#) fails when Φ includes functions with non-zero higher order derivatives within the ε of the maximally robust classifier. In practice, this failure manifests itself as various forms of gradient masking or gradient obfuscation where the model has almost zero gradient near the data but large higher-order derivatives [6].

Various regularization methods have been proposed for adversarial robustness that penalize the gradient norm and can be studied using the framework of maximally robust

classification [168, 186, 123, 139] Strong gradient or curvature regularization methods can suffer from gradient masking [123].

For general family of non-linear functions, the interplay with implicit bias of optimization and regularization methods remains to be characterized. The solution to the regularized problem in Definition 5.4.1 is not necessarily unique. In such cases, the implicit bias of the optimizer biases the robustness.

B.5 Extended Experiments

B.5.1 Details of Linear Classification Experiments

For experiments with linear classifiers, we sample n training data points from the $\mathcal{N}(0, \mathbb{I}_d)$, d -dimensional standard normal distribution centered at zero. We label data points $y = \text{sign}(\mathbf{w}^\top \mathbf{x})$, using a ground-truth linear separator sampled from $\mathcal{N}(0, \mathbb{I}_d)$. For $n < d$, the generated training data is linearly separable. This setting is similar to a number of recent theoretical works on the implicit bias of optimization methods in deep learning and specifically the double descent phenomenon in generalization [138, 41]. We focus on robustness against norm-bounded attacks centered at the training data, in particular, ℓ_2 , ℓ_∞ , ℓ_1 and Fourier- ℓ_∞ bounded attacks.

Because the constraints and the objective in the minimum norm linear classification problem are convex, we can use off-the-shelf convex optimization toolbox to find the solution for small enough d and n . We use the CVXPY library [42]. We evaluate the following approaches based on the implicit bias of optimization: Gradient Descent (GD), Coordinate Descent (CD), and Sign Gradient Descent (SignGD) on fully-connected networks as well as GD on linear two-layer convolutional networks (discussed in Section 5.3). We also compare with explicit regularization methods (discussed in Section 5.4) trained using proximal gradient methods [154]. We do not use gradient descent because ℓ_p norms can be non-differentiable at some points (e.g., ℓ_1 and ℓ_∞) and we seek a global minima of the regularized empirical risk. We also compare with adversarial training. As we discussed in

Hyperparameter	Values
Random seed	0,1,2
d	100
d/n	1, 2, 4, 8, 16, 32
Training steps	10000
Learning rate	$1e-5$, $3e-5$, $1e-4$, $3e-4$, $1e-3$, $3e-3$, $1e-2$, $3e-2$, $1e-1$, $3e-1$, 1, 2, 3, 6, 9, 10, 20, 30, 50
Reg. coefficient	$1e-7$, $1e-6$, $1e-5$, $1e-4$, $1e-3$, $1e-2$, $1e-1$, 1, 10, $3e-3$, $5e-3$, $3e-2$, $5e-2$, $3e-1$, $5e-1$
Line search max step	1, 10, 100, 1000
Adv. Train steps	10
Adv. Train learning rate	0.1
Runtime (line search/prox. method)	< 20 minutes
Runtime (others)	< 2 minutes

Table B.1: **Range of Hyperparameters.** Each run uses 2 CPU cores.

[Section 5.2.1](#) we need to provide the value of maximally robust ε to adversarial training for finding a maximally robust classifier. In our experiments, we give an advantage to adversarial training by providing it with the maximally robust ε . We also use the steepest descent direction corresponding to the attack norm to solve the inner maximization.

For regularization methods a sufficiently small regularization coefficient achieves maximal robustness. Adversarial training given the maximal ε also converges to the same solution. We tune all hyper-parameters for all methods including learning rate regularization coefficient and maximum step size in line search. We provide a list of values in [Table B.1](#).

B.5.2 Details of CIFAR-10 experiments

For [Figs. 5.4c](#) and [5.4d](#), the model is a WRN-28-10. We use SGD momentum (momentum set to 0.9) with a learning rate schedule that warms up from 0 to LR for 10 epochs, then decays slowly using a cosine schedule back to zero over 200 epochs. LR is set to $0.1 * BS / 256$, where batch size, BS, is set to 1024. Experiments runs on Google Cloud TPUv3 over 32 cores. All models are trained from scratch and uses the default initialization from

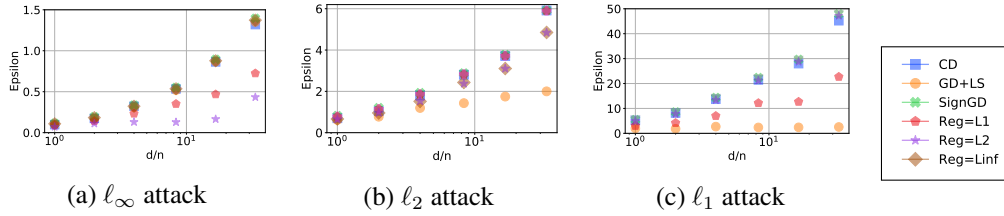


Figure B.1: **Margin of models in Fig. 5.2.** Models are trained to be robust against ℓ_∞ , ℓ_2 , ℓ_1 attacks. For each attack, there exists one optimizer and one regularization method that finds the maximally robust classifier. Adversarial training also finds the solution given the maximal ε .

JAX/Haiku. We use the KL loss and typical adversarial loss for adversarial training. The inner optimization either maximizes the KL divergence (for TRADES) or the cross-entropy loss (for AT) and we use Adam with a step-size of 0.1.

For the evaluation, we use 40 PGD steps (with Adam as the underlying optimizer and step-size 0.1). Instead of optimizing the cross-entropy loss, we used the margin-loss [22].

For Fig. 5.5, we evaluate the models in Table B.2 against our Fourier- ℓ_p attack with varying ε in the range $[0, 8] \times 255$ with step size 0.5. We report the largest ε at which the robust test accuracy is at most 1% lower than standard test accuracy of the model. We run the attack for 20 iterations with no restarts and use apgd-ce, and apgd-dlr methods from AutoAttack.

B.5.3 Margin Figures

A small gap exists between the solution found using CVXPY compared with coordinate descent. That is because of limited number of training iterations. The convergence of coordinate descent to minimum ℓ_1 norm solution is slower than the convergence of gradient descent to minimum ℓ_2 norm solution. There is also a small gap between the solution of ℓ_1 regularization and CVXPY. The reason is the regularization coefficient has to be infinitesimal but in practice numerical errors prevent us from training using very small regularization coefficients.

Model name	Robust training type
Standard	-
Gowal2020Uncovering_70_16_extra	Linf
Gowal2020Uncovering_28_10_extra	Linf
Wu2020Adversarial_extra	Linf
Carmon2019Unlabeled	Linf
Sehwag2020Hydra	Linf
Gowal2020Uncovering_70_16	Linf
Gowal2020Uncovering_34_20	Linf
Wang2020Improving	Linf
Wu2020Adversarial	Linf
Hendrycks2019Using	Linf
Gowal2020Uncovering_extra	L2
Gowal2020Uncovering	L2
Wu2020Adversarial	L2
Augustin2020Adversarial	L2
Engstrom2019Robustness	L2
Rice2020Overfitting	L2
Rice2020Overfitting	L2
Rony2019Decoupling	L2
Ding2020MMA	L2
Hendrycks2020AugMix_ResNeXt	corruptions
Hendrycks2020AugMix_WRN	corruptions
Kireev2021Effectiveness_RLATAugMixNoJSD	corruptions
Kireev2021Effectiveness_AugMixNoJSD	corruptions
Kireev2021Effectiveness_Gauss50percent	corruptions
Kireev2021Effectiveness_RLAT	corruptions

Table B.2: List of models evaluated in Fig. 5.5.

B.5.4 Visualization of Fourier Adversarial Attacks

In Figs. B.3, B.5 and B.7 we visualize adversarial samples for models available in Robust-Bench [36]. Fourier- ℓ_∞ adversarial samples are qualitatively different from ℓ_∞ adversarial samples as they concentrate on the object.

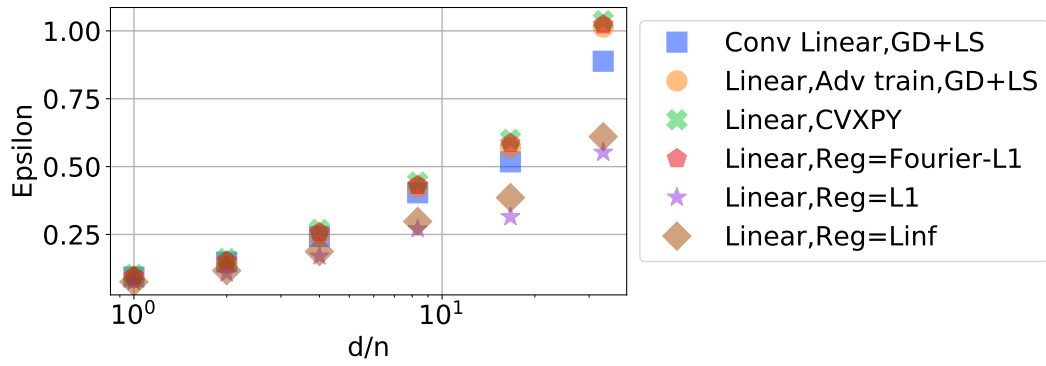


Figure B.2: **Fourier- ℓ_1 margin of Linear Convolutional Models.**

B.6 Visualization of Norm-balls

To reach an intuition of the norm-ball for Fourier ℓ_∞ norm, we visualize a number of common norm-balls in 3D in Fig. B.9. Norm-balls have been visualized in prior work [10] but we are not aware of any visualization of Fourier- ℓ_∞ .

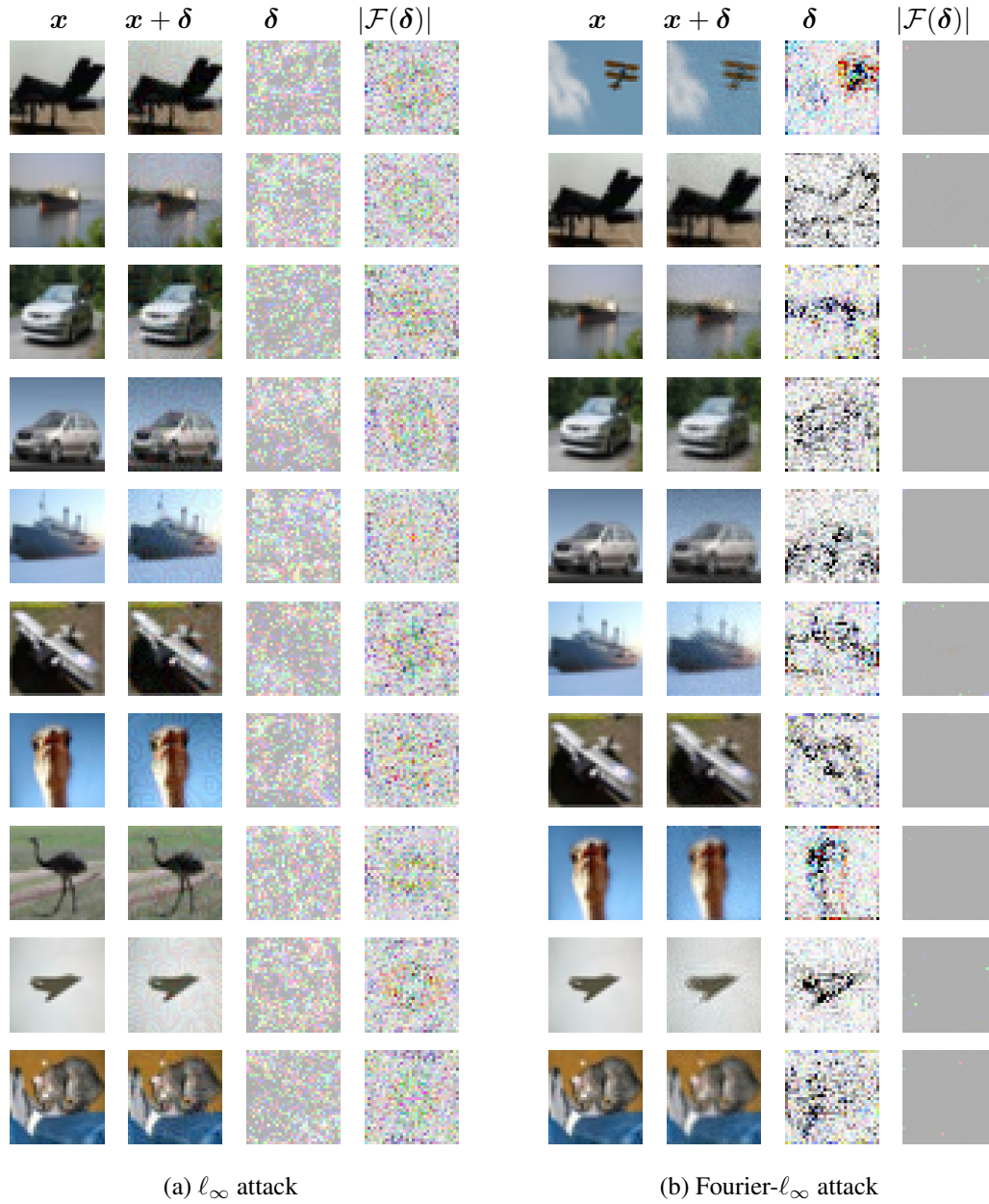


Figure B.3: **Adversarial attacks (ℓ_∞ and Fourier- ℓ_∞) against CIFAR-10 with standard training.** WideResNet-28-10 model with standard training. The attack methods are APGD-CE and APGD-DLR with default hyper-parameters in RobustBench. We use $\varepsilon = 8/255$ for both attacks. Fourier- ℓ_∞ perturbations are more concentrated on the object. Darker color in perturbations means larger magnitude. The optimal Fourier attack step is achieved when the magnitude in the Fourier domain is equal to the constraints.

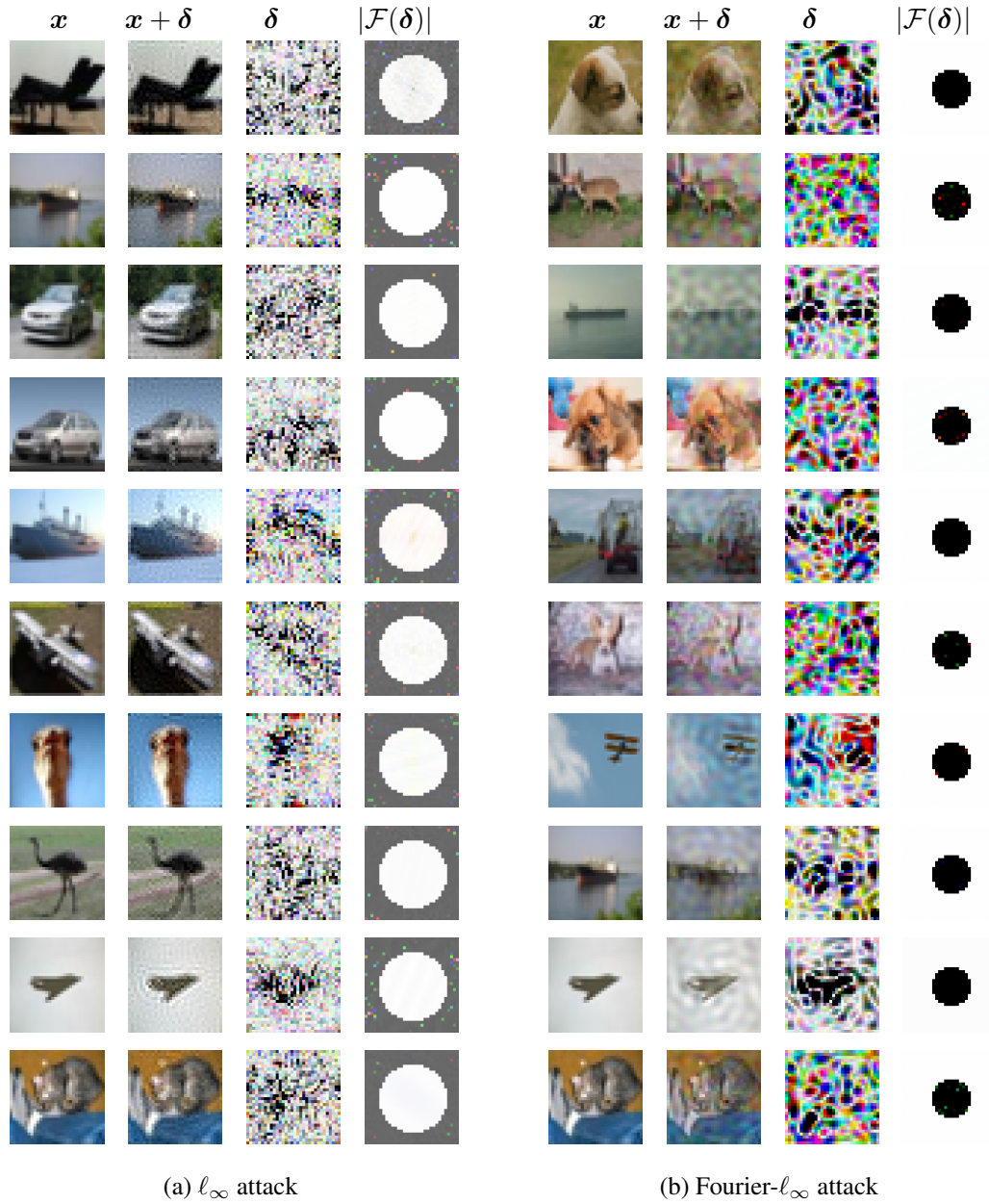


Figure B.4: **Adversarial attacks (High and low frequency Fourier- ℓ_∞) against CIFAR-10 with standard training.** WideResNet-28-10 model with standard training. The attack methods are APGD-CE and APGD-DLR with default hyper-parameters in RobustBench. We use $\varepsilon = 15/255, 45/255$ respectively for high and low frequency. Darker color in perturbations means larger magnitude. The optimal Fourier attack step is achieved when the magnitude in the Fourier domain is equal to the constraints.

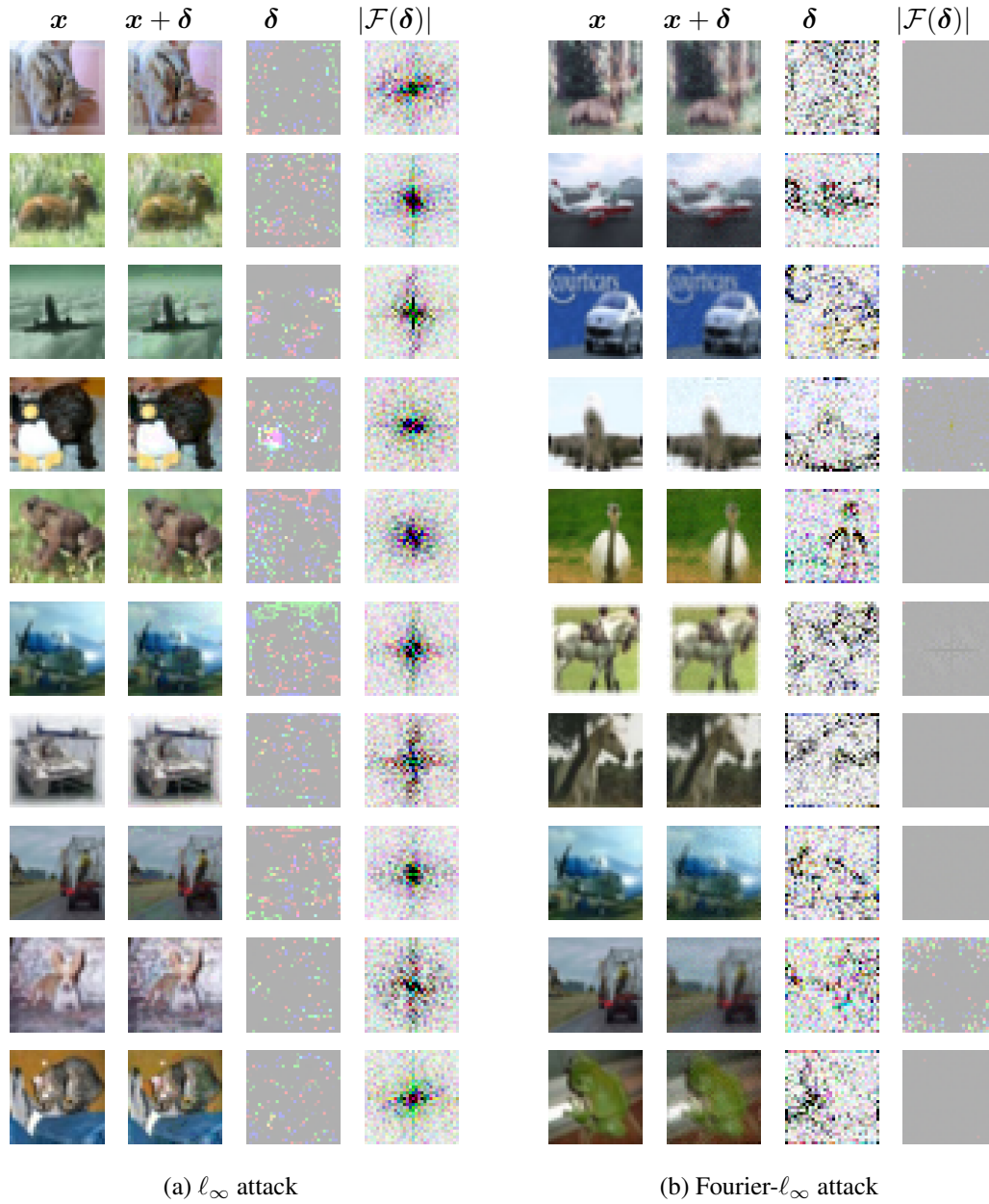


Figure B.5: **Adversarial attacks (ℓ_∞ and Fourier- ℓ_∞) against CIFAR-10 ℓ_∞ model of [23].** Adversarially trained model against ℓ_∞ attacks. The attack methods are APGD-CE and APGD-DLR with default hyper-parameters in RobustBench. We use $\varepsilon = 8/255$ for both attacks. Fourier- ℓ_∞ perturbations are more concentrated on the object. Darker color in perturbations means larger magnitude. The optimal Fourier attack step is achieved when the magnitude in the Fourier domain is equal to the constraints.

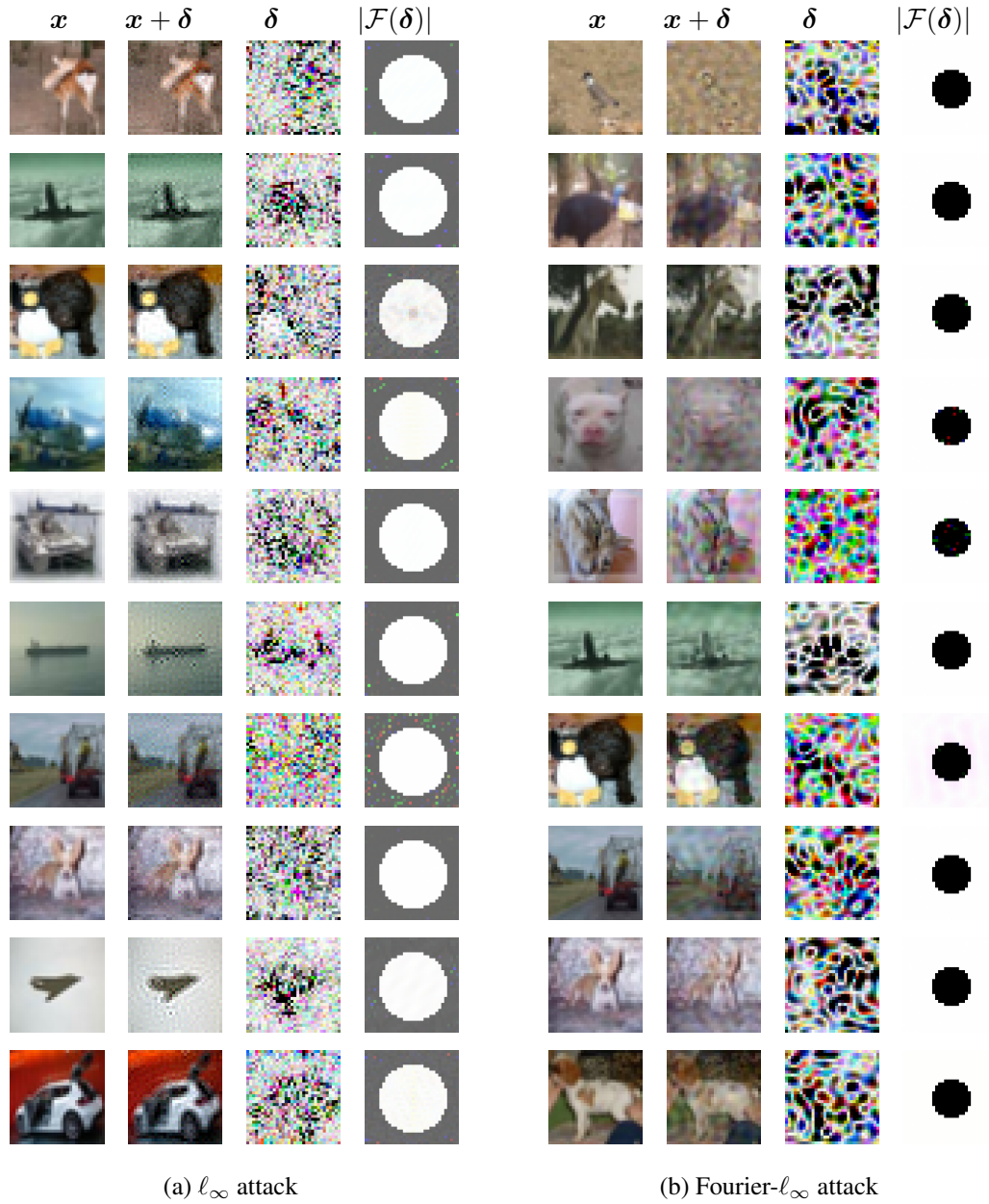


Figure B.6: **Adversarial attacks (High and low frequency Fourier- l_∞) against CIFAR-10 l_∞ model of [23].** WideResNet-28-10 model with standard training. The attack methods are APGD-CE and APGD-DLR with default hyper-parameters in RobustBench. We use $\varepsilon = 15/255, 45/255$ respectively for high and low frequency. Darker color in perturbations means larger magnitude. The optimal Fourier attack step is achieved when the magnitude in the Fourier domain is equal to the constraints.

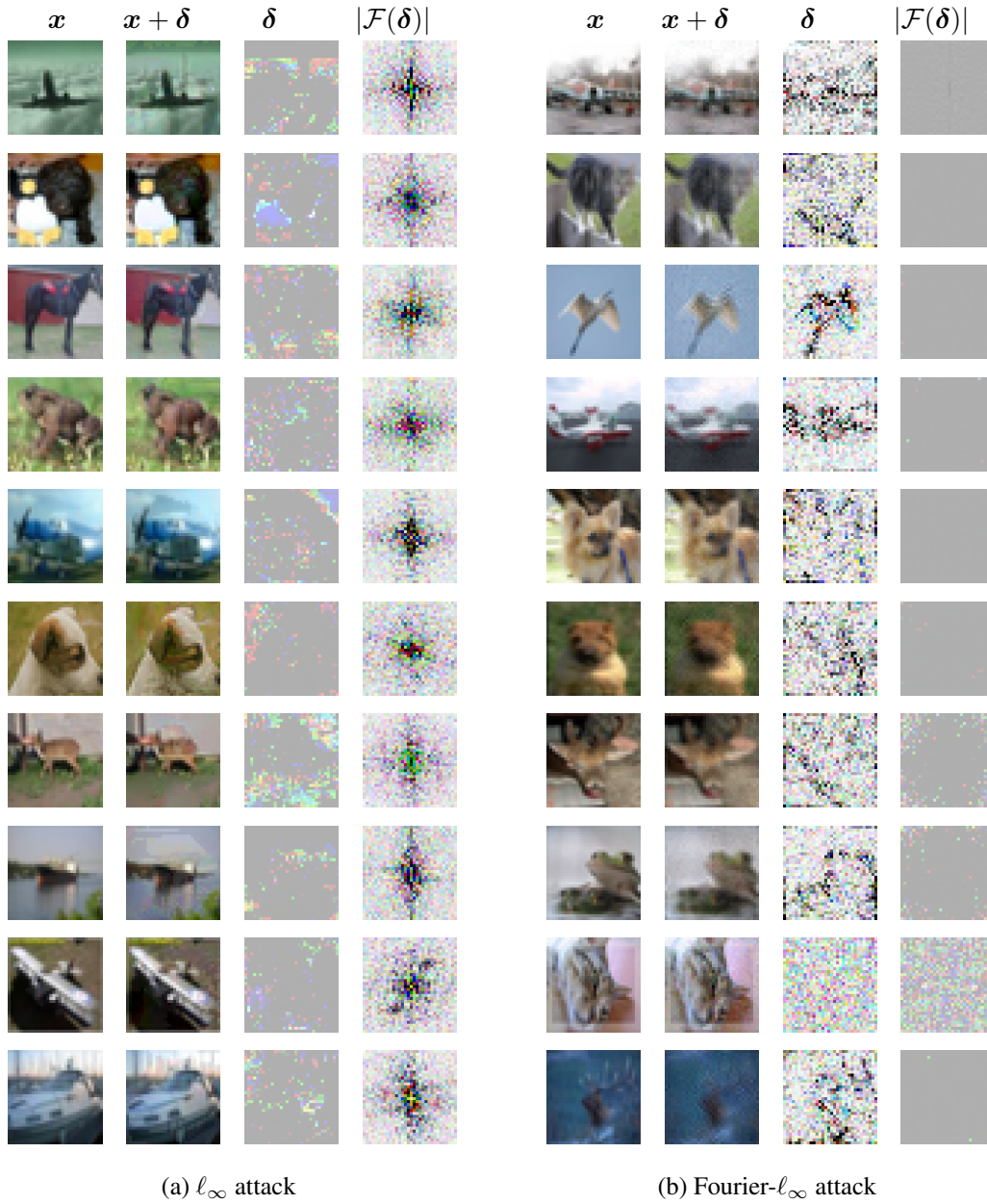


Figure B.7: **Adversarial attacks (l_∞ and Fourier- l_∞) against CIFAR-10 l_2 model of [7].** Adversarially trained model against l_2 attacks. The attack methods are APGD-CE and APGD-DLR with default hyper-parameters in RobustBench. We use $\varepsilon = 8/255$ for both attacks. Fourier- l_∞ perturbations are more concentrated on the object. Darker color in perturbations means larger magnitude. The optimal Fourier attack step is achieved when the magnitude in the Fourier domain is equal to the constraints.

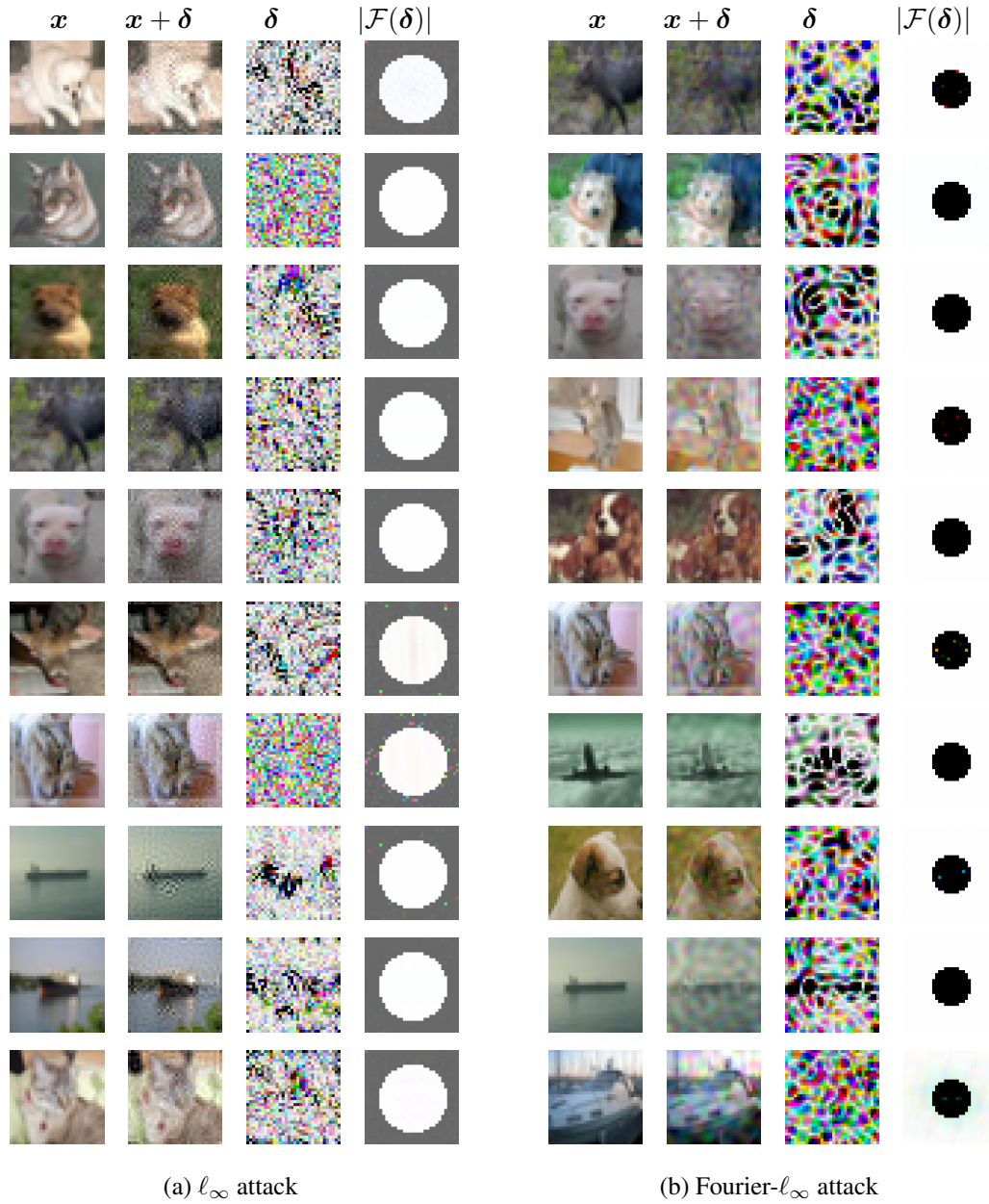


Figure B.8: **Adversarial attacks (High and low frequency Fourier- ℓ_∞) against CIFAR-10 ℓ_2 model of [7].** WideResNet-28-10 model with standard training. The attack methods are APGD-CE and APGD-DLR with default hyper-parameters in RobustBench. We use $\varepsilon = 15/255, 45/255$ respectively for high and low frequency. Darker color in perturbations means larger magnitude. The optimal Fourier attack step is achieved when the magnitude in the Fourier domain is equal to the constraints.

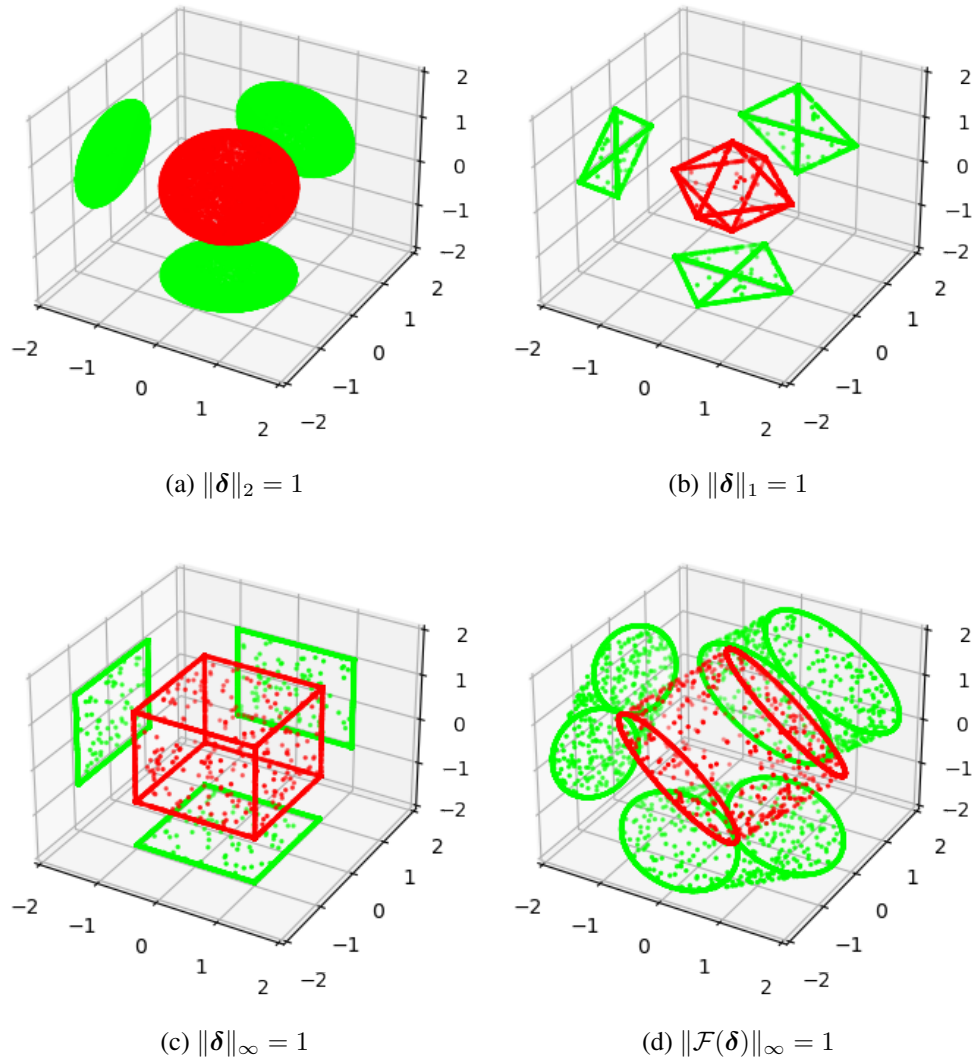


Figure B.9: Unit norm balls in 3-D (red) and their 2-D projections (green). Linear models trained with gradient descent are maximally robust to ℓ_2 perturbations. Two-layer linear convolutional networks trained with gradient descent are maximally robust to perturbations with bounded Fourier- ℓ_∞ .

Bibliography

- [1] Aishwarya Agrawal, Jiasen Lu, Stanislaw Antol, Margaret Mitchell, C Lawrence Zitnick, Devi Parikh, and Dhruv Batra. “VQA: Visual question answering”. In: *International Journal of Computer Vision (IJCV)* 123.1 (2017), pp. 4–31.
- [2] Guillaume Alain, Alex Lamb, Chinnadhurai Sankar, Aaron Courville, and Yoshua Bengio. “Variance Reduction in SGD by Distributed Importance Sampling”. In: *arXiv e-prints*, arXiv:1511.06481 (Nov. 2015), arXiv:1511.06481. arXiv: [1511.06481](https://arxiv.org/abs/1511.06481) [stat.ML].
- [3] Shun-Ichi Amari. “Natural gradient works efficiently in learning”. In: *Neural computation* 10.2 (1998), pp. 251–276.
- [4] Shun-ichi Amari, Jimmy Ba, Roger Grosse, Xuechen Li, Atsushi Nitanda, Taiji Suzuki, Denny Wu, and Ji Xu. “When Does Preconditioning Help or Hurt Generalization?” In: *arXiv preprint arXiv:2006.10732* (2020).
- [5] Rohan Anil, Vineet Gupta, Tomer Koren, Kevin Regan, and Yoram Singer. “Scalable second order optimization for deep learning”. In: *arXiv preprint arXiv:2002.09018* 7 (2021), p. 15.
- [6] Anish Athalye, Nicholas Carlini, and David Wagner. “Obfuscated gradients give a false sense of security: Circumventing defenses to adversarial examples”. In: *arXiv preprint arXiv:1802.00420* (2018).

- [7] Maximilian Augustin, Alexander Meinke, and Matthias Hein. “Adversarial robustness on in-and out-distribution improves explainability”. In: *European Conference on Computer Vision*. Springer. 2020, pp. 228–245.
- [8] George Awad, Asad A. Butt, Keith Curtis, Yooyoung Lee, Jonathan Fiscus, Afzal Godil, Andrew Delgado, Jesse Zhang, Eliot Godard, Lukas Diduch, Jeffrey Liu, Alan F. Smeaton, Yvette Graham, Gareth J. F. Jones, Wessel Kraaij, and Georges Quénot. “TRECVID 2020: comprehensive campaign for evaluating video retrieval tasks across multiple application domains”. In: *Proceedings of TRECVID 2020*. NIST, USA. 2020.
- [9] Muhammad Awais, Fahad Shamshad, and Sung-Ho Bae. “Towards an Adversarially Robust Normalization Approach”. In: *CoRR abs/2006.11007* (2020).
- [10] Francis Bach, Rodolphe Jenatton, Julien Mairal, Guillaume Obozinski, et al. “Structured sparsity through convex optimization”. In: *Statistical Science* 27.4 (2012), pp. 450–468.
- [11] Sue Becker, Yann Le Cun, et al. “Improving the convergence of back-propagation learning with second order methods”. In: *Proceedings of the 1988 connectionist models summer school*. San Matteo, CA: Morgan Kaufmann. 1988, pp. 29–37.
- [12] Aharon Ben-Tal, Laurent El Ghaoui, and Arkadi Nemirovski. *Robust optimization*. Vol. 28. Princeton University Press, 2009.
- [13] Yoshua Bengio and Jean-Sébastien Senecal. “Adaptive Importance Sampling to Accelerate Training of a Neural Probabilistic Language Model”. In: *IEEE Trans. Neural Networks* 19.4 (2008), pp. 713–722.
- [14] Yoshua Bengio, Jérôme Louradour, Ronan Collobert, and Jason Weston. “Curriculum learning”. In: *International Conference on Machine Learning (ICML)*. Vol. 382. ACM International Conference Proceeding Series. ACM, 2009, pp. 41–48.
- [15] Christopher M. Bishop. *Pattern recognition and machine learning*. Springer, 2007.

- [16] Ondřej Bojar, Christian Buck, Christian Federmann, Barry Haddow, Philipp Koehn, Johannes Leveling, Christof Monz, Pavel Pecina, Matt Post, Herve Saint-Amand, et al. “Findings of the 2014 workshop on statistical machine translation”. In: *Proceedings of the ninth workshop on statistical machine translation*. 2014, pp. 12–58.
- [17] Léon Bottou, Frank E Curtis, and Jorge Nocedal. “Optimization methods for large-scale machine learning”. In: *arXiv preprint arXiv:1606.04838* (2016).
- [18] Léon Bottou, Frank E. Curtis, and Jorge Nocedal. “Optimization Methods for Large-Scale Machine Learning”. In: *SIAM Review* 60.2 (2018), pp. 223–311.
- [19] Stephen Boyd and Lieven Vandenberghe. *Convex optimization*. Cambridge university press, 2004.
- [20] Tom B. Brown, Dandelion Mané, Aurko Roy, Martín Abadi, and Justin Gilmer. “Adversarial Patch”. In: *arXiv e-prints*, arXiv:1712.09665 (Dec. 2017), arXiv:1712.09665. arXiv: [1712.09665 \[cs.CV\]](https://arxiv.org/abs/1712.09665).
- [21] Tom B. Brown, Benjamin Mann, Nick Ryder, Melanie Subbiah, Jared Kaplan, Prafulla Dhariwal, Arvind Neelakantan, Pranav Shyam, Girish Sastry, Amanda Askell, Sandhini Agarwal, Ariel Herbert-Voss, Gretchen Krueger, Tom Henighan, Rewon Child, Aditya Ramesh, Daniel M. Ziegler, Jeffrey Wu, Clemens Winter, Christopher Hesse, Mark Chen, Eric Sigler, Mateusz Litwin, Scott Gray, Benjamin Chess, Jack Clark, Christopher Berner, Sam McCandlish, Alec Radford, Ilya Sutskever, and Dario Amodei. “Language Models are Few-Shot Learners”. In: *Neural Information Processing Systems (NeurIPS)*. 2020.
- [22] Nicholas Carlini and David Wagner. “Towards evaluating the robustness of neural networks”. In: *2017 IEEE Symposium on Security and Privacy (SP)*. IEEE. 2017, pp. 39–57.

- [23] Yair Carmon, Aditi Raghunathan, Ludwig Schmidt, John C. Duchi, and Percy Liang. “Unlabeled Data Improves Adversarial Robustness”. In: *NeurIPS*. 2019, pp. 11190–11201.
- [24] Josue Ortega Caro, Yilong Ju, Ryan Pyle, and Ankit Patel. “Using Learning Dynamics to Explore the Role of Implicit Regularization in Adversarial Examples”. In: *arXiv preprint arXiv:2006.11440* (2020).
- [25] Olivier Chapelle, Quoc Le, and Alex Smola. “Large margin optimization of ranking measures”. In: *NIPS workshop: Machine learning for Web search*. 2007.
- [26] Gal Chechik, Varun Sharma, Uri Shalit, and Samy Bengio. “Large scale online learning of image similarity through ranking”. In: *Journal of Machine Learning Research (JMLR)* 11.Mar (2010), pp. 1109–1135.
- [27] Beidi Chen, Yingchen Xu, and Anshumali Shrivastava. “Fast and Accurate Stochastic Gradient Estimation”. In: *Neural Information Processing Systems (NeurIPS)*. 2019, pp. 12339–12349.
- [28] Hongming Chen, Ola Engkvist, Yinhai Wang, Marcus Olivecrona, and Thomas Blaschke. “The rise of deep learning in drug discovery”. In: *Drug discovery today* 23.6 (2018), pp. 1241–1250.
- [29] Jiacheng Chen, Hexiang Hu, Hao Wu, Yuning Jiang, and Changhu Wang. “Learning the best pooling strategy for visual semantic embedding”. In: *Proceedings of the IEEE/CVF Conference on Computer Vision and Pattern Recognition*. 2021, pp. 15789–15798.
- [30] Ting Chen, Simon Kornblith, Mohammad Norouzi, and Geoffrey Hinton. “A simple framework for contrastive learning of visual representations”. In: *arXiv preprint arXiv:2002.05709* (2020).
- [31] Xinlei Chen, Haoqi Fan, Ross Girshick, and Kaiming He. “Improved baselines with momentum contrastive learning”. In: *arXiv preprint arXiv:2003.04297* (2020).

- [32] Lenaic Chizat and Francis Bach. “Implicit bias of gradient descent for wide two-layer neural networks trained with the logistic loss”. In: *Conference on Learning Theory*. PMLR, 2020, pp. 1305–1338.
- [33] Dami Choi, Christopher J Shallue, Zachary Nado, Jaehoon Lee, Chris J Maddison, and George E Dahl. “On empirical comparisons of optimizers for deep learning”. In: *arXiv preprint arXiv:1910.05446* (2019).
- [34] Jeremy M Cohen, Elan Rosenfeld, and J Zico Kolter. “Certified adversarial robustness via randomized smoothing”. In: *arXiv preprint arXiv:1902.02918* (2019).
- [35] Francesco Croce and Matthias Hein. “Reliable evaluation of adversarial robustness with an ensemble of diverse parameter-free attacks”. In: *ICML*. Vol. 119. Proceedings of Machine Learning Research. PMLR, 2020, pp. 2206–2216.
- [36] Francesco Croce, Maksym Andriushchenko, Vikash Sehwal, Nicolas Flammarion, Mung Chiang, Prateek Mittal, and Matthias Hein. “RobustBench: a standardized adversarial robustness benchmark”. In: *arXiv preprint arXiv:2010.09670* (2020).
- [37] Dominik Csiba and Peter Richtárik. “Importance sampling for minibatches”. In: *The Journal of Machine Learning Research* 19.1 (2018), pp. 962–982.
- [38] Navneet Dalal and Bill Triggs. “Histograms of oriented gradients for human detection”. In: *IEEE Conference on Computer Vision and Pattern Recognition (CVPR)*. Vol. 1. IEEE, 2005, pp. 886–893.
- [39] Aaron Defazio and Léon Bottou. “On the Ineffectiveness of Variance Reduced Optimization for Deep Learning”. In: *Neural Information Processing Systems (NeurIPS)*. 2019, pp. 1753–1763.
- [40] Jia Deng, Wei Dong, Richard Socher, Li-Jia Li, Kai Li, and Fei-Fei Li. “ImageNet: A large-scale hierarchical image database”. In: *IEEE Conference on Computer Vision and Pattern Recognition (CVPR)*. IEEE Computer Society, 2009, pp. 248–255.

- [41] Zeyu Deng, Abba Kammoun, and Christos Thrampoulidis. “A Model of Double Descent for High-dimensional Binary Linear Classification”. In: *arXiv e-prints*, arXiv:1911.05822 (Nov. 2019), arXiv:1911.05822. arXiv: [1911.05822](https://arxiv.org/abs/1911.05822) [[stat.ML](#)].
- [42] Steven Diamond and Stephen Boyd. “CVXPY: A Python-embedded modeling language for convex optimization”. In: *Journal of Machine Learning Research* 17.83 (2016), pp. 1–5.
- [43] Gavin Weiguang Ding, Yash Sharma, Kry Yik Chau Lui, and Ruitong Huang. “Max-Margin Adversarial (MMA) Training: Direct Input Space Margin Maximization through Adversarial Training”. In: *CoRR* abs/1812.02637 (2018). arXiv: [1812.02637](https://arxiv.org/abs/1812.02637). URL: <http://arxiv.org/abs/1812.02637>.
- [44] Edgar Dobriban, Hamed Hassani, David Hong, and Alexander Robey. “Provable tradeoffs in adversarially robust classification”. In: *arXiv e-prints*, arXiv:2006.05161 (June 2020), arXiv:2006.05161. arXiv: [2006.05161](https://arxiv.org/abs/2006.05161) [[cs.LG](#)].
- [45] John Duchi, Elad Hazan, and Yoram Singer. “Adaptive subgradient methods for online learning and stochastic optimization”. In: *Journal of Machine Learning Research* 12.Jul (2011), pp. 2121–2159.
- [46] Aviv Eisenschat and Lior Wolf. “Linking Image and Text with 2-Way Nets”. In: (2017).
- [47] Gamaleldin F. Elsayed, Dilip Krishnan, Hossein Mobahi, Kevin Regan, and Samy Bengio. *Large Margin Deep Networks for Classification*. 2018. arXiv: [1803.05598](https://arxiv.org/abs/1803.05598) [[stat.ML](#)].
- [48] Fartash Faghri, David Duvenaud, David J Fleet, and Jimmy Ba. “A Study of Gradient Variance in Deep Learning”. In: *arXiv preprint arXiv:2007.04532* (2020).
- [49] Fartash Faghri, Iman Tabrizian, Ilia Markov, Dan Alistarh, Daniel M. Roy, and Ali Ramezani-Kebrya. “Adaptive Gradient Quantization for Data-Parallel SGD”. In: *NeurIPS*. 2020.

- [50] Fartash Faghri, David J. Fleet, Jamie Ryan Kiros, and Sanja Fidler. “VSE++: Improving Visual-Semantic Embeddings with Hard Negatives”. In: *British Machine Vision Conference 2018, BMVC 2018, Newcastle, UK, September 3-6, 2018*. BMVA Press, 2018, p. 12. URL: <http://bmvc2018.org/contents/papers/0344.pdf>.
- [51] Alhussein Fawzi, Hamza Fawzi, and Omar Fawzi. “Adversarial vulnerability for any classifier”. In: *Advances in neural information processing systems*. 2018, pp. 1178–1187.
- [52] Alhussein Fawzi, Omar Fawzi, and Pascal Frossard. “Analysis of classifiers’ robustness to adversarial perturbations”. In: *Machine Learning* 107.3 (2018), pp. 481–508.
- [53] Pedro F Felzenszwalb, Ross B Girshick, David McAllester, and Deva Ramanan. “Object detection with discriminatively trained part-based models”. In: *IEEE Transactions on Pattern Analysis and Machine Intelligence (PAMI)* 32.9 (2010), pp. 1627–1645.
- [54] Chelsea Finn, Pieter Abbeel, and Sergey Levine. “Model-agnostic meta-learning for fast adaptation of deep networks”. In: *International Conference on Machine Learning*. PMLR. 2017, pp. 1126–1135.
- [55] Michael P Friedlander and Mark Schmidt. “Hybrid deterministic-stochastic methods for data fitting”. In: *SIAM Journal on Scientific Computing* 34.3 (2012), A1380–A1405.
- [56] Andrea Frome, Greg S Corrado, Jon Shlens, Samy Bengio, Jeff Dean, Tomas Mikolov, et al. “Devise: A deep visual-semantic embedding model”. In: *Neural Information Processing Systems (NeurIPS)*. 2013, pp. 2121–2129.
- [57] Andrea Frome, Yoram Singer, Fei Sha, and Jitendra Malik. “Learning globally-consistent local distance functions for shape-based image retrieval and classification”. In: *International Conference in Computer Vision (ICCV)*. IEEE. 2007, pp. 1–8.

- [58] Angus Galloway, Anna Golubeva, Thomas Tanay, Medhat Moussa, and Graham W. Taylor. “Batch Normalization is a Cause of Adversarial Vulnerability”. In: *CoRR* abs/1905.02161 (2019).
- [59] Amirata Ghorbani, Abubakar Abid, and James Zou. “Interpretation of neural networks is fragile”. In: *Proceedings of the AAAI Conference on Artificial Intelligence*. Vol. 33. 01. 2019, pp. 3681–3688.
- [60] Justin Gilmer, Luke Metz, Fartash Faghri, Samuel S. Schoenholz, Maithra Raghu, Martin Wattenberg, and Ian Goodfellow. “Adversarial Spheres”. In: *arXiv e-prints*, arXiv:1801.02774 (Jan. 2018), arXiv:1801.02774. arXiv: [1801.02774 \[cs.CV\]](#).
- [61] Xavier Glorot and Yoshua Bengio. “Understanding the difficulty of training deep feedforward neural networks”. In: *Proceedings of the thirteenth international conference on artificial intelligence and statistics*. 2010, pp. 249–256.
- [62] Gabriel Goh. “Why Momentum Really Works”. In: *Distill* (2017). DOI: [10.23915/distill.00006](#). URL: <http://distill.pub/2017/momentum>.
- [63] Noah Golmant, Nikita Vemuri, Zhewei Yao, Vladimir Feinberg, Amir Gholami, Kai Rothauge, Michael W. Mahoney, and Joseph Gonzalez. “On the Computational Inefficiency of Large Batch Sizes for Stochastic Gradient Descent”. In: *arXiv e-prints*, arXiv:1811.12941 (Nov. 2018), arXiv:1811.12941. arXiv: [1811.12941 \[cs.LG\]](#).
- [64] Ian Goodfellow. “Efficient Per-Example Gradient Computations”. In: *arXiv e-prints*, arXiv:1510.01799 (Oct. 2015), arXiv:1510.01799. arXiv: [1510.01799 \[stat.ML\]](#).
- [65] Ian Goodfellow, Yoshua Bengio, Aaron Courville, and Yoshua Bengio. *Deep learning*. Vol. 1. MIT press Cambridge, 2016.
- [66] Ian Goodfellow, Jean Pouget-Abadie, Mehdi Mirza, Bing Xu, David Warde-Farley, Sherjil Ozair, Aaron Courville, and Yoshua Bengio. “Generative Adversarial Nets”. In: *Neural Information Processing Systems (NeurIPS)*. Ed. by Z. Ghahramani, M. Welling, C. Cortes, N. D. Lawrence, and K. Q. Weinberger. Curran Associates,

- Inc., 2014, pp. 2672–2680. URL: <http://papers.nips.cc/paper/5423-generative-adversarial-nets.pdf>.
- [67] Ian J Goodfellow, Jonathon Shlens, and Christian Szegedy. “Explaining and harnessing adversarial examples”. In: *arXiv preprint arXiv:1412.6572* (2014).
- [68] Ian J. Goodfellow and Oriol Vinyals. “Qualitatively characterizing neural network optimization problems”. In: *International Conference on Learning Representations (ICLR)*. 2015.
- [69] Sven Gowal, Krishnamurthy Dvijotham, Robert Stanforth, Rudy Bunel, Chongli Qin, Jonathan Uesato, Relja Arandjelovic, Timothy Mann, and Pushmeet Kohli. “On the Effectiveness of Interval Bound Propagation for Training Verifiably Robust Models”. In: *arXiv e-prints*, arXiv:1810.12715 (Oct. 2018), arXiv:1810.12715. arXiv: [1810.12715 \[cs.LG\]](https://arxiv.org/abs/1810.12715).
- [70] Sven Gowal, Chongli Qin, Jonathan Uesato, Timothy Mann, and Pushmeet Kohli. “Uncovering the Limits of Adversarial Training against Norm-Bounded Adversarial Examples”. In: *arXiv e-prints*, arXiv:2010.03593 (Oct. 2020), arXiv:2010.03593. arXiv: [2010.03593 \[stat.ML\]](https://arxiv.org/abs/2010.03593).
- [71] Sorin Grigorescu, Bogdan Trasnea, Tiberiu Cocias, and Gigel Macesanu. “A survey of deep learning techniques for autonomous driving”. In: *Journal of Field Robotics* 37.3 (2020), pp. 362–386.
- [72] Suriya Gunasekar, Jason Lee, Daniel Soudry, and Nathan Srebro. “**Characterizing implicit bias in terms of optimization geometry**”. In: *arXiv preprint arXiv:1802.08246* (2018).
- [73] Suriya Gunasekar, Jason D Lee, Daniel Soudry, and Nati Srebro. “Implicit bias of gradient descent on linear convolutional networks”. In: *Advances in Neural Information Processing Systems*. 2018, pp. 9461–9471.

- [74] Chuan Guo, Jared S. Frank, and Kilian Q. Weinberger. “Low Frequency Adversarial Perturbation”. In: *Proceedings of the Thirty-Fifth Conference on Uncertainty in Artificial Intelligence, UAI 2019, Tel Aviv, Israel, July 22-25, 2019*. Ed. by Amir Globerson and Ricardo Silva. Vol. 115. Proceedings of Machine Learning Research. AUAI Press, 2019, pp. 1127–1137. URL: <http://proceedings.mlr.press/v115/guo20a.html>.
- [75] Yiwen Guo, Long Chen, Yurong Chen, and Changshui Zhang. “On connections between regularizations for improving dnn robustness”. In: *IEEE transactions on pattern analysis and machine intelligence* (2020).
- [76] Raia Hadsell, Sumit Chopra, and Yann LeCun. “Dimensionality Reduction by Learning an Invariant Mapping”. In: *IEEE Conference on Computer Vision and Pattern Recognition (CVPR)*. IEEE Computer Society, 2006, pp. 1735–1742.
- [77] Trevor Hastie, Andrea Montanari, Saharon Rosset, and Ryan J. Tibshirani. “Surprises in High-Dimensional Ridgeless Least Squares Interpolation”. In: *arXiv e-prints*, arXiv:1903.08560 (Mar. 2019), arXiv:1903.08560. arXiv: [1903.08560](https://arxiv.org/abs/1903.08560) [[math.ST](https://arxiv.org/abs/1903.08560)].
- [78] Kaiming He, Xiangyu Zhang, Shaoqing Ren, and Jian Sun. “Deep Residual Learning for Image Recognition”. In: *IEEE Conference on Computer Vision and Pattern Recognition (CVPR)*. IEEE Computer Society, 2016, pp. 770–778.
- [79] Kaiming He, Xiangyu Zhang, Shaoqing Ren, and Jian Sun. “Delving deep into rectifiers: Surpassing human-level performance on imagenet classification”. In: *Proceedings of the IEEE international conference on computer vision*. 2015, pp. 1026–1034.
- [80] Kaiming He, Haoqi Fan, Yuxin Wu, Saining Xie, and Ross Girshick. “Momentum contrast for unsupervised visual representation learning”. In: *Proceedings of the IEEE/CVF Conference on Computer Vision and Pattern Recognition*. 2020, pp. 9729–9738.

- [81] Matthias Hein and Maksym Andriushchenko. “Formal guarantees on the robustness of a classifier against adversarial manipulation”. In: *Advances in neural information processing systems*. 2017, pp. 2266–2276.
- [82] Sepp Hochreiter. “The vanishing gradient problem during learning recurrent neural nets and problem solutions”. In: *International Journal of Uncertainty, Fuzziness and Knowledge-Based Systems* 6.02 (1998), pp. 107–116.
- [83] Sepp Hochreiter, A Steven Younger, and Peter R Conwell. “Learning to learn using gradient descent”. In: *International Conference on Artificial Neural Networks*. Springer. 2001, pp. 87–94.
- [84] Micah Hodosh, Peter Young, and Julia Hockenmaier. “Framing image description as a ranking task: Data, models and evaluation metrics”. In: *Journal of Artificial Intelligence Research* 47 (2013), pp. 853–899.
- [85] Thomas Hofmann, Aurélien Lucchi, Simon Lacoste-Julien, and Brian McWilliams. “Variance Reduced Stochastic Gradient Descent with Neighbors”. In: *Neural Information Processing Systems (NeurIPS)*. 2015, pp. 2305–2313.
- [86] Yan Huang, Wei Wang, and Liang Wang. “Instance-aware Image and Sentence Matching with Selective Multimodal LSTM”. In: (2017).
- [87] Andrew Ilyas, Shibani Santurkar, Dimitris Tsipras, Logan Engstrom, Brandon Tran, and Aleksander Madry. “Adversarial examples are not bugs, they are features”. In: *Advances in Neural Information Processing Systems*. 2019, pp. 125–136.
- [88] Arthur Jacot, Clément Hongler, and Franck Gabriel. “Neural Tangent Kernel: Convergence and Generalization in Neural Networks”. In: *Neural Information Processing Systems (NeurIPS)*. 2018, pp. 8580–8589.
- [89] Adel Javanmard and Mahdi Soltanolkotabi. “Precise Statistical Analysis of Classification Accuracies for Adversarial Training”. In: *arXiv e-prints*, arXiv:2010.11213 (Oct. 2020), arXiv:2010.11213. arXiv: [2010.11213 \[stat.ML\]](https://arxiv.org/abs/2010.11213).

- [90] Adel Javanmard, Mahdi Soltanolkotabi, and Hamed Hassani. “Precise Tradeoffs in Adversarial Training for Linear Regression”. In: *COLT*. Vol. 125. Proceedings of Machine Learning Research. PMLR, 2020, pp. 2034–2078.
- [91] Ziwei Ji and Matus Telgarsky. “Directional convergence and alignment in deep learning”. In: *NeurIPS*. 2020.
- [92] Ziwei Ji and Matus Telgarsky. “Gradient descent aligns the layers of deep linear networks”. In: *arXiv preprint arXiv:1810.02032* (2018).
- [93] Angela H Jiang, Daniel L-K Wong, Giulio Zhou, David G Andersen, Jeffrey Dean, Gregory R Ganger, Gauri Joshi, Michael Kaminsky, Michael Kozuch, Zachary C Lipton, et al. “Accelerating Deep Learning by Focusing on the Biggest Losers”. In: *arXiv preprint arXiv:1910.00762* (2019).
- [94] Lu Jiang, Zhengyuan Zhou, Thomas Leung, Li-Jia Li, and Li Fei-Fei. “MentorNet: Learning Data-Driven Curriculum for Very Deep Neural Networks on Corrupted Labels”. In: *arXiv e-prints*, arXiv:1712.05055 (Dec. 2017), arXiv:1712.05055. arXiv: [1712.05055 \[cs.CV\]](https://arxiv.org/abs/1712.05055).
- [95] Rie Johnson and Tong Zhang. “Accelerating Stochastic Gradient Descent using Predictive Variance Reduction”. In: *Neural Information Processing Systems (NeurIPS)*. 2013, pp. 315–323.
- [96] Tyler B Johnson and Carlos Guestrin. “Training deep models faster with robust, approximate importance sampling”. In: *Advances in Neural Information Processing Systems* 31 (2018), pp. 7265–7275.
- [97] Ryo Karakida, Shotaro Akaho, and Shun-ichi Amari. “Pathological spectra of the Fisher information metric and its variants in deep neural networks”. In: *arXiv preprint arXiv:1910.05992* (2019).
- [98] Andrej Karpathy and Li Fei-Fei. “Deep visual-semantic alignments for generating image descriptions”. In: *IEEE Conference on Computer Vision and Pattern Recognition (CVPR)*. 2015, pp. 3128–3137.

- [99] Angelos Katharopoulos and François Fleuret. “Biased Importance Sampling for Deep Neural Network Training”. In: *arXiv e-prints*, arXiv:1706.00043 (May 2017), arXiv:1706.00043. arXiv: [1706.00043 \[cs.LG\]](https://arxiv.org/abs/1706.00043).
- [100] Nitish Shirish Keskar, Dheevatsa Mudigere, Jorge Nocedal, Mikhail Smelyanskiy, and Ping Tak Peter Tang. “On Large-Batch Training for Deep Learning: Generalization Gap and Sharp Minima”. In: *International Conference on Learning Representations (ICLR)*. OpenReview.net, 2017.
- [101] Pieter-Jan Kindermans, Sara Hooker, Julius Adebayo, Maximilian Alber, Kristof T Schütt, Sven Dähne, Dumitru Erhan, and Been Kim. “The (un) reliability of saliency methods”. In: *Explainable AI: Interpreting, Explaining and Visualizing Deep Learning*. Springer, 2019, pp. 267–280.
- [102] Diederik Kingma and Jimmy Ba. “Adam: A method for stochastic optimization”. In: (2015).
- [103] Ryan Kiros, Ruslan Salakhutdinov, and Richard S Zemel. “Unifying visual-semantic embeddings with multimodal neural language models”. In: (2014).
- [104] Benjamin Klein, Guy Lev, Gil Sadeh, and Lior Wolf. “Associating neural word embeddings with deep image representations using fisher vectors”. In: *IEEE Conference on Computer Vision and Pattern Recognition (CVPR)*. 2015, pp. 4437–4446.
- [105] Alex Krizhevsky et al. “Learning multiple layers of features from tiny images”. In: (2009).
- [106] Frederik Kunstner, Philipp Hennig, and Lukas Balles. “Limitations of the empirical Fisher approximation for natural gradient descent”. In: *Neural Information Processing Systems (NeurIPS)*. 2019, pp. 4158–4169.
- [107] Alexey Kurakin, Ian J. Goodfellow, and Samy Bengio. “Adversarial examples in the physical world”. In: *ICLR (Workshop)*. OpenReview.net, 2017.

- [108] Quoc Le and Alexander Smola. “Direct optimization of ranking measures”. In: *arXiv preprint arXiv:0704.3359* (2007).
- [109] Nicolas Le Roux, Yoshua Bengio, and Andrew Fitzgibbon. “Improving first and second-order methods by modeling uncertainty”. In: *Optimization for Machine Learning* (2011), p. 403.
- [110] Nicolas Le Roux, Mark Schmidt, and Francis R. Bach. “A Stochastic Gradient Method with an Exponential Convergence Rate for Finite Training Sets”. In: *Neural Information Processing Systems (NeurIPS)*. 2012, pp. 2672–2680.
- [111] Yann LeCun, Léon Bottou, Yoshua Bengio, and Patrick Haffner. “Gradient-based learning applied to document recognition”. In: *Proceedings of the IEEE* 86.11 (1998), pp. 2278–2324.
- [112] Hang Li. “Learning to rank for information retrieval and natural language processing”. In: *Synthesis Lectures on Human Language Technologies 7.3* (2014), pp. 1–121.
- [113] Sijin Li, Weichen Zhang, and Antoni B Chan. “Maximum-margin structured learning with deep networks for 3d human pose estimation”. In: *International Conference in Computer Vision (ICCV)*. 2015, pp. 2848–2856.
- [114] Yan Li, Ethan X Fang, Huan Xu, and Tuo Zhao. “Implicit bias of gradient descent based adversarial training on separable data”. In: *International Conference on Learning Representations*. 2019.
- [115] Yangyan Li, Hao Su, Charles Ruizhongtai Qi, Noa Fish, Daniel Cohen-Or, and Leonidas J Guibas. “Joint embeddings of shapes and images via CNN image purification.” In: 34.6 (2015), pp. 234–1.
- [116] Tao Lin, Sebastian U. Stich, Kumar Kshitij Patel, and Martin Jaggi. “Don’t Use Large Mini-batches, Use Local SGD”. In: *International Conference on Learning Representations (ICLR)*. OpenReview.net, 2020.

- [117] Tsung-Yi Lin, Priya Goyal, Ross Girshick, Kaiming He, and Piotr Dollár. “Focal loss for dense object detection”. In: *Proceedings of the IEEE international conference on computer vision*. 2017, pp. 2980–2988.
- [118] Tsung-Yi Lin, Michael Maire, Serge Belongie, James Hays, Pietro Perona, Deva Ramanan, Piotr Dollár, and C Lawrence Zitnick. “Microsoft coco: Common objects in context”. In: *European Conference on Computer Vision (ECCV)*. Springer. 2014, pp. 740–755.
- [119] Hsueh-Ti Derek Liu, Michael Tao, Chun-Liang Li, Derek Nowrouzezahrai, and Alec Jacobson. “Beyond Pixel Norm-Balls: Parametric Adversaries using an Analytically Differentiable Renderer”. In: *ICLR (Poster)*. OpenReview.net, 2019.
- [120] David Lopez-Paz et al. “Gradient Episodic Memory for Continual Learning”. In: *Advances in Neural Information Processing Systems*. 2017, pp. 6470–6479.
- [121] Chunchuan Lyu, Kaizhu Huang, and Hai-Ning Liang. “A unified gradient regularization family for adversarial examples”. In: *2015 IEEE International Conference on Data Mining*. IEEE. 2015, pp. 301–309.
- [122] Kaifeng Lyu and Jian Li. “Gradient Descent Maximizes the Margin of Homogeneous Neural Networks”. In: *International Conference on Learning Representations (ICLR)*. OpenReview.net, 2020.
- [123] Avery Ma, Fartash Faghri, and Amir-massoud Farahmand. “Adversarial Robustness through Regularization: A Second-Order Approach”. In: *arXiv e-prints*, arXiv:2004.01832 (Apr. 2020), arXiv:2004.01832. arXiv: [2004.01832 \[cs.LG\]](https://arxiv.org/abs/2004.01832).
- [124] Linhai Ma and Liang Liang. “Increasing-Margin Adversarial (IMA) Training to Improve Adversarial Robustness of Neural Networks”. In: *CoRR* abs/2005.09147 (2020). arXiv: [2005.09147](https://arxiv.org/abs/2005.09147). URL: <https://arxiv.org/abs/2005.09147>.

- [125] Shuang Ma, Zhaoyang Zeng, Daniel McDuff, and Yale Song. “Active Contrastive Learning of Audio-Visual Video Representations”. In: *International Conference on Learning Representations*. 2021. URL: https://openreview.net/forum?id=OMizHuea_HB.
- [126] Aleksander Madry, Aleksandar Makelov, Ludwig Schmidt, Dimitris Tsipras, and Adrian Vladu. “Towards deep learning models resistant to adversarial attacks”. In: *arXiv preprint arXiv:1706.06083* (2017).
- [127] Pratyush Maini, Eric Wong, and Zico Kolter. “Adversarial robustness against the union of multiple perturbation models”. In: *International Conference on Machine Learning*. PMLR. 2020, pp. 6640–6650.
- [128] Mateusz Malinowski, Marcus Rohrbach, and Mario Fritz. “Ask Your Neurons: A Neural-based Approach to Answering Questions about Images”. In: *International Conference in Computer Vision (ICCV)*. 2015.
- [129] Tomasz Malisiewicz, Abhinav Gupta, and Alexei A Efros. “Ensemble of exemplar-svm for object detection and beyond”. In: *International Conference in Computer Vision (ICCV)*. IEEE. 2011, pp. 89–96.
- [130] James Martens. “Deep learning via Hessian-free optimization.” In: *ICML*. Vol. 27. 2010, pp. 735–742.
- [131] James Martens. “New insights and perspectives on the natural gradient method”. In: *arXiv e-prints*, arXiv:1412.1193 (Dec. 2014), arXiv:1412.1193. arXiv: [1412.1193](https://arxiv.org/abs/1412.1193) [[cs.LG](https://arxiv.org/abs/1412.1193)].
- [132] James Martens and Roger Grosse. “Optimizing neural networks with kronecker-factored approximate curvature”. In: *International conference on machine learning*. 2015, pp. 2408–2417.
- [133] James Martens and Roger B. Grosse. “Optimizing Neural Networks with Kronecker-factored Approximate Curvature”. In: *International Conference on Machine Learn-*

- ing (ICML)*. Vol. 37. JMLR Workshop and Conference Proceedings. JMLR.org, 2015, pp. 2408–2417.
- [134] James Martens and Ilya Sutskever. “Training deep and recurrent networks with hessian-free optimization”. In: *Neural networks: Tricks of the trade*. Springer, 2012, pp. 479–535.
- [135] Dominic Masters and Carlo Luschi. “Revisiting Small Batch Training for Deep Neural Networks”. In: *arXiv e-prints*, arXiv:1804.07612 (Apr. 2018), arXiv:1804.07612. arXiv: [1804.07612 \[cs.LG\]](https://arxiv.org/abs/1804.07612).
- [136] Song Mei and Andrea Montanari. “The generalization error of random features regression: Precise asymptotics and double descent curve”. In: *arXiv e-prints*, arXiv:1908.05355 (Aug. 2019), arXiv:1908.05355. arXiv: [1908.05355 \[math.ST\]](https://arxiv.org/abs/1908.05355).
- [137] Shakir Mohamed, Mihaela Rosca, Michael Figurnov, and Andriy Mnih. “Monte Carlo Gradient Estimation in Machine Learning.” In: *J. Mach. Learn. Res.* 21.132 (2020), pp. 1–62.
- [138] Andrea Montanari, Feng Ruan, Youngtak Sohn, and Jun Yan. “The generalization error of max-margin linear classifiers: High-dimensional asymptotics in the overparametrized regime”. In: *arXiv preprint arXiv:1911.01544* (2019).
- [139] Seyed-Mohsen Moosavi-Dezfooli, Alhussein Fawzi, Jonathan Uesato, and Pascal Frossard. “Robustness via curvature regularization, and vice versa”. In: *Proceedings of the IEEE Conference on Computer Vision and Pattern Recognition*. 2019, pp. 9078–9086.
- [140] Edward Moroshko, Blake E. Woodworth, Suriya Gunasekar, Jason D. Lee, Nati Srebro, and Daniel Soudry. “Implicit Bias in Deep Linear Classification: Initialization Scale vs Training Accuracy”. In: (2020). Ed. by Hugo Larochelle, Marc’Aurelio Ranzato, Raia Hadsell, Maria-Florina Balcan, and Hsuan-Tien Lin. URL: <https://proceedings.neurips.cc/paper/2020/hash/fc2022c89b61c76bbef978f1370660bf-Abstract.html>.

- [141] Eric Moulines and Francis Bach. “Non-asymptotic analysis of stochastic approximation algorithms for machine learning”. In: *Advances in neural information processing systems* 24 (2011), pp. 451–459.
- [142] Kevin Murphy. *Machine learning, a probabilistic perspective*. 2014.
- [143] Mor Shpigel Nacson, Jason Lee, Suriya Gunasekar, Pedro Henrique Pamplona Savarese, Nathan Srebro, and Daniel Soudry. “Convergence of gradient descent on separable data”. In: *The 22nd International Conference on Artificial Intelligence and Statistics*. PMLR. 2019, pp. 3420–3428.
- [144] Zachary Nado, Justin M Gilmer, Christopher J Shallue, Rohan Anil, and George E Dahl. “A large batch optimizer reality check: Traditional, generic optimizers suffice across batch sizes”. In: *arXiv preprint arXiv:2102.06356* (2021).
- [145] Preetum Nakkiran, Gal Kaplun, Yamini Bansal, Tristan Yang, Boaz Barak, and Ilya Sutskever. “Deep Double Descent: Where Bigger Models and More Data Hurt”. In: *CoRR* abs/1912.02292 (2019). arXiv: [1912.02292](https://arxiv.org/abs/1912.02292). URL: <http://arxiv.org/abs/1912.02292>.
- [146] Hyeonseob Nam, Jung-Woo Ha, and Jeonghee Kim. “Dual attention networks for multimodal reasoning and matching”. In: (2017).
- [147] Radford M Neal. “Bayesian Learning for Neural Networks”. PhD thesis. University of Toronto, 1995.
- [148] Deanna Needell, Rachel Ward, and Nathan Srebro. “Stochastic Gradient Descent, Weighted Sampling, and the Randomized Kaczmarz algorithm”. In: *Neural Information Processing Systems (NeurIPS)*. 2014, pp. 1017–1025.
- [149] Yurii Nesterov. “A method for unconstrained convex minimization problem with the rate of convergence $O(1/k^2)$ ”. In: *Doklady AN USSR*. Vol. 269. 1983, pp. 543–547.
- [150] Jorge Nocedal and Stephen Wright. *Numerical optimization*. Springer Science & Business Media, 2006.

- [151] Greg Ongie, Rebecca Willett, Daniel Soudry, and Nathan Srebro. “A Function Space View of Bounded Norm Infinite Width ReLU Nets: The Multivariate Case”. In: *International Conference on Learning Representations (ICLR)*. OpenReview.net, 2020.
- [152] Aaron van den Oord, Yazhe Li, and Oriol Vinyals. “Representation learning with contrastive predictive coding”. In: *arXiv preprint arXiv:1807.03748* (2018).
- [153] Guillermo Ortiz-Jimenez, Apostolos Modas, Seyed-Mohsen Moosavi-Dezfooli, and Pascal Frossard. “Hold me tight! Influence of discriminative features on deep network boundaries”. In: *arXiv preprint arXiv:2002.06349* (2020).
- [154] Neal Parikh and Stephen Boyd. “**Proximal algorithms**”. In: *Foundations and Trends in Optimization* (2013).
- [155] Jeffrey Pennington, Samuel Schoenholz, and Surya Ganguli. “Resurrecting the sigmoid in deep learning through dynamical isometry: theory and practice”. In: *Advances in neural information processing systems*. 2017, pp. 4785–4795.
- [156] Boris T Polyak. “Some methods of speeding up the convergence of iteration methods”. In: *USSR Computational Mathematics and Mathematical Physics* 4.5 (1964), pp. 1–17.
- [157] Martin Popel, Marketa Tomkova, Jakub Tomek, Łukasz Kaiser, Jakob Uszkoreit, Ondřej Bojar, and Zdeněk Žabokrtský. “Transforming machine translation: a deep learning system reaches news translation quality comparable to human professionals”. In: *Nature communications* 11.1 (2020), pp. 1–15.
- [158] Chongli Qin, James Martens, Sven Gowal, Dilip Krishnan, Krishnamurthy Dvijotham, Alhussein Fawzi, Soham De, Robert Stanforth, and Pushmeet Kohli. “Adversarial robustness through local linearization”. In: *Advances in Neural Information Processing Systems*. 2019, pp. 13847–13856.

- [159] Alec Radford, Jong Wook Kim, Chris Hallacy, Aditya Ramesh, Gabriel Goh, Sandhini Agarwal, Girish Sastry, Amanda Askell, Pamela Mishkin, Jack Clark, et al. “Learning transferable visual models from natural language supervision”. In: *arXiv preprint arXiv:2103.00020* (2021).
- [160] Maithra Raghu, Justin Gilmer, Jason Yosinski, and Jascha Sohl-Dickstein. “SVCCA: Singular Vector Canonical Correlation Analysis for Deep Learning Dynamics and Interpretability”. In: *Neural Information Processing Systems (NeurIPS)*. 2017, pp. 6076–6085.
- [161] Aditi Raghunathan, Sang Michael Xie, Fanny Yang, John Duchi, and Percy Liang. “Understanding and mitigating the tradeoff between robustness and accuracy”. In: *arXiv preprint arXiv:2002.10716* (2020).
- [162] Ali Rahimi and Benjamin Recht. “Random Features for Large-Scale Kernel Machines”. In: *NIPS*. Curran Associates, Inc., 2007, pp. 1177–1184.
- [163] Aditya Ramesh, Mikhail Pavlov, Gabriel Goh, Scott Gray, Chelsea Voss, Alec Radford, Mark Chen, and Ilya Sutskever. *Zero-Shot Text-to-Image Generation*. 2021. arXiv: [2102.12092](https://arxiv.org/abs/2102.12092) [cs.CV].
- [164] Ali Ramezani-Kebrya, Fartash Faghri, Ilya Markov, Vitalii Aksenov, Dan Alistarh, and Daniel M Roy. “NUQSGD: Provably Communication-efficient Data-parallel SGD via Nonuniform Quantization”. In: *Journal of Machine Learning Research* 22.114 (2021), pp. 1–43.
- [165] Scott Reed, Zeynep Akata, Xinchen Yan, Lajanugen Logeswaran, Bernt Schiele, and Honglak Lee. “Generative adversarial text to image synthesis”. In: (2016).
- [166] Scott Reed, Zeynep Akata, Honglak Lee, and Bernt Schiele. “Learning deep representations of fine-grained visual descriptions”. In: *IEEE Conference on Computer Vision and Pattern Recognition (CVPR)*. 2016, pp. 49–58.
- [167] Herbert Robbins and Sutton Monro. “A stochastic approximation method”. In: *The annals of mathematical statistics* (1951), pp. 400–407.

- [168] Andrew Ross and Finale Doshi-Velez. “Improving the adversarial robustness and interpretability of deep neural networks by regularizing their input gradients”. In: *Proceedings of the AAAI Conference on Artificial Intelligence*. Vol. 32. 2018.
- [169] Saharon Rosset, Ji Zhu, and Trevor J Hastie. “Margin maximizing loss functions”. In: *Advances in neural information processing systems*. 2004, pp. 1237–1244.
- [170] David E Rumelhart, Geoffrey E Hinton, and Ronald J Williams. “Learning representations by back-propagating errors”. In: *nature* 323.6088 (1986), p. 533.
- [171] Shiori Sagawa, Aditi Raghunathan, Pang Wei Koh, and Percy Liang. “An investigation of why overparameterization exacerbates spurious correlations”. In: *International Conference on Machine Learning (ICML)*. PMLR. 2020, pp. 8346–8356.
- [172] Tim Salimans, Jonathan Ho, Xi Chen, Szymon Sidor, and Ilya Sutskever. “Evolution strategies as a scalable alternative to reinforcement learning”. In: *arXiv preprint arXiv:1703.03864* (2017).
- [173] Hadi Salman, Greg Yang, Huan Zhang, Cho-Jui Hsieh, and Pengchuan Zhang. “A convex relaxation barrier to tight robustness verification of neural networks”. In: *Advances in Neural Information Processing Systems*. 2019, pp. 9835–9846.
- [174] Hadi Salman, Andrew Ilyas, Logan Engstrom, Ashish Kapoor, and Aleksander Madry. “Do Adversarially Robust ImageNet Models Transfer Better?” In: *NeurIPS*. 2020.
- [175] Andrew M Saxe, James L McClelland, and Surya Ganguli. “Exact solutions to the nonlinear dynamics of learning in deep linear neural networks”. In: *arXiv preprint arXiv:1312.6120* (2013).
- [176] Ludwig Schmidt, Shibani Santurkar, Dimitris Tsipras, Kunal Talwar, and Aleksander Madry. “Adversarially robust generalization requires more data”. In: *Advances in Neural Information Processing Systems*. 2018, pp. 5014–5026.

- [177] Mark Schmidt and Nicolas Le Roux. “Fast convergence of stochastic gradient descent under a strong growth condition”. In: *arXiv preprint arXiv:1308.6370* (2013).
- [178] Robin M. Schmidt, Frank Schneider, and Philipp Hennig. “Descending through a Crowded Valley - Benchmarking Deep Learning Optimizers”. In: *Proceedings of the 38th International Conference on Machine Learning, ICML 2021, 18-24 July 2021, Virtual Event*. Ed. by Marina Meila and Tong Zhang. Vol. 139. Proceedings of Machine Learning Research. PMLR, 2021, pp. 9367–9376. URL: <http://proceedings.mlr.press/v139/schmidt21a.html>.
- [179] Florian Schroff, Dmitry Kalenichenko, and James Philbin. “Facenet: A unified embedding for face recognition and clustering”. In: *IEEE Conference on Computer Vision and Pattern Recognition (CVPR)*. 2015, pp. 815–823.
- [180] Ayon Sen, Xiaojin Zhu, Liam Marshall, and Robert Nowak. “Should Adversarial Attacks Use Pixel p-Norm?” In: *arXiv e-prints*, arXiv:1906.02439 (June 2019), arXiv:1906.02439. arXiv: [1906.02439 \[cs.LG\]](https://arxiv.org/abs/1906.02439).
- [181] Christopher J. Shallue, Jaehoon Lee, Joseph Antognini, Jascha Sohl-Dickstein, Roy Frostig, and George E. Dahl. “Measuring the Effects of Data Parallelism on Neural Network Training”. In: *arXiv e-prints*, arXiv:1811.03600 (Nov. 2018), arXiv:1811.03600. arXiv: [1811.03600 \[cs.LG\]](https://arxiv.org/abs/1811.03600).
- [182] Mahmood Sharif, Lujo Bauer, and Michael K. Reiter. “On the Suitability of Lp-Norms for Creating and Preventing Adversarial Examples”. In: *CVPR Workshops*. IEEE Computer Society, 2018, pp. 1605–1613.
- [183] Yash Sharma, Gavin Weiguang Ding, and Marcus Brubaker. “On the effectiveness of low frequency perturbations”. In: *arXiv preprint arXiv:1903.00073* (2019).
- [184] John Shawe-Taylor, Peter L. Bartlett, Robert C. Williamson, and Martin Anthony. “Structural Risk Minimization Over Data-Dependent Hierarchies”. In: *IEEE Trans. Inf. Theory* 44.5 (1998), pp. 1926–1940.

- [185] David Silver, Julian Schrittwieser, Karen Simonyan, Ioannis Antonoglou, Aja Huang, Arthur Guez, Thomas Hubert, Lucas Baker, Matthew Lai, Adrian Bolton, et al. “Mastering the game of go without human knowledge”. In: *nature* 550.7676 (2017), pp. 354–359.
- [186] Carl-Johann Simon-Gabriel, Yann Ollivier, Leon Bottou, Bernhard Schölkopf, and David Lopez-Paz. “First-order adversarial vulnerability of neural networks and input dimension”. In: *International Conference on Machine Learning*. PMLR, 2019, pp. 5809–5817.
- [187] Karen Simonyan and Andrew Zisserman. “Very deep convolutional networks for large-scale image recognition”. In: (2015).
- [188] Umut Simsekli, Levent Sagun, and Mert Gürbüzbalaban. “A Tail-Index Analysis of Stochastic Gradient Noise in Deep Neural Networks”. In: *International Conference on Machine Learning (ICML)*. Vol. 97. Proceedings of Machine Learning Research. PMLR, 2019, pp. 5827–5837.
- [189] Richard Socher, Andrej Karpathy, Quoc V Le, Christopher D Manning, and Andrew Y Ng. “Grounded compositional semantics for finding and describing images with sentences”. In: 2 (2014), pp. 207–218.
- [190] Jure Sokolić, Raja Giryes, Guillermo Sapiro, and Miguel RD Rodrigues. “Robust large margin deep neural networks”. In: *IEEE Transactions on Signal Processing* 65.16 (2017), pp. 4265–4280.
- [191] Nitish Srivastava, Geoffrey Hinton, Alex Krizhevsky, Ilya Sutskever, and Ruslan Salakhutdinov. “Dropout: A simple way to prevent neural networks from overfitting”. In: *The Journal of Machine Learning Research* 15.1 (2014), pp. 1929–1958.
- [192] Emma Strubell, Ananya Ganesh, and Andrew McCallum. “Energy and Policy Considerations for Deep Learning in NLP”. In: *ACL (1)*. Association for Computational Linguistics, 2019, pp. 3645–3650.

- [193] Niko Sünderhauf, Oliver Brock, Walter Scheirer, Raia Hadsell, Dieter Fox, Jürgen Leitner, Ben Upcroft, Pieter Abbeel, Wolfram Burgard, Michael Milford, et al. “The limits and potentials of deep learning for robotics”. In: *The International Journal of Robotics Research* 37.4-5 (2018), pp. 405–420.
- [194] Ilya Sutskever, James Martens, George Dahl, and Geoffrey Hinton. “On the importance of initialization and momentum in deep learning”. In: *International conference on machine learning*. 2013, pp. 1139–1147.
- [195] Richard S Sutton. “Two problems with backpropagation and other steepest-descent learning procedures for networks”. In: *Proceedings of Eighth Annual Conference of the Cognitive Science Society, 1986*. 1986.
- [196] Christian Szegedy, Wojciech Zaremba, Ilya Sutskever, Joan Bruna, Dumitru Erhan, Ian Goodfellow, and Rob Fergus. “Intriguing properties of neural networks”. In: *arXiv preprint arXiv:1312.6199* (2013).
- [197] Christian Szegedy, Vincent Vanhoucke, Sergey Ioffe, Jonathon Shlens, and Zbigniew Wojna. “Rethinking the Inception Architecture for Computer Vision”. In: *IEEE Conference on Computer Vision and Pattern Recognition (CVPR)*. IEEE Computer Society, 2016, pp. 2818–2826.
- [198] Terence Tao. *Topics in random matrix theory*. Vol. 132. American Mathematical Soc., 2012.
- [199] Matus Telgarsky. “Margins, Shrinkage, and Boosting”. In: *ICML (2)*. Vol. 28. JMLR Workshop and Conference Proceedings. JMLR.org, 2013, pp. 307–315.
- [200] Valentin Thomas, Fabian Pedregosa, Bart van Merriënboer, Pierre-Antoine Manzagol, Yoshua Bengio, and Nicolas Le Roux. “On the interplay between noise and curvature and its effect on optimization and generalization”. In: *International Conference on Artificial Intelligence and Statistics (AISTATS)*. 2020.

- [201] Tijmen Tieleman and Geoffrey Hinton. “Lecture 6.5-RMSProp: Divide the gradient by a running average of its recent magnitude”. In: *COURSERA: Neural networks for machine learning* 4.2 (2012), pp. 26–31.
- [202] Florian Tramèr and Dan Boneh. “Adversarial Training and Robustness for Multiple Perturbations”. In: *NeurIPS*. 2019, pp. 5858–5868.
- [203] Florian Tramer, Nicholas Carlini, Wieland Brendel, and Aleksander Madry. “On Adaptive Attacks to Adversarial Example Defenses”. In: *arXiv e-prints*, arXiv:2002.08347 (Feb. 2020), arXiv:2002.08347. arXiv: [2002.08347 \[cs.LG\]](https://arxiv.org/abs/2002.08347).
- [204] Dimitris Tsipras, Shibani Santurkar, Logan Engstrom, Alexander Turner, and Aleksander Madry. “Robustness may be at odds with accuracy”. In: *arXiv preprint arXiv:1805.12152* (2018).
- [205] Ioannis Tsochantaridis, Thorsten Joachims, Thomas Hofmann, and Yasemin Altun. “Large margin methods for structured and interdependent output variables”. In: *Journal of Machine Learning Research (JMLR)* 6.Sep (2005), pp. 1453–1484.
- [206] Yusuke Tsuzuku and Issei Sato. “On the structural sensitivity of deep convolutional networks to the directions of fourier basis functions”. In: *Proceedings of the IEEE Conference on Computer Vision and Pattern Recognition*. 2019, pp. 51–60.
- [207] Vladimir Naumovich Vapnik. “An overview of statistical learning theory”. In: *IEEE transactions on neural networks* 10.5 (1999), pp. 988–999.
- [208] Cristina Vasconcelos, Hugo Larochelle, Vincent Dumoulin, Nicolas Le Roux, and Ross Goroshin. “An Effective Anti-Aliasing Approach for Residual Networks”. In: *CoRR* abs/2011.10675 (2020).
- [209] Sharan Vaswani, Reza Babanezhad, Jose Gallego, Aaron Mishkin, Simon Lacoste-Julien, and Nicolas Le Roux. “To Each Optimizer a Norm, To Each Norm its Generalization”. In: *CoRR* abs/2006.06821 (2020). arXiv: [2006.06821](https://arxiv.org/abs/2006.06821). URL: <https://arxiv.org/abs/2006.06821>.

- [210] Ivan Vendrov, Ryan Kiros, Sanja Fidler, and Raquel Urtasun. “Order-embeddings of images and language”. In: (2016).
- [211] Oriol Vinyals, Charles Blundell, Tim Lillicrap, Koray Kavukcuoglu, and Daan Wierstra. “Matching Networks for One Shot Learning”. In: *Advances in Neural Information Processing Systems 29: Annual Conference on Neural Information Processing Systems 2016, December 5-10, 2016, Barcelona, Spain*. Ed. by Daniel D. Lee, Masashi Sugiyama, Ulrike von Luxburg, Isabelle Guyon, and Roman Garnett. 2016, pp. 3630–3638. URL: <https://proceedings.neurips.cc/paper/2016/hash/90e1357833654983612fb05e3ec9148c-Abstract.html>.
- [212] Kailas Vodrahalli, Ke Li, and Jitendra Malik. “Are All Training Examples Created Equal? An Empirical Study”. In: *arXiv e-prints*, arXiv:1811.12569 (Nov. 2018), arXiv:1811.12569. arXiv: [1811.12569](https://arxiv.org/abs/1811.12569) [cs.LG].
- [213] Haoran Wang, Ying Zhang, Zhong Ji, Yanwei Pang, and Lin Ma. “Consensus-aware visual-semantic embedding for image-text matching”. In: *European Conference on Computer Vision (ECCV)*. Springer. 2020, pp. 18–34.
- [214] Liwei Wang, Yin Li, and Svetlana Lazebnik. “Learning Two-Branch Neural Networks for Image-Text Matching Tasks”. In: *IEEE Transactions on Pattern Analysis and Machine Intelligence (PAMI)* (2018).
- [215] Colin Wei, Jason D Lee, Qiang Liu, and Tengyu Ma. “Regularization matters: Generalization and optimization of neural nets vs their induced kernel”. In: *Advances in Neural Information Processing Systems*. 2019, pp. 9712–9724.
- [216] Kilian Q Weinberger and Lawrence K Saul. “Distance metric learning for large margin nearest neighbor classification.” In: *Journal of machine learning research* 10.2 (2009).
- [217] Yeming Wen, Kevin Luk, Maxime Gazeau, Guodong Zhang, Harris Chan, and Jimmy Ba. “An Empirical Study of Large-Batch Stochastic Gradient Descent with

- Structured Covariance Noise”. In: *International Conference on Artificial Intelligence and Statistics (AISTATS)*. 2019. arXiv: [1902.08234](https://arxiv.org/abs/1902.08234).
- [218] Eric Wong and Zico Kolter. “Provable defenses against adversarial examples via the convex outer adversarial polytope”. In: *International Conference on Machine Learning*. PMLR. 2018, pp. 5286–5295.
- [219] Chao-Yuan Wu, R Manmatha, Alexander J Smola, and Philipp Krähenbühl. “Sampling Matters in Deep Embedding Learning”. In: (2017).
- [220] Jingfeng Wu, Wenqing Hu, Haoyi Xiong, Jun Huan, Vladimir Braverman, and Zhanxing Zhu. “On the noisy gradient descent that generalizes as sgd”. In: *International Conference on Machine Learning*. PMLR. 2020, pp. 10367–10376.
- [221] Xiaoxia Wu, Ethan Dyer, and Behnam Neyshabur. “When Do Curricula Work?” In: *9th International Conference on Learning Representations, ICLR 2021, Virtual Event, Austria, May 3-7, 2021*. OpenReview.net, 2021. URL: <https://openreview.net/forum?id=tW4QEInpni>.
- [222] Cihang Xie, Mingxing Tan, Boqing Gong, Alan L. Yuille, and Quoc V. Le. “Smooth Adversarial Training”. In: *CoRR* abs/2006.14536 (2020).
- [223] Dong Yin, Raphael Gontijo Lopes, Jon Shlens, Ekin Dogus Cubuk, and Justin Gilmer. “A fourier perspective on model robustness in computer vision”. In: *Advances in Neural Information Processing Systems 32* (2019), pp. 13276–13286.
- [224] Peter Young, Alice Lai, Micah Hodosh, and Julia Hockenmaier. “From image descriptions to visual denotations: New similarity metrics for semantic inference over event descriptions”. In: *2* (2014), pp. 67–78.
- [225] Chun-Nam John Yu and Thorsten Joachims. “Learning structural svms with latent variables”. In: *International Conference on Machine Learning (ICML)*. ACM. 2009, pp. 1169–1176.

- [226] Chulhee Yun, Shankar Krishnan, and Hossein Mobahi. “A Unifying View on Implicit Bias in Training Linear Neural Networks”. In: *arXiv e-prints*, arXiv:2010.02501 (Oct. 2020), arXiv:2010.02501. arXiv: [2010.02501 \[cs.LG\]](https://arxiv.org/abs/2010.02501).
- [227] Chiyuan Zhang, Samy Bengio, Moritz Hardt, Benjamin Recht, and Oriol Vinyals. “Understanding deep learning requires rethinking generalization”. In: *arXiv preprint arXiv:1611.03530* (2016).
- [228] Chiyuan Zhang, Samy Bengio, Moritz Hardt, Benjamin Recht, and Oriol Vinyals. “Understanding deep learning requires rethinking generalization”. In: *International Conference on Learning Representations (ICLR)*. OpenReview.net, 2017.
- [229] Guodong Zhang, Lala Li, Zachary Nado, James Martens, Sushant Sachdeva, George E. Dahl, Christopher J. Shallue, and Roger B. Grosse. “Which Algorithmic Choices Matter at Which Batch Sizes? Insights From a Noisy Quadratic Model”. In: *Neural Information Processing Systems (NeurIPS)*. 2019, pp. 8194–8205.
- [230] Hongyang Zhang, Yaodong Yu, Jiantao Jiao, Eric P. Xing, Laurent El Ghaoui, and Michael I. Jordan. “Theoretically Principled Trade-off between Robustness and Accuracy”. In: *arXiv e-prints*, arXiv:1901.08573 (Jan. 2019), arXiv:1901.08573. arXiv: [1901.08573 \[cs.LG\]](https://arxiv.org/abs/1901.08573).
- [231] Jingzhao Zhang, Sai Praneeth Karimireddy, Andreas Veit, Seungyeon Kim, Sashank J. Reddi, Sanjiv Kumar, and Suvrit Sra. “Why ADAM Beats SGD for Attention Models”. In: *CoRR* abs/1912.03194 (2019). arXiv: [1912.03194](https://arxiv.org/abs/1912.03194). URL: <http://arxiv.org/abs/1912.03194>.
- [232] Peilin Zhao and Tong Zhang. “Accelerating Minibatch Stochastic Gradient Descent using Stratified Sampling”. In: *arXiv e-prints*, arXiv:1405.3080 (May 2014), arXiv:1405.3080. arXiv: [1405.3080 \[stat.ML\]](https://arxiv.org/abs/1405.3080).
- [233] Peilin Zhao and Tong Zhang. “Stochastic optimization with importance sampling for regularized loss minimization”. In: *international conference on machine learning*. PMLR. 2015, pp. 1–9.

- [234] Zhengyu Zhao, Zhuoran Liu, and Martha Larson. “Adversarial Color Enhancement: Generating Unrestricted Adversarial Images by Optimizing a Color Filter”. In: *arXiv e-prints*, arXiv:2002.01008 (Feb. 2020), arXiv:2002.01008. arXiv: [2002.01008](https://arxiv.org/abs/2002.01008) [cs.CV].
- [235] Yukun Zhu, Ryan Kiros, Rich Zemel, Ruslan Salakhutdinov, Raquel Urtasun, Antonio Torralba, and Sanja Fidler. “Aligning Books and Movies: Towards Story-like Visual Explanations by Watching Movies and Reading Books”. In: *International Conference in Computer Vision (ICCV)*. 2015.
- [236] Zhanxing Zhu, Jingfeng Wu, Bing Yu, Lei Wu, and Jinwen Ma. “The Anisotropic Noise in Stochastic Gradient Descent: Its Behavior of Escaping from Sharp Minima and Regularization Effects”. In: *International Conference on Machine Learning (ICML)*. Vol. 97. Proceedings of Machine Learning Research. PMLR, 2019, pp. 7654–7663.
- [237] C Lawrence Zitnick, Aishwarya Agrawal, Stanislaw Antol, Margaret Mitchell, Dhruv Batra, and Devi Parikh. “Measuring machine intelligence through visual question answering”. In: *AI Magazine* (2016).
- [238] Will Y Zou, Richard Socher, Daniel Cer, and Christopher D Manning. “Bilingual word embeddings for phrase-based machine translation”. In: *Empirical Methods in Natural Language Processing (EMNLP)*. 2013, pp. 1393–1398.